Experimental Investigation and Modeling of Growth Cone Adaptation in the Development of Topographic Projections

(Experimentelle Untersuchung und Modellierung der Wachstumskegel-
Adaptation bei der Entwicklung topographischer Karten)

Zur Erlangung des akademischen Grades eines

DOKTORS DER NATURWISSENSCHAFTEN
(Dr. rer. nat.)

von der KIT-Fakultät für Chemie und Biowissenschaften
des Karlsruher Instituts für Technologie (KIT)

genehmigte

DISSERTATION

von

Felix Fiederling
aus Oberkirch

Dekan: Prof. Dr. Willem Klopper
Referent: Prof. Dr. Martin Bastmeyer
Korreferent: Prof. Dr. Peter Nick
Tag der mündlichen Prüfung: 22.07.2016

ABSTRACT

The retinotectal projection is a model to investigate the development of topographic projections, which are defined by the preservation of neighborhood relationships upon projection. Topographic projections are an abundant motif of brain connectivity. In the visual system, retinal ganglion cell growth cones (GCs) are mapped onto the optic tectum in the midbrain. Counter-gradients of EphA receptor tyrosine kinases and their ephrin-A ligands along both, the retinal temporo-nasal and the tectal antero-posterior axes provide decisive chemoaffinity cues guiding retinal axons to their topographically appropriate tectal destinations.

Topographic precision relies on a faithful read-out of guidance cue concentrations. A comprehensive computational model of our group, in which GCs are led towards a balance of total EphA/ ephrin-A forward and ephrin-A/ EphA reverse signaling is able to explain major experimental *in vitro* and *in vivo* evidence gained on this system. Surprisingly, however, retinal GCs can adapt to these signals. *In vitro*, GCs desensitize towards soluble and substrate-bound ephrin-A5 and, as I show in this work, EphA3 signals. In absence of either cue, they quickly resensitize.

In an updated version of our computational model, now including adaptation, I propose a proportional co-variation of EphA and ephrin-A activities to explain the inconsistency of adaptation with topographic precision. Implementing this assumption, the model faithfully reproduces the results of *in vitro* adaptation assays and can still explain topographic map formation.

Notably, the models' assumption of strict co-regulation of both sensors during adaptation (here termed co-adaptation) could be confirmed by *in*

vitro experiments. Here I show, that GCs desensitize towards ephrin-A5 even without having migrated on it but on EphA3 instead and *vice versa*. In agreement with this, we could previously show a massive reduction of surface bound ephrin-A5 on GCs growing on either EphA3 or ephrin-A5 fields by transfecting axons with a SNAP-tagged ephrin-A5 expression construct. In this work, I provide evidence that the sensors are internalized via clathrin-mediated endocytosis during desensitization and are recycled back to the surface upon resensitization.

In sum, I present co-adaptation as a novel mechanism of signal integration, potentially involving recycling endosomes. Results from the computational model support a potential role for (co-) adaptation in target innervation, explaining why retinal axons can enter the anterior tectum, a region with highest expression of repulsive EphAs.

ZUSAMMENFASSUNG

Die Retinotectale Projektion ist ein Modellsystem zur Untersuchung der Entwicklung topografischer Projektionen, die sich durch eine nachbarschaftstreue Verknüpfung der beteiligten Neurone auszeichnen und in der Architektur des Gehirns allgegenwärtig sind. Im visuellen System projizieren Wachstumskegel retinaler Ganglionzellen auf das optische Tectum im Mittelhirn. Gegenläufige Gradienten aus EphA Rezeptortyrosinkinasen und deren ephrin-A Liganden entlang der retinalen temporo-nasalen und entlang der tectalen antero-posterioren Achsen, dienen dabei als ausschlaggebende Lenkungssignale, die retinale Axone an ihre korrekten Ziele führen. Ein präzises Auslesen der lokalen Konzentration dieser Lenkungsmoleküle ist für eine genaue Zielfindung essenziell.

Ein umfassendes Computermodell unserer Gruppe erklärt einen Großteil der auf diesem Gebiet gesammelten *in vitro* und *in vivo* Evidenzen, indem es Wachstumskegel eine Balancierung der eingehenden EphA/ ephrin-A 'forward' und ephrin-A/ EphA 'reverse' Signale anstreben lässt. Überraschenderweise adaptieren retinale Wachstumskegel an diese Signale: *In vitro* verlieren Wachstumskegel ihre Sensitivität gegenüber gelöstem und substratgebundenem ephrin-A5 und, wie ich in dieser Arbeit zeige, auch gegenüber EphA3. In Abwesenheit beider Proteine stellt sich die ursprüngliche Sensitivität wieder ein.

In einer erweiterten Modellversion, die jetzt Adaptation enthält, schlage ich eine proportionale Koregulation der EphA und ephrin-A Aktivitäten vor, um die scheinbare Unvereinbarkeit von Adaptation und topografischer Präzision aufzulösen. Durch die Implementierung dieser Annahme ist das Modell in der Lage die Ergebnisse der *in vitro*

Adaptationsexperimente sowie eine topografische Projektion zu reproduzieren.

In dieser Arbeit konnte ich die Annahme des Modells über eine strikte Koregulierung beider Sensoren während der Adaptation (Ko-Adaptation) experimentell bestätigen. Wachstumskegel, die auf EphA3 auswachsen, desensitivieren gegenüber ephrin-A5, obwohl sie ephrin-A5 zuvor nie wahrnehmen konnten. Umgekehrt ko-adaptieren ephrin-A5 adaptierende Wachstumskegel an EphA3. Damit übereinstimmend, konnten unsere Arbeitsgruppe in Wachstumskegeln, die ein SNAP-markiertes ephrin-A5 Konstrukt exprimieren, eine starke Reduktion des membranständigen Anteils an ephrin-A5 nachweisen, sowohl wenn diese auf EphA3, als auch auf ephrin-A5 beschichteten Flächen migrieren. Daten dieser Arbeit deuten darauf, dass diese Sensoren während der Desensitivierung durch Clathrin-abhängige Endozytose internalisiert und durch endosomales Recycling während der Resensitivierung wieder zurück and die Zelloberfläche gebracht werden.

Zusammenfassend bietet diese Arbeit deutliche Hinweise auf die Existenz eines neuartigen Ko-Adaptation Mechanismus, der spezifisch EphA und ephrin-A Signale moduliert. Ergebnisse des Computermodells unterstützen eine mögliche Rolle der Ko-Adaptation bei der Innervation des Zielgebietes und erklären warum retinale Axone in das anteriore Tectum einwachsen können, obwohl dort repulsive EphAs maximal exprimiert werden.

ERKLÄRUNG

Der experimentelle Teil der vorliegenden Arbeit wurde in der Zeit von August 2012 bis April 2016 am Zoologischen Institut in der Abteilung für Zell- und Neurobiologie, des Karlsruher Instituts für Technologie (KIT) durchgeführt.

Hiermit versichere ich, dass ich diese Arbeit selbstständig verfasst und nur die angegebenen Quellen und Hilfsmittel verwendet habe. Wörtlich oder inhaltlich übernommene Stellen sind als solche gekennzeichnet. Die Satzung des Karlsruher Instituts für Technologie (KIT) zur Sicherung guter wissenschaftlicher Praxis habe ich in der gültigen Fassung beachtet. Die Arbeit wurde in keiner Form einer anderen Prüfungsbehörde vorgelegt. Ich verischere, dass die beigelegte, elektronische Version der Arbeit mit der schriftlichen übereinstimmt.

Karlsruhe, den 27.07.2016

Felix Fiederling

CONTENTS

<u>INTRODUCTION</u>

Topographic Projections

The perplexingly complex function of the brain is mainly encoded in the connectional architecture of its vast number of neurons. To construct a network of such dimensions necessitates sophisticated developmental mechanisms enabling neurons to target their correct connection partners with high precision at preferably low wiring costs. Topographic projections, in which neighboring neurons project to neighboring targets, are excellent examples of economic wiring motives (Chklovskii and Koulakov, 2004) and can be found in the visual, auditory, somatosensory and motor systems but also deep inside the brain (Wedeen et al., 2012; Cang and Feldheim, 2013). Their ostensibly simple developmental self-organization is mainly genetically instructed and best studied for the retinotectal/ retinocullicular projection connecting retinal ganglion cells (RGCs) in the eye with the midbrains *tectum opticum/ superior colliculus* (Lemke and Reber, 2005; Luo and Flanagan, 2007; Feldheim and O'Leary, 2010). However, despite being in the focus of research for several decades, there is still no fully consistent developmental model for the formation of topographic projections to date.

The Retinotectal Projection

Within the retinotectal/ retinocollicular projection, RGC axons leaving the retinal cup in the optic nerve cross the chiasm and grow within the optic tract towards the *colliculi superiores* (in mammals) or the *tectum opticum* (in amphibians, fishes and birds). Whereas, in mammals, the

visual information is transmitted from the *superior colliculus* (SC) to the primary visual nuclei in the thalamus (*corpora geniculata lateralia*) and then to the visual areas of the cortex for processing, in lower vertebrates the optic tectum directly serves as the main processing unit. This is also reflected in the enormous size of the tectum, for example in chicken embryos, what made them, beside the genetically better accessible mice, key model organisms to investigate retinotectal map formation (Thanos and Mey, 2001).

The topographic organization in the chicken retinotectal system results in the projection of the temporo-nasal (t-n) axis of the retina onto the antero-posterior (a-p) axis of the tectum and, for the representation of the second main axis of the two-dimensional visual field, the projection of the retinal dorso-ventral axis onto the tectal latero-medial (l-m) axis (Figure 1). This basic organization is similar in all studied model organisms, however, there are differences in the mode of map formation. In mammals, all retinal axons first grow straight to the posterior end of the SC and then, via interstitial (back-)branching, form terminal arborizations at the topographically correct positions. The overshooting parts of the axons are pruned later (Simon and O'Leary, 1992). In contrast, in amphibians, fishes and chicken, the axons directly target their correct positions (Holt and Harris, 1983), although there is also a minor overshoot of axons in chicken (Nakamura and O'Leary, 1989; Yates et al., 2001), indicating a general imprecision of the initial map.

The Mechanisms of Map Formation

Seminal to the understanding of the development of the retinotectal map was the work of Roger Sperry, who first proposed graded distributions of chemical guidance cues on the tectal target to provide

for the directional an positional information to guide retinal growth cones to their topographically correct positions, based on their affinities towards these cues (Sperry, 1963). Following Sperry's chemoaffinity hypothesis, research over the last decades indeed identified molecular components essential for RGCs along the n-t axis to map onto the a-p axis of the tectum and established the retinotectal projection as a model system for topographic projections. Today, it is commonly accepted that opposing graded distributions of ephrin-As (low anterior, high posterior; Drescher et al., 1995; Cheng et al, 1995) and EphAs (high anterior, low posterior; Connor et al., 1998) on the tectum guide RGC axons to their target positions.
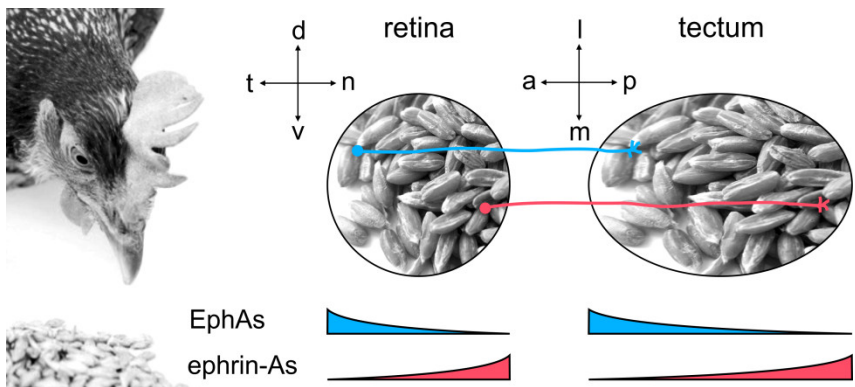
Figure 1: The retinotectal projection.

The topographic projection in the chicken visual system connects $>10^6$ RGCs from the retina to the midbrains' optic tectum. The temporo-nasal (t-n) axis of the retina is mapped onto the antero-posterior (a-p) axis of the tectum, whereas the retinal dorso-ventral (d-v) axis projects onto the latero-medial (l-m) axis of the tectum. With this, the visual information of an object in the retina is transferred to the tectum as a scaled, but ordered representation. Retinal growth cones are guided to their tectal targets by repulsive signals originating from counter-gradient distributions of ephrin-A (red) and EphA (blue) guidance cues, expressed in the tectum in p>a and a>p gradients, respectively. Detection of these cues is mediated via EphA and, due to a bidirectional signaling, ephrin-A sensors, which are expressed in the retina in t>n and n>t gradients, respectively.

The physical aspect of guidance, i.e. movement within the target field, is achieved by a motile structure at the axons' tip, the growth cone. Growth cones, first described by Ramón y Cajal in 1890 as 'cone- like lump[s] with a peripheral base' (Cajal, 1890; translation taken from Tamariz and Varela-Echavarria, 2015) act as a chemotactic sensors reading the guidance information by probing the environment with highly dynamic filopodia and lamellipodia, which they extend and retract by modulating their actin (Gomez and Letourneau, 2014; Nichol IV et al., 2016) and microtubule (Liu and Dwyer, 2014; Bearce et al., 2015) cytoskeletal network. In addition, local endo- and exocytosis of membrane allow for rapid morphological transformations and changes in the direction of growth in response to guidance cues (Tojima et al., 2014; Akiyama et al., 2016).

Somehow confusingly, RGCs utilize the very same EphAs and ephrin-As for the detection of tectal cues, which they express in different levels along the retinal n-t axis (EphAs: low nasal, high temporal; Cheng et al., 1995; Connor et al., 1998; ephrin-As: high nasal, low temporal; Hornberger et al., 1999; Menzel et al., 2001) in addition to some homogeneously expressed EphA/ ephrin-A subfamily members of unknown function (Connor et al., 1998; Marin et al., 2001)[1].

This is possible, because Eph/ ephrin signaling is bidirectional, meaning that both classes of molecules can function as ligands or receptors (reviewed in Kullander and Klein, 2002). To discriminate between the direction of signaling, the signal transmitted into an Eph expressing cell is termed 'forward', whereas the signal transmitted into an ephrin expressing cell is termed 'reverse'. Both pathways have been shown to transduce repulsive signals to the navigating growth cone.

---

[1]: Expression levels of individual EphA and ephrin-A family members differ between mouse and chick and were recently summarized in Weth et al., 2014.

Being GPI-anchored, ephrin-As rely on co-receptors for reverse signaling, which were identified to be p75NTR (in mouse; Lim et al., 2008) and TrkB (in chick; Marler et al., 2008).

In the tectal gradient field RGC growth cones target a position with a distribution of EphAs and ephrin-As matching their own endowment. Depending on the EphA/ ephrin-A expression levels, and therefore on the origin of individual RGCs along the retinal n-t axis, this mechanism assigns the individual chemoaffinity information to the growth cones needed for topographic a-p mapping. However, to date, an explicit proof, that EphA/ ephrin-A signaling is sufficient to guide retinal growth cones along this axis is yet missing.

Still little is known about a-p independent, m-l mapping of RGCs originating from the retinal d-v axis.

Fiber-Fiber Interactions

Although a large body of experimental evidence can be explained by the abovementioned guidance mechanism, based on the interactions of growth cones with the tectal cues, several experiments are not consistent with rigid fiber-target (FT) mapping.

As a prominent example, an ingenious knock-in study by Brown and colleagues revealed the importance of interactions among fibers for mapping. In Islet2/ EphA3 mice, in which a random population of about 50% of all RGCs expresses a constant amount of EphA3 in addition to the native EphAs, they observed two segregated topographic maps, one formed by the knock-in and one by the wild-type fibers. Remarkably, the map of knock-in fibers (which is compressed to the anterior SC, due to the hyper-sensitivity of knock-in fibers towards ephrin-As on the target) pushes the wild-type fibers away from their normal targets to more posterior positions (Brown et al., 2000). Thus, interactions between

fibers can 'overwrite' the information on the target and shift fibers to positions they would normally avoid. Notably, fiber-fiber (FF) interactions do not just amount to non-specific competition, but are topographically selective and can correctly sort retinal fibers in the tectum (Gaze et al., 1963; Gaze and Sharma 1970; Yoon, 1971; Sharma, 1972; Schmidt et al., 1978). Therefore, topographic mapping must be assumed to be instructed by (at least) two autonomous mechanisms: FT and FF interactions. As fibers can self-sort themselves against the markers on the target (Yoon, 1972; Meyer, 1979), FF signals seem to be even stronger than FT signals.

In addition to FF interactions between two fibers (in *trans*), Ephs and ephrins can also interact on the same fiber (in *cis*; Hornberger et al., 1999; Yin et al., 2004; Marquardt et al., 2005; Carvalho et al., 2006). Whether *cis* interactions mask sensors and prevent them from *trans* signaling, or also produce a signal is still under debate and will be discussed later (cf. *Discussion*: '*How Sensor Trafficking Controls Sensitivity - Predictions of the Model*').

In sum, there are three different modes of signaling (FT, FF and *cis* FF), each in forward and reverse direction, amounting to six dimensions of signaling. We have recently discussed the relative importance of all interactions for topographic mapping in Weth et al., 2014.

Modeling Retinotopic Mapping

To evaluate, how FT and FF interactions might integrate into the guidance of retinal growth cones within the optic tectum, our group previously developed a comprehensive computational model (Gebhardt et al., 2012). In this model, we suggest growth cones to be guided by a

guidance potential, which is determined by calculating the ratio of all instantaneous ephrin-A/ EphA reverse and EphA/ ephrin-A forward signals, each comprising FT, FF and *cis* FF signals. A growth cone has reached its target, when this potential is minimized, i.e., when total forward and reverse signals are balanced.

The model, in addition to explaining topographic mapping, is able to reproduce a large body of experimental *in vitro* and *in vivo* evidence including single- and double-cue stripe assays, Islet2/EphA3 knock-in and regeneration experiments, as reviewed in Weth et al., 2014.

Eph/ Ephrin Signaling

The Eph receptor tyrosine kinases (RTKs) have been classified into EphA and EphB subfamilies, based on their affinities to bind GPI-anchored ephrin-A or transmembrane ephrin-B ligands[2]. To date, in the mouse nine EphA family members (EphA1-8 and 10) and five EphBs (EphB1-4 and 6) have been identified to promiscuously bind five ephrin-As (ephrin-A1-5) and three ephrin-Bs (ephrin-B1-3), respectively. Exceptions are EphA4, also binding to ephrin-Bs (Gale et al., 1996) and EphB2, which also binds to ephrin-A5 (Himanen et al., 2004).

Ephs consist of an extracellular part, comprising a ligand binding domain (LBD), a cysteine-rich domain (CRD) and two fibronectin type III repeats (FNIII), followed by a transmembrane domain and an intracellular part. The latter is build from a kinase domain, a sterile alpha motif (SAM) and a PDZ (PSD-95/ disc large/ zonula occludens-1) binding motif (Himanen et al., 2004; Pasquale, 2005).

---

[2]: Nomenclature according to the Eph Nomenclature Committee, 1997.

Upon ligand binding, Ephs have been shown to get activated by the autophosphorylation of a juxtamembrane Tyrosine (Tyr) residue, enabling Eph dimerization and the subsequent trans-phosphorylation of a second Tyr residue in this domain; a mechanism known to mediate the activation of most RTKs (Schlessinger, 2000). The smallest Eph/ ephrin signaling unit, thus, comprises of two Eph/ ephrin dimers, which have been found to assemble into a ring shaped hetero-tetramer, connecting each ephrin with two Ephs (Lackmann et al., 1997; Wimmer-Kleikamp et al., 2004; Day et al., 2005).

EphA activation typically results in a repulsive cellular response, mediated by the recruitment of specific intracellular effectors that initiate cytoskeletal rearrangements by regulating the balance between activation and inactivation of small GTPases. Effectors have been reported to involve proteins like Src, Abl or PI3 family kinases, the adaptors Nck or Crk and the guanosine nucleotide excahange factors (GEFs) Vav and ephexin (Lisabeth et al., 2014; Kania and Klein, 2016). Upon activation, most of these effectors interact with the GTPase activating proteins (GAPs) RhoA, Rac1 or α2-chimerin, linking EphA activity to the actin cytoskeleton and endocytosis, respectively, eventually controlling growth cone turning, retraction or collapse (Kania and Klein, 2016). Other effectors are involved also in proliferation, size and survival of cells (Lisabeth et al., 2014).

For ephrin-A reverse signaling, Src family kinases and the co-receptors p75NTR and TrkB have been identified as crucial effectors (Lisabeth et al., 2014), although the exact mechanisms of how they mediate repulsive responses are less well understood.

Structural studies on Eph crystals and Eph/ ephrin co-crystals, moreover revealed homophilic binding via different domains in the

Ephs' extracellular part and, together with functional studies, suggest that clustering of Ephs is crucial to signaling (Himanen, 2012).

Starting from a hetero-tetrameric seed, clusters are thought to expand laterally by the binding of additional, unligated Ephs via LBD-FNIII or LBD-CRD interactions, potentially allowing for a faster availability of unbound receptors to a site of signaling (Smith et al., 2004; Wimmer-Kleikamp et al., 2004; Xu et al., 2013). Additionally, LBD-LBD and CRD-CRD interactions have been proposed to contribute to EphA clustering (Himanen et al., 2010; Seiradake et al., 2010).

Notably, different Ephs seem to have distinct clustering properties. While EphA2 has been reported to form large, multimeric clusters, EphA4 was shown to induce much smaller, oligomeric clusters upon stimulation with ephrin-A5, potentially explaining the functional differences in EphA2 and EphA4 signaling, observed in HeLa cells (cell adhesion versus cell rounding; Seiradake et al., 2013).

More recent findings, however, challenge the model of high-order clusters being essential for signaling. In 2014, Schaupp and co-workers showed, that already small EphB2 clusters (trimers and tetramers) mediate strong cellular responses and suggest the relative number of active Eph/ ephrin multimers over inactive Eph dimers to determine the strength of signaling, rather than the absolute size of the cluster (Schaupp et al., 2014). Notably, Ephs have been reported to dimerize via their intracellular SAM domains even in the absence of ligands and, thereby, negatively regulate the formation of signaling clusters (Schaupp et al., 2014; Singh et al., 2015). Clustering might, thus, also be initiated by pre-formed Eph dimers, that assemble into bigger aggregates upon ligand binding, in contrast to the previously described seeding mechanism model.

Although the formation of clusters is not well understood and has been studied only for few Eph/ ephrin combinations, clustering seems to provide a means to diversify the response to the signals from a limited number of possible Eph/ ephrin pairs, possibly explaining the highly divergent roles of Eph/ ephrin signaling during development.

To terminate signaling, ligand activated EphAs and ephrin-As have been proposed to be internalized via endocytosis and targeted for degradation through ubiquitination (Goh and Sorkin, 2013), or be inactivated via phosphatases like PTP1B (Nievergall et al., 2010; Wimmer-Kleikamp et al., 2008). To convert the contact dependent interaction of EphAs and ephrin-As into a repulsive event, metalloproteases, like ADAM10, have been reported to detach EphA-bound ephrin-As either in *cis*, or in *trans* from the opposing membrane and, thus, enable the internalization of the receptor-ligand complex into the Eph expressing cell (Hattori et al., 2000; Janes et al., 2005; Atapattu et al., 2012). Others observe a so-called 'trans-endocytosis', that does not require the shedding of ephrins, but involves the uptake of Eph/ ephrin complexes together with parts of the other cell's membrane. Trans-endocytosis has been reported to occur in forward and reverse direction upon interaction of EphBs and ephrin-Bs, but is most likely limited to the forward direction in the EphA/ ephrin-A system, as there is no evidence for an ephrin-A reverse trans-endocytosis (Mann et al. 2003; Marston et al. 2003; Zimmer et al. 2003; Lauterbach and Klein 2006; Trinidad et al., 2010).

A fully consistent picture of Eph/ ephrin signaling has not emerged yet.

Growth Cone Adaptation Towards Guidance Cues

In addition to the abovementioned mechanisms modulating signaling, growth cones have also been shown to adapt towards guidance cues. Adaptation, i.e. the ability to re-adjust sensitivity according to the strength of a stimulus, has been suggested to occur towards attractive and repulsive signals, based on the following observations:

Growth cones of *Xenopus* spinal neurons lose their ability to turn towards an attractive gradient of soluble Netrin-1 or BDNF in a dose dependent manner upon bath application of the respective cue, just before the gradient was presented. Growth cones regain their sensitivity again and turn towards the source of the gradient, when the previous uniform application of the cue is prolonged to 120 minutes (Ming et al., 2002). Thus, growth cones rapidly desensitize towards basal levels of chemoattractants, but resensitize in presence of the cue over time.

Similarly, Piper and co-workers showed adaptation of retinal *Xenopus* axons towards repulsive Sema3A and Netrin-1 signals. In collapse assays, they showed that application of a low concentration of either cue, which itself does not induce a collapse, significantly reduces the response of growth cones towards a subsequently applied higher dose, that normally triggers a strong collapse response. Again, when the low concentration was applied for a longer period, growth cones resensitize and show a strong response to the high concentration, similar to growth cones that were not pre-treated (Piper et al., 2005).

In both studies, the authors could show that desensitization is dependent on endocytosis, whereas resensitization could be prevented by the application of drugs inhibiting protein synthesis (Ming et al., 2002; Piper et al., 2005). This adaptation, thus, seems to be achieved via the internalization of receptors, leading to a desensitization of growth

cones towards the respective guidance cues, and the subsequent local synthesis of new receptor proteins, which brings back sensitivity.

Notably, studies with chick retinal growth cones exposed to gradients of posterior tectal membranes or purified ephrin-A5, demonstrate that adaptation also occurs towards guidance cues involved in topographic mapping (Rosentreter et al., 1998; von Philipsborn et al., 2006b). Rosentreter and colleagues report temporal growth cones to reach higher absolute concentrations in a gradient of posterior tectal membranes (known to be enriched in ephrin-As) before they stop, when they were grown from a pedestal of posterior membranes, revealing their desensitized state. In gradients of purified ephrin-A5, von Philipsborn and co-workers showed that growth cones tolerate higher absolute concentrations when growing into steep, compared to shallow gradients, indicating a 'signaling history' dependent adjustment of sensitivity. The strongest evidence for adaptation towards ephrin-A5, however, comes from so called 'gap assays', showing that growth cones desensitize when growing on substrate-bound ephrin-A5, but resensitize when they leave an ephrin-A5 covered area and grow on laminin instead (cf. *Results*: '*I. GROWTH CONE ADAPTATION AND RETINOTOPIC MAPPING*'). It is unknown, whether desensitization towards ephrin-A5 depends on the endocytosis of receptors, however, in contrast to resensitization towards other guidance cues, resensitization towards ephrin-A5 is independent on local protein synthesis (von Philipsborn, 2007).

Adaptation is typically used in biological systems to keep a signaling system in its dynamic range upon changing ligand concentrations. In bacterial chemotaxis, for example, adaptation is used to continuously 'reset' the microorganisms' sensitivity towards signals from increasing ligand concentrations, enabling them to find the sink/ source of a

chemical gradient (reviewed in Micali and Endres, 2016). Adaptation in this system thereby eradicates the positional information of the gradient and leaves behind only the directional information. The same is true for the growth cones in the studies by Ming and Piper (Ming et al., 2002; Piper et al., 2005) mentioned earlier.

In this regard, however, adaptation towards guidance cues in a topographic system is highly counter intuitive, as the positional information of the gradient system is essential for mapping. Growth cones that desensitize towards EphAs or ephrin-As in the tectal gradients *in vivo*, should not be able to stop at their topographically correct target position and, thus, adaptation seems incompatible with topographic mapping.

Questions and Aims

To evaluate the role of adaptation in topographic axon guidance, the work presented here addresses the following questions:

I. Do retinal growth cones also adapt towards EphAs and, therefore, towards both sources of positional and directional information within the tectum for the mapping of the retinal n-t axis onto its a-p axis?

II. Is adaptation limited to fiber-target signals, or can retinal growth cones also adapt towards fiber-fiber signals?

III. What are the cellular mechanisms of adaptation? Is growth cone desensitization dependent on the endocytosis of receptors as observed in other systems?

IV. How can adaptation and topographic mapping be reconciled?

V. What is the function of adaptation?

The aim of this work was to combine theoretical modeling and *in vitro* experiments to better understand the concept of growth cone adaptation towards guidance cues and to search for its potential function in retinotopic mapping.

MATERIALS AND METHODS

MATERIALS AND METHODS

MATERIALS

Unless otherwise stated, chemicals were obtained from Sigma Aldrich (Merck KGaA, Darmstadt, Germany) and Carl Roth (Carl Roth GmbH & Co. KG, Karlsruhe, Germany).

H_2O was deionized in a TKA MicroLab Pure Water System (TKA, Niederelbert, Germany).

Protein stock solutions were prepared according to the corresponding product datasheet and stored at -20°C or -80°C.

Organisms

Chicken embryos (*Gallus gallus domesticus*) were bred to E6-E7 (Hamburger & Hamilton stage 29-30) from fertilized eggs (Geflügelzucht Hockenberger, Eppingen, Germany) in an automated breeder at 37°C, 60% air humidity. Until breeding, eggs were kept at 18°C up to 12 days.

Proteins and Enzymes

Name	Stock	Distributor
Accutase cell dissociation reagent	n.a.	Thermo Fisher Scientific, #A11105
Bovine Serum Albumin (BSA)	powder	Sigma Aldrich, #A3059
EphA3 Fc chimera, mouse	100μg/ml	R&D Systems, #640-A3

Ephrin-A5 Fc chimera, human	200μg/ml	R&D Systems, #374-EA,
Fc fragment, human IgG	1.7mg/ml	Merck, #401104,
Laminin, mouse natural	1mg/ml	Thermo Fisher Scientific, #23017-015,
Semaphorin3A Fc, mouse	100μg/ml	Thermo Fisher Scientific, #50631-M01H
Slit2, domain2	100μg/ml	Gift by Andrew McCarthy, EMBL, Grenoble, France

Antibodies and Fluorescent Labels

Name	Stock	Distributor
1,1'-Dioctadecyl-3,3,3',3'-tetramethylindocarbocyanine perchlorate (DiI)	powder	Thermo Fisher Scientific, #D-282
3,3'-Dioctadecyloxacarbo-cyanine perchlorate (DiO)	powder	Thermo Fisher Scientific, #D-275
Goat anti human IgG (H+L), Alexa Fluor488	2mg/ml	Thermo Fisher Scientific, #A11013
Goat anti human IgG (H+L), Alexa Fluor594	2mg/ml	Thermo Fisher Scientific, #A11014
Goat anti mouse IgG, Alexa Fluor647	2mg/ml	Thermo Fisher Scientific, #A-21236
Mouse anti fluorescein IgG	1mg/ml	Thermo Fisher Scientific, #A-6421
SNAP Cell fluorescein	1mM	New England Biolabs, #S9107S
SNAP Surface block	4mM	New England Biolabs, #S9143S

Phalloidin, Alexa Fluor488	200U/ml	Thermo Fisher Scientific, #A12379
Phalloidin, Alexa Fluor568	200U/ml	Thermo Fisher Scientific, #A12380

Media, Buffers and Solutions

H_2O was used as solvent, if not explicitly stated.

Name	Components	Concentration
Dimethylformamide (DMF)	pure	≥99.8%
Dimethylsulfoxide (DMSO)	pure	≥99,9%
F12	F12 nutrient mixture, Sigma Aldrich, #N6760	
	Fetal Bovine Serum (FBS), Merck, #S0615	10% (v/v)
	Chicken Serum (CS), Thermo Fisher Scientific, #16110	2% (v/v)
	$NaHCO_3$	1.176g/l
	L-Glutamine	146mg/l
	Penicillin/Streptomycin	10U/ml
F12-MC	F12	
	Methylcellulose	0.4% (w/v)
Fixative	Saccharose	113g/l
	Paraformaldehyde	4% (w/v)
	Glutaraldehyde	0.1% (w/v)
	in PBS, pH=7.4	

Hanks' Balanced Salt Solution (HBSS)	NaCl	8g/l
	KCl	0.4g/l
	NaH_2PO_4	60mg/l
	$Na_2HPO_4 \bullet 2H_2O$	60mg/l
	$NaHCO_3$	0.35g/l
	Glucose	1g/l
	HEPES	4.8g/l
	Phenol red	10mg/l
	pH=7.4	
Mowiol embedding medium	Mowiol 4-88	16,67% (w/v)
	Glycerol	33,33% (v/v)
	Thimerosal	0,1% (v/v)
	n-Propylgallate	small amount
	in PBS, pH=8.5	
Phosphate Buffered Saline (PBS)	NaCl	8g/l
	KCl	0.2g/l
	$Na_2HPO_4 \bullet 2H2O$	1.15g/l
	KH_2PO_4	0.2g/l
	pH=7.4	

Other Chemicals and Consumables

Name	Distributor	Details
(3-Glycidoxypropyl)-trimethoxysilane	abcr	n.a.
Coverslips Ø 18 mm	VWR	n.a.
Nitrocellulose membrane filters (ME 25/31 ST)	Whatman	soaked in HBSS
PDMS Elastosil RT625 A/B	Wacker Chemie	9:1 - 10:1 curing

Pitstop2	Abcam	50mM in DMSO
Poly-L-lysine (PLL)	Sigma-Aldrich	1mg/ml
Triton-X100	Sigma-Aldrich	n.a.

Hard- and Software

Name	Distributor	Details
CUY21SC electroporator	NepaGene	n.a.
CUY700P20 electrodes	NepaGene	n.a.
Glass bottom dishes	MatTek	n.a.
Plasma System 100-E	Tepla	0.5Torr (air), 300W
Tissue Chopper	McIlwaine	n.a.
Zeiss Axioimager Z1	Carl Zeiss	CCD camera & ApoTome-module
Zeiss AxioVert200M	Carl Zeiss	heatable chamber for time lapse
ImageJ	Wayne Rasband (NIH)	V1.5i
Matlab	Mathworks	V8.4
Zeiss Zen	Carl Zeiss	Blue version

METHODS

Explant Cultures

Retinae of E6-E7 (Hamburger Hamilton 29-30) chicken embryos were dissected in ice-cold Hanks' balanced salt solution (HBSS). In short, embryos were decapitated and an eye was taken from the head. After removing sclera, pigment epithelium, lens and vitreous body, the retina was spread with its inner side up on a nitrocellulose filter. The flat-mounted retina was then attached to the filter by vacuum suction and cut into 250-300μm wide strips, orthogonal to the naso-temporal axis, with a tissue chopper. Either nasal or temporal explant strips were placed with the retinal tissue down on substrates immediately after dissection, weighted with small metal blocks to prevent detachment from the substrate and grown in F12-MC medium at 37°C and 4% CO_2 routinely for 20-24 hours.

Cleaning and Activation of Coverslips

Coverslips were first sonicated in 50% H_2O/ 50% ethanol for 15min, degreased in 50% acetone/ 50% ethanol overnight, rinsed in ethanol and finally air dried and baked at 200°C. Cleaned coverslips were additionally plasmacleaned for 2min at 300W, 0.5Torr (air) and activated with 1% (3-glycidoxypropyl)-trimethoxysilane in absolute ethanol, pH=5.5 (adjusted with acetic acid) for 5min, when used for protein contact printing. After epoxysilanization, coverslips were washed twice in absolute ethanol, air dried and covered with 200μg/ml poly-L-lysine in PBS overnight. After washing in H_2O and air drying, PLL-coated coverslips were stored up to one week at 4°C.

Gap Assays

Gap patterns consist of homogeneously covered protein fields separated by protein-free areas of different width (65, 90, 115 and 215μm) and were produced by direct contact printing as described previously (von Philipsborn et al., 2006a).

Gap stamps were cast from molds produced by photolithography from SU-8 photoresist in the group of Dr. Bastian Rapp, IMT, KIT. PDMS was mixed in a ratio of 9:1 (Elastosil RT625A: Elastosil RT625B), degassed by centrifugation (4700rpm, 5min) and cured at RT over night.

Stamps were then covered with the appropriate protein solution for 2 hours at 37°C. For single-cue gap assays either 15μg/ml ephrin-A5-Fc or 15μg/ml EphA3-Fc in PBS was used. For double-cue gap assays, the stamp was incised 1-2mm deep inside the gap with a razor blade and a snippet of Parafilm was inserted vertically into the notch, physically separating both sides of the stamp. Each side was subsequently covered with a different protein solution (combinations of 15μg/ml ephrin-A5-Fc, 15μg/ml EphA3-Fc, 25μg/ml Semaphorin3A-Fc and 15μg/ml Slit2 domain2 in PBS). Neither protein was mixed with antibodies for visualization. After protein adsorption, the stamp was rinsed in H_2O, dried under a stream of nitrogen gas (in case of double-cue gap stamps, Parafilm was removed now) and then stamped onto an epoxysilanized and PLL-covered glass coverslip (15 min at 37°C). After lifting the stamp off, the substrate was covered with 20μg/ml laminin in HBSS (1 hour at 37°C), rinsed in H_2O, covered with F12 medium and kept at 37°C until imminent usage.

Quantification of gap assay results was performed using a custom-written MATLAB code to count fibers in and immediately behind the gap (for details see the *Supplement* section of this work: '*III. GUI and Code of the Fiber-Counting Tool*'). In short, grayscale images of phalloidin

stained axons were manually thresholded and two rectangular regions of interest (ROIs) were drawn in parallel to the edge of the gap (ROI 1 in the gap, ROI 2 immediately behind the gap; both ~20μm wide and over the complete lateral extension of the gap; cf. Figure S2). ROIs were then line-scanned and a histogram of each pixel row was evaluated counting signal peaks. Peaks broader than average axon widths were either divided into several counts, or excluded from evaluation when reaching the average size of a growth cone. Counts from all pixel rows in one ROI were averaged and the percentage of stopping fibers was calculated from mean counts in ROI 1 and ROI 2 (% $F_{stopping}$ = 100-[(F_{ROI2}*100)/F_{ROI1}]).

Collapse Assays

RGC explant cultures were grown for 20-24 hours on coverslips coated with 20μg/ml laminin in F12-MC. The medium was then carefully replaced with pre-warmed F12-MC containing 0.25 or 1μg/ml of ephrin-A5-Fc, 15μg/ml EphA3-Fc or an equimolar concentration of human IgG Fc fragment in control experiments. After incubation for 20 or 120min, explants were fixed and stained.

For inhibitor experiments, 30μM Pitstop2 in F12-MC was first applied solely 15min before addition of the guidance protein or control and thereafter in combination with ephrin-A5-Fc, EphA3-Fc or Fc fragment for 20 or 120min.

For quantification, two 10x images (phalloidin channel) from representative spots of each sample were taken with a conventional fluorescence microscope and collapsed/total growth cones were count manually in an analysis that was blinded to the experimental conditions.

Collision Experiments

Growth cone encounters between axons of two populations (either temporal and nasal, temporal and temporal, or nasal and nasal) in naive or adapted states were monitored using a Zeiss AxioVert200M time lapse microscope. For unambiguous assignment of growth cones to each population, the temporal and nasal halves of each retina were stained with DiI and DiO, respectively. To this end, DiI/DiO was dissolved in DMF (10mg/ml at 50°C) and then precipitated at a final concentration of 200µg/ml by dilution in HBSS. To obtain preferably small DiI/DiO crystals, the solution was forced through a syringe several times. Whole-mount retinae were cut into 250-300µm wide strips and treated with 100µl ice-cold Accutase solution for 5min at RT to digest basal lamina. The temporal and nasal halves of a retina attached to the nitrocellulose filter were then placed each into a 50ml centrifugation tube cut to ~30ml and filled up to ~25ml with PDMS and covered with 1ml of DiI or DiO-HBSS solution (Figure 3A). Dye crystals were deposited onto the retinal tissue by centrifugation at 2800rpm, 4°C for 6 minutes. Stained explants were placed on laminin-coated glass bottom dishes and grown for 20-24 hours. In collision experiments with adapted axons, one or both explants were put on contact printed fields of 15µg/ml ephrin-A5-Fc (contact printing as described for gap assays, but on untreated glass). For time lapse videos, cultures were placed into a heatable chamber on the microscope at 37°C, 5% CO_2 and imaged using phase contrast at 5min intervals. Fluorescent labels were recorded only in the first and the last frame of a video, to prevent phototoxic effects on the growth cones.

Expression Constructs and *ex vivo* Electroporation

For RGC transfection, whole-mount retinae were cut into 250-300µm wide strips and treated with 100µl ice-cold Accutase solution for 5min at RT to digest basal lamina. After stopping the enzymatic digest in F12 medium, retinae were rinsed in HBSS, sucked dry, placed with the retinal tissue facing up onto a plate electrode (∅=2cm), serving as anode and covered with 50µl of ice-cold 330ng/µl SNAP-ephrin-A5 plasmid in 0.5x PBS. The cathode was positioned approximately 1mm away from the cathode and a pulse protocol of five 50ms pulses (950ms off time), 15V each was applied. Immediately after electroporation the retina was transferred into ice-cold HBSS to minimize thermal damage and used for explant cultures.

The SNAP-ephrin-A5 plasmid (pSNAP-ephrin-A5-IRES-GFP) under the control of the CAG enhancer/promoter was produced in our lab as described in Weschenfelder, 2014.

Fixation, Staining and Image Acquisition

Explants were fixed with pre-warmed fixative for 15min at RT. Unless stated otherwise, antibodies and stains were diluted in 1% BSA in PBS. In most experiments, and if not declared, actin was stained with Alexa Fluor488 or Alexa Fluor568 coupled phalloidin (1:50 - 1:100) without permeabilization for 2 hours at RT.

Substrate-bound ephrin-A5-Fc, EphA3-Fc and Semaphorin3A-Fc were visualized with Alexa Fluor488 or Alexa Fluor594 coupled anti human goat IgG (1:200).

SNAP-ephrin-A5 staining was performed applying 1µg/ml SNAP Substrate in warm F12-MC for 40min at 37°C to the living explant

cultures followed by washing with warm F12 and a subsequent recovery phase in F12-MC for 15min at 37°C.

To evaluate SNAP-ephrin-A5 recycling, surface SNAP-ephrin-A5 was first blocked by treatment with 1μg/ml SNAP Surface Block in warm F12-MC for 40min followed by washing with warm F12-MC. Intracellular SNAP-ephrin-A5 was subsequently labeled with 1μg/ml SNAP Cell fluorescein in warm F12-MC again for 40min followed by washing with warm F12-MC. Explants were cultured for another 20-22 hours before anti fluorescein mouse IgG (1:200) in pre-warmed F12-MC was added to the living explants for 15min in order to label extracellularly exposed targets only. After washing out the antibody with warm F12-MC, explants were fixed, permeabilized and stained with anti mouse Alexa Fluor647 goat IgG (1:400, 1 hour) for recycled SNAP-ephrin-A5. The whole staining procedure is depicted in Figure 7A.

After staining, samples were mounted in embedding medium and images were acquired using a Zeiss Axioimager Z1 with ApoTome-module. For image acquisition and processing Zeiss ZenBlue software was used.

For quantification, mean SNAP signal intensities were measured in ImageJ within a hand drawn mask covering a growth cone (drawn in the actin channel) and normalized to the mean GFP signal in this area to eliminate differences in strength of expression.

Computational Modeling

All simulations were performed using MATLAB 8.4 (The MathWorks, Natrick, MA, USA). A previously published computational model of our group (Gebhardt et al., 2012) was updated to include adaptation without changing its basic performance. In short, the model builds on

the minimization of a guidance potential, D, which is calculated from total EphA forward (*FWD*) and ephrin-A reverse (*REV*) signals. Both signaling directions comprise fiber-target (FT) signals, fiber-fiber (FF) signals and cellular *cis* signals in total amounting to six signaling dimensions. All dimensions are calculated from mass action of EphAs (R) and ephrin-As (L) ($FWD = k_1 K R_F L$ and $REV = k_{-1} K L_F R$, with k_1, k_{-1} and K being proportionality and binding constants) and weighted equally (all constants being set to one), except *trans* FF signals, which increase in strength with iteration number to conceptually reflect the developmental increase in terminal number and size. With this, forward and reverse signals detected at position x'_T, y'_T and iteration i by fiber F with the sensors R_F and L_F from interactions with ligands on the target (L_T, R_T), on the same fiber (L_F, R_F) or on other fibers (L_f, R_f) integrate into D with:

$$D_{F,i}\left(x'_T, y'_T\right) = \left|\ln\left(\frac{\sum_{x_T,y_T} L_F(x_T,y_T)[R_T(x_T,y_T)+R_F(x_T,y_T)+c(i)\ R_f(x_T,y_T)]}{\sum_{x_T,y_T} R_F(x_T,y_T)[(L_T(x_T,y_T)+L_F(x_T,y_T)+c(i)\ L_f(x_T,y_T)]}\right)\right|$$

A growth cone has reached its target position when the impinging total *FWD* and *REV* signals are balanced (*REV*/*FWD*=1) and, therefore, the potential is minimized (abs(ln(1))=0). For more details see Gebhardt et al., 2012).

Adaptation is implemented in terms of de- and resensitizing forces regulating the levels of EphA and ephrin-A sensors ($S= R_F, L_F$) on a growth cone and thereby modulating the strength of incoming signals.

Depending on the recent history h of guidance potential D, adaptation coefficient a:

$$a(i) = \frac{\sum_{j=1}^{h} j\left(\frac{1}{1+\mu D(i-h+j)}\right)}{\sum_{j=1}^{h} j}$$

at iteration *i* deflects both sensors *S:*

$$S(i + 1) = \left(\frac{1}{a(i)}\right) S(i) + f(i)$$

with *f:*

$$f(i) = \lambda(S(0) - S(i))$$

being the resensitizing force driving sensor levels back to original values. λ and μ are constants.

If not explicitly stated, a unique set of parameters was used in all simulations: number of terminals n=100; target field 50x8; iterations i=10000; k_1=k$_{-1}$=K=1; forward drive q_x=0. FF interaction parameters: C_0=100, j=i/2, s=5; σ=0.12. Adaptation parameters: μ=0.006, λ=0.0045, h=10.

The full model code is shared in the *Supplement* section of this work ('*II. Model Code*').

RESULTS

I. GROWTH CONE ADAPTATION AND RETINOTOPIC MAPPING

Adaptive responses of growth cones, which do not map topographically, have been described to occur towards attractive as well as repulsive guidance cues (Ming et al., 2002; Piper et al., 2005). Albeit unexpected, evidence for adaptation of topographically mapping growth cones has mainly been gathered in our lab and includes the following observations: (i) RGC growth cones collapse upon treatment with soluble ephrin-A5, but show a complete recovery after 120 minutes despite the presence of fully active ephrin-A5 (Fritz, 2012). (ii) Axons initially grow out from a retinal explant in permanent presence of soluble ephrin-A5, applied at a concentration that triggers collapse of naïve growth cones (von Philipsborn et al., 2006b). (iii) Axons also grow out on substrate-bound ephrin-A5, which is strongly avoided when axons have the choice to grow on ephrin-free substrate (von Philipsborn, 2007). (iv) Growth cones on substrate-bound ephrin-A5 no longer collapse upon treatment with soluble ephrin-A5 (von Philipsborn et al., 2006b). (v) Growth cones growing in the presence of soluble ephrin-A5 no longer avoid substrate-bound ephrin-A5 (von Philipsborn, 2007).

The critical reader could argue at this position, that the growth cones might only react to changes in ephrin-A5 concentration, rather than to the absolute concentration, or be saturated (iv, v) and that the observed growth cone behaviors therefore must not compellingly be interpreted as adaptation. To exclude these possibilities, our lab developed an elegant *in vitro* assay, the 'gap assay'. In ephrin-A5 gap assays a patterned substrate containing two homogeneously covered fields of ephrin-A5-Fc divided by a gap of variable width is used. A retinal

explant is placed on one of the two fields. If axons, growing out on the first field of ephrin, in fact would adapt their forward signal transduction, they should easily overgrow the edge to the second ephrin field after a small gap, even though this means ignoring a sharp change in ephrin concentration (no ephrin-A5-Fc in the gap). To ensure the repulsive action of ephrin-A5-Fc in these assays, control experiments in which RGC axons grow from homogeneous laminin towards an identical field of ephrin-A5 are performed. In these controls, naïve temporal axons show a clear stop reaction in front of the ephrin field (Figure 2A, left). In contrast, however, axons growing from homogeneous ephrin-A5-Fc no longer stop in front of the second ephrin field in gap assays with small gaps (Figure 2A, middle), clearly revealing the desensitized state of their growth cones. Notably, the proportion of growth cones able to cross the gap declines with increasing gap sizes. While only 15.3% of temporal axons stop in assays with 50µm wide gaps, 43.0% stop after 75µm gaps, 59.2% after 100µm gaps and 81.0% after having crossed 200µm wide gaps (cf. Figure 2A, right and C; quantification of von Philipsborn's unpublished data[3]).

These findings suggest, that axons desensitize towards forward signals, when growing on the first ephrin-A5 field and regain their original sensitivity, when they grow on permissive laminin in the ephrin-free gap. Such an adjustment of sensitivity (desensitization and resensitization) according to the strength of a stimulus is generally defined as adaptation.

Whether RGC axons also adapt towards EphA, i.e. reverse signaling, however, has not been investigated in detail so far.

---

[3]: von Philipsborn used 8µg/ml ephrin-A5-Fc and micro-structured gap patterns were created by a lift-off technique (von Philipsborn et al., 2006a). In own experiments, patterns were produced by direct contact-printing of 15µg/ml ephrin-A5-Fc, offering slightly different gap sizes (65, 90, 115 and 215µm). Results from both experiments were quantified and did not show significant differences (data not shown).

Reverse Signal Adaptation in EphA3 Gap Assays

To check for a potential adaptation towards reverse signals, I performed EphA gap assays using 15µg/ml EphA3-Fc. In my previous work, I could successfully establish a method to transfer functionally active EphA3 protein onto epoxysilanized and poly-L-lysine-covered glass coverslips, which previously had not been possible using the standard printing protocol (Fiederling, 2012).

For EphA3 gap experiments, nasal explants were chosen, since those RGCs express the highest ephrin-A levels and should therefore be most sensitive towards reverse signals (Hornberger et al., 1999). In control experiments with naïve nasal axons, growth cones show a clear stop reaction at the edge to a field of contact-printed EphA3-Fc (92.6% stopping; Figure 2B, left and C), corroborating the repulsive action of EphA reverse signaling. Notably, and as observed in ephrin-A gap assays, growth cones no longer stop in front of an identical field after a small gap, when grown on EphA3 from the beginning (65µm: 25.0% stopping; Figure 2B, middle and C), indicating a loss of sensitivity towards reverse signals. Again, they gradually regain sensitivity with increasing gap sizes (90µm: 39.9% stopping; 115µm: 60.1% stopping; 215µm: 75.8% stopping; Figure 2B, right and C) displaying a similar gap-size dependence as ephrin-A5 resensitization. Temporal growth cones on these EphA3 gap patterns show the same trend of de- and resensitization (data not shown). Negative controls with naïve axons growing towards a field printed with 8µg/ml human Fc fragment, which show very little axon reactivity to the boundary, demonstrate the specificity of the ephrin-A5-Fc and EphA3-Fc responses (naïve: 28.8% stopping; von Philipsborn, 2007; Figure 2C).

Together, these results show for the first time, that RGC growth cones strongly adapt not only their forward but also reverse signaling *in vitro*, when exposed to substrate-bound ephrin-A5 or EphA3, respectively.

A

naïve eA5   65 μm gap   215 μm gap

axons   eA5   axons   eA5   axons   eA5

B

naïve EA3   65 μm gap   215 μm gap

axons   EA3   axons   EA3   axons   EA3

C

% of axons stopping

***
***
***
***

100
80
60
40
20
0

N=4 (8)   N=9 (14)   N=3 (7)   N=3 (11)   N=4 (15)   N=4 (13)   N=3 (4)   N=3 (4)   N=7 (16)   N=7 (21)   N=5 (11)

***   ***   ***   **   ***   ***   ***   *

naïve | naïve | 50 μm | 75 μm | 100 μm | 200 μm | naïve | 65 μm | 90 μm | 115 μm | 215 μm

Fc   **ephrin-A5**   **EphA3**
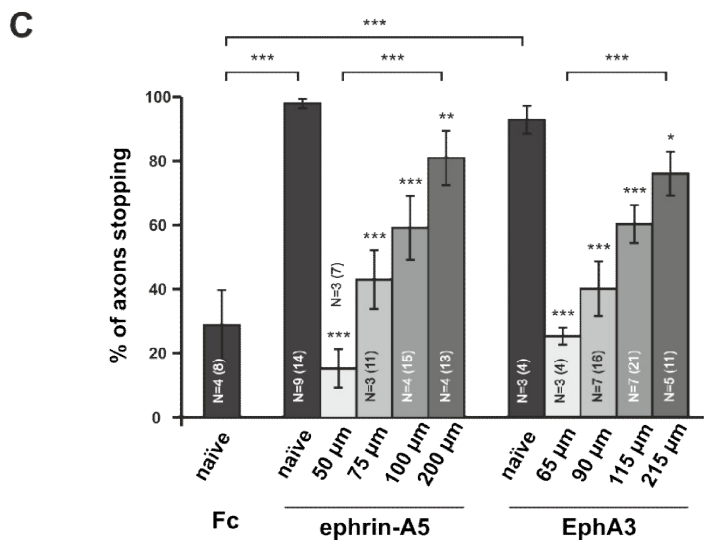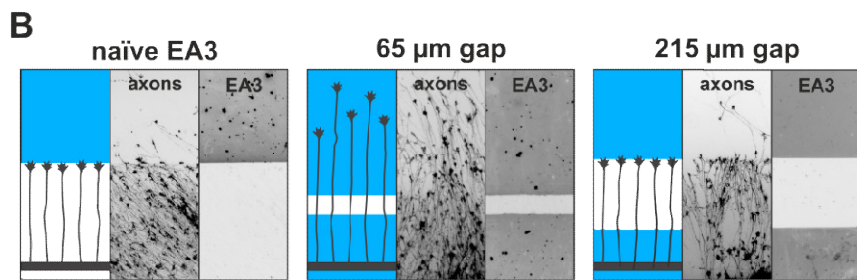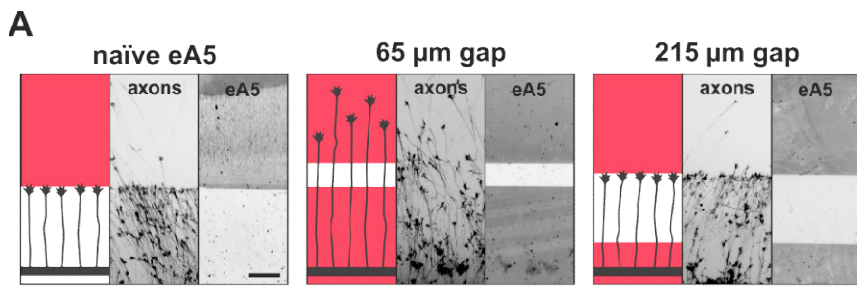
Figure 2: Adaptation of retinal growth cones towards ephrin-A5 and EphA3 in single-cue gap assays.

Subfigures in A and B each display a cartoon illustrating the experimental setup (left) consisting of explant (black stripe), axons and printed guidance protein (colored field(s)), the inverted signal of fluorescent phalloidin stained axonal actin (middle; explant not shown) and the underlying, antibody-labeled substrate (right) in a detailed view of a representative microscopic image (scale: 100µm). All explants are from chicken E7 retinae; gap patterns were printed using 15µg/ml Fc-fusion proteins.

A: Ephrin-A5 gap assays. Naïve temporal axons stop in front of a homogeneous field of ephrin-A5-Fc (eA5, red), but do not react to an identical boundary when initially grown on homogeneous ephrin-A5 after a 65µm wide gap. After having crossed a 215µm wide gap, axons show a stop reaction again.

B: EphA3 gap assays. Nasal RGC axons show a similar behavior on EphA3-Fc (EA3, blue) gap substrates as described for ephrin-A5 gap assays.

C: Quantification of gap assays. Stop reactions were quantified as the percentage ratio between the average number of fibers directly in front and directly behind the edge to a protein field, counted with a custom-written image analysis tool (see *Material and Methods* for details). Fc: naïve: 28.8% stopping. eA5: naïve: 98.0%, 50µm: 15.3%, 75µm: 43.0%, 100µm: 59.2%, 200µm: 81.0% stopping (quantification of von Philipsborn's experiments). EA3: naïve: 92.6% stopping, 65µm: 25.0%, 90µm: 39.9%, 115µm: 60.1%, 215µm: 75.8% stopping. N: independent experimental days; n: analyzed culture dishes. Error bars represent standard errors. T-test with *: $\alpha<0.05$, **: $\alpha<0.01$, ***: $\alpha<0.001$.

Adaptation of Fiber-Fiber *trans* Signaling

Fiber-target (FT) adaptation is potentially incompatible with mapping that critically relies on precise quantitative signaling from the tectal gradients. According to our previous work, however, mapping is anyhow mainly instructed by fiber-fiber (FF) interactions (Gebhardt et al., 2012; Weth et al., 2014). Is topography possibly rescued because adaptation only modulates FT, but not FF interactions? To tackle this question, I monitored events of encounter between two axons of both

temporal, both nasal, or mixed retinal origin in naïve and adapted states via time lapse microscopy.

RGC growth cones have been demonstrated to be sensitive towards guidance cues presented on the surface of other fibers (Raper and Grunewald, 1990). We have previously shown, that these interactions are in fact due to EphA/ ephrin-A interactions in RGCs (Lutz, 2011).

To enable unambiguous identification of temporal and nasal axons in a densely growing culture, temporal and nasal explants were differentially labeled by centrifugation of DiI or DiO crystals into the retinal tissue (Figure 3A, see *Materials and Methods* for details). With this method, about 30% of all axons showed a strong fluorescent signal after staining.

In accordance with previous studies (Raper and Grunewald, 1990; Lutz, 2011), naïve temporal growth cones (which express high EphA levels) collapse and retract or collapse and stop, when encountering naïve nasal axons (expressing high levels of ephrinAs), whereas nasal growth cones do not react upon contact with temporal axons, for reasons that are not understood (Figure 3B). Growth cones of matching origin (both naïve or adapted) completely ignore each other. Notably, however, ephrin-A5-Fc adapted temporal growth cones are no longer repelled from naïve nasal axons (Figure 3B), indicating a loss of sensitivity towards axonal ephrin-As, presented on the nasal axons' surface.
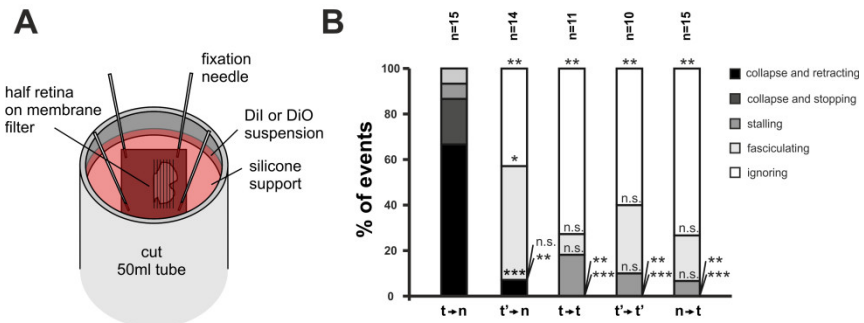
Figure 3: Adaptation of fiber-fiber *trans* signals.

A: DiI/ DiO staining of flat-mounted retinae. Nasal or temporal halves of a flat-mounted retina were placed into a custom-build centrifugation tray made of a cut tube filled with PDMS silicone and then covered with HBSS containing DiI or DiO crystals. Dye crystals were subsequently sedimented onto the tissue by gentle centrifugation.

B: Quantification of growth cone encounters. Growth cones' reactions upon contact with axons from the other explant were grouped into five categories: collapse and retracting, collapse and stopping, stalling, fasciculating and ignoring. Naïve temporal (t) growth cones encountering naïve nasal (n) axons show a strong repulsive response (t-n: 66.7% collapse and retracting, 20% collapse and stopping, 6.7% stalling, 6.7% fasciculating, 0% ignoring). When adapted on ephrin-A5-Fc, however, temporal (t') growth cones are no longer repelled from naïve nasal axons (t'-n: 7.1% collapse and retracting, 0% collapse and stopping, 0% stalling, 50% fasciculating, 42.9% ignoring). Both, temporal - temporal and adapted temporal - adapted temporal encounters were predominantly classified as ignoring (t-t: 72.7% and t'-t': 60%). Naïve nasal growth cones do not react upon contact with naïve temporal axons (n-t: 73.3% ignoring), as previously observed by others. n: number of observed encounters; X^2-test with n.s.: $\alpha \geq 0.05$; *: $\alpha < 0.05$, **: $\alpha < 0.01$, ***: $\alpha < 0.001$.

Adaptation, therefore, has to be considered to desensitize not only FT, but also FF interactions.

Mathematical Modeling of Growth Cone Adaptation and Mapping

Observing growth cone adaptation to change sensor activities of forward and reverse FT and FF signaling *in vitro*, directly prompts the question of how adapted growth cones can still find their topographically correct target positions during map formation *in vivo*, in a system that critically relies on precise quantitative signaling.

To conceptually address this problem, I updated a previously published computational model of our group (Gebhardt et al., 2012) to include adaptation (Figure 4A; see *Materials and Methods* for details). In its

original form this model, in addition to reproducing crucial *in vivo* evidence from regeneration and genetic experiments, explains both, topographically differential behavior of axons *in vitro* (as observed in ephrin-A and EphA single-cue stripe assays) as well as topographically appropriate binary decisions *in vitro* (as shown with ephrin-A/ EphA double-cue stripe assays; Gebhardt et al., 2012; Weth et al., 2014). The basic model builds on the minimization of a guidance potential, *D*, which is calculated from total forward (fwd: FT, FF, *cis*) and reverse (rev: FT, FF, *cis*) signals:

$$D = \left| \ln\left(\frac{\text{rev}}{\text{fwd}}\right) \right|$$

$$= \left| \ln\left(\frac{FT_{rev} + cisFF_{rev} + c * FF_{rev}}{FT_{fwd} + cisFF_{fwd} + c * FF_{fwd}}\right) \right|$$

with *c* scaling the influence of FF interactions. Every interaction is calculated from mass action, e.g.:

$$FT_{rev} = L_F * R_T$$

A growth cone has reached its target position when this potential is minimized, i.e. when impinging total forward and reverse signals are balanced (Figure 4A and B, dark gray squares; Gebhardt et al., 2012).

The updated model now additionally involves a de- and a resensitizing force, modulating forward and reverse signals of a growth cone depending on the recent history of the guidance potential. Critically, to retain topography, adaptation might scale the potential, but must not change its fundamental topology. This can be achieved only, when forward and reverse signaling are modified concordantly. Intuitively, we first assumed that desensitization might correspond to a reduction of both, forward and reverse signaling. Therefore, a factorial modifier, *a*,

which depends on the potential with strong influence distant from the target (high potential) and approximating 1 close to the target (low potential) was used:

$$a(i) = \frac{\sum_{j=1}^{h} j\left(\frac{1}{1+\mu D(i-h+j)}\right)}{\sum_{j=1}^{h} j}$$

Depending on the recent history h of guidance potential D, adaptation coefficient a at iteration i deflects both sensors S ($S = R_F, L_F$). A resensitization force, f, was set to counteract a and to bring sensor levels back to original values, when $D=0$.

$$f(i) = \lambda(S(0) - S(i))$$

The absolute terms λ and μ regulate the speed of adaptation. Upon application it turned out that this implementation is not potential preserving. Applying the inverse adaptation factor, however, does. With this, we arrive at:

$$S(i + 1) = \left(\frac{1}{a(i)}\right) S(i) + f(i)$$

This means, in the model, desensitization of growth cones is achieved by up regulating the growth cones' Eph and ephrin sensor activities. Adaptation thereby modulates the balance between FT and FF *cis* interactions, as *cis* interactions increase with the square of a, while FT interactions only with a. The more the FF *cis* signals outbalance FT signals, the less sensitive is a growth cone.

A
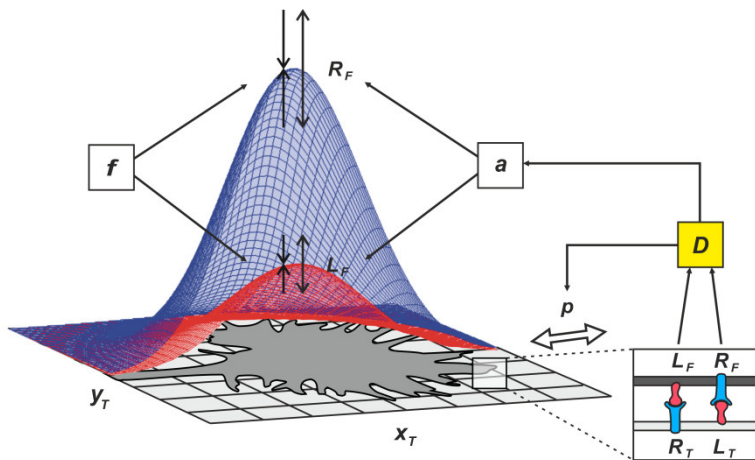
B
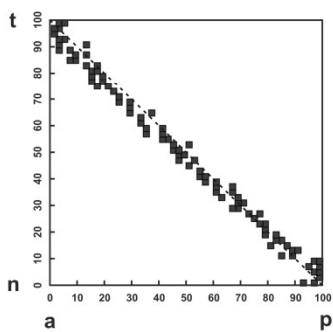
C
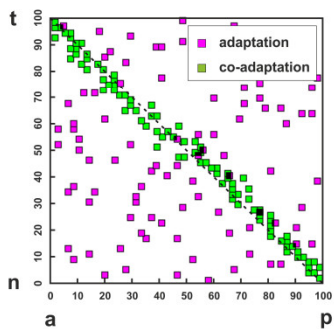
D
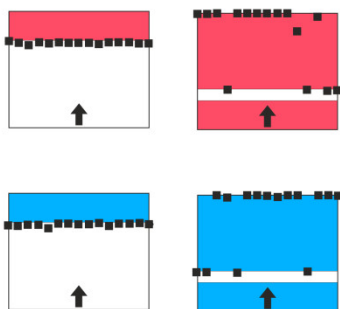
E
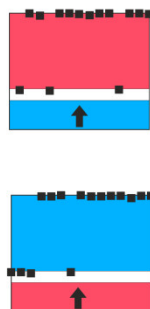
Figure 4: Modeling growth cone adaptation and mapping.

A: Computational model of adaptation and topographic mapping. Fiber terminals are modeled as circular discs bearing Gaussian-shaped distributions of EphAs (R_F, blue) and ephrin-As (L_F, red), according to their retinal origin, moving on a target field x_T, y_T. Fiber-target and fiber-fiber (*cis* and *trans*) interactions and resulting forward and reverse signals integrate into a guidance potential, *D*, which determines the probability *p* to change position (only FT interactions are illustrated in the inset). Additionally, *D* is used to calculate adaptation coefficient, *a*, which in turn proportionally deflects sensor levels R_F and L_F. A resetting force, *f*, counteracts *a*.

B: Mapping without adaptation. Mapping of n=100 fiber terminals using the model without adaptation. The antero-posterior (a-p) position of a terminal is plotted as a function of naso-temporal (n-t) origin in this graphs (perfect topography is indicated by all terminals targeting the main diagonal). Non-adapting terminals (dark gray squares) find their topographically correct target positions with little scatter. Model parameters: Number of terminals *n*=100; target field 50x8; iterations *i*=10000; k_1=k_{-1}=K=1; forward drive q_x=0; FF interaction parameters: C_0=100, *j*=*i*/2, *s*=5; σ=0.12.

C: Adaptation and Mapping. Mapping of n=100 fiber terminals using different implementations of adaptation. Terminals enabled to regulate sensors independent from each other are widely scattered across the target field (magenta squares), indicating a loss of topography, whereas co-adapted terminals (regulating sensors in proportion) find their topographically correct target positions (green squares), as seen with non-adapting terminals (cf. B). Adaptation parameters: μ=0.006, λ=0.0045, *h*=10; τ=1000.

D: Simulation of gap assays. Naïve terminals stop in front of a field of high ephrin-A or EphA (L_T=4, red; R_T=4, blue), respectively, but ignore it in simulated gap assays with small gap size (gap size=20). In simulations with wider gaps (gap size=100), terminals stop again in front of the second field. *n*=15; *i*=2000; target field: 200x8; C_0=1; q_x=0.3.

E: Simulation of double-cue gap assays. Modeling predicts co-adaptation with EphA adapted terminals ignoring a field of high ephrin-A after a small gap and *vice versa*. Gap size=20; *n*=15; *i*=2000; target field: 200x8; C_0=1; q_x=0.3.

Including such a form of adaptation, which is termed 'co-adaptation' in this work, the model faithfully reproduces the experimental results of ephrin-A and EphA gap assays (Figure 4D) and is still able to form an accurate topographic map (Figure 4C, green squares).

In contrast, allowing the system to adjust the strength of incoming signals independent from each other (as typically expected in an adapting system) with:

$$a_R(i) = \ln((1/R_F(0)) * L_T) \quad \text{and} \quad a_L(i) = \ln((1/L_F(0)) * R_T)$$

independently driving sensor activities R_F and L_F to minimize the signal from the current position x_T, y_T:

$$R_F(i+1) = (R_F(i) - R_T(x_T, y_T)) * e^{(-|\tau * a_R(i)^2|)} + R_T(x_T, y_T)$$

$$L_F(i+1) = \left(L_F(i) - L_T(x_T, y_T)\right) * e^{(-|\tau * a_L(i)^2|)} + L_T(x_T, y_T)$$

with τ regulating the speed of adaptation, inevitably destroys the guidance potential and, thus, map formation (Figure 4C, magenta squares).

Modeling therefore suggests a relative up regulation of *cis* FF signals over FT signals during growth cone desensitization and a co-regulated form of adaptation being needed to reconcile adaptation and mapping. Ultimately, this predicts a novel cellular mechanism enabling growth cones to adjust their EphA activity not only upon forward signaling, but also when exposed to reverse signals and *vice versa* for ephrin-A activity. If true, axons adapted on an ephrin-A substrate should ignore a field of EphA in a 'double-cue' gap assay with small gap size. Similarly, EphA adapted axons should ignore a field of ephrin-A, as predicted by the model (simulations in Figure 4E).

Co-Adaptation in Ephrin-A5/ EphA3 Double-Cue Gap Assays

To test the model's prediction of the existence of co-adaptation, I developed an *in vitro* double-cue gap assay with substrates comprising two different cues on the fields to either side of the gap (see *Materials and Methods*). With these substrates, it was possible to evaluate the sensitivity of forward signal adapted growth cones towards reverse signals and *vice versa*. In ephrin-A5/ EphA3 double-cue gap assays, for example, temporal axons were grown on 15µg/ml ephrin-A5-Fc and confronted with 15µg/ml EphA3-Fc on the other side of the gap. Remarkably, ephrin-A5 adapted growth cones clearly ignore the EphA3 field after a small gap (<100µm, 26.9% stopping), in front of which they naïvely stop (naïve: 93.4% stopping; Figure 5A left and B). Since these growth cones have not experienced substrate-bound EphAs before they meet the EphA3-Fc field behind the gap, their insensitivity towards reverse signals can only be explained through a co-regulation of ephrin-As and EphAs, while they adapt their forward signal on the ephrin-A5 field. Similar to the observations in ephrin-A5/ EphA3 double-cue gap assays, RGC growth cones co-adapt their forward signal, when growing on an EphA3 field in EphA3/ ephrin-A5 double-cue gap assays (Figure 5A middle and B). Nasal EphA3 adapted growth cones show a significantly reduced stop reaction (40.3% stopping) as compared to naïve growth cones (91.6% stopping), when confronted to ephrin-A5 after a small gap (<100µm). Consistent with the findings in ephrin-A5 or EphA3 single-cue gap assays, the strength of co-adaptation abates on neutral substrates with increased gap width (eA5-EA3, >100µm: 76.3% stopping; EA3-eA5, >100µm: 77.1% stopping).
Moreover, co-adaptation seems to be ephrin/ Eph specific, as seen by the fact that, for example, ephrin-A5 adapted temporal growth cones are still sensitive towards other repulsive guidance molecules like Sema3A

A

naïve EA3 | axons | EA3

naïve eA5 | axons | eA5

naïve S3A | axons | S3A

eA5 - EA3 | axons | EA3 | eA5

EA3 - eA5 | axons | eA5 | EA3

eA5 - S3A | axons | S3A | eA5
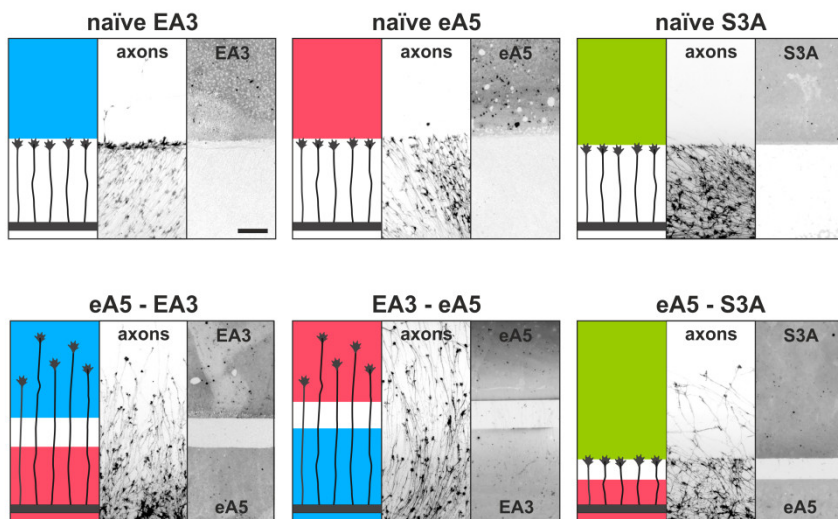
B
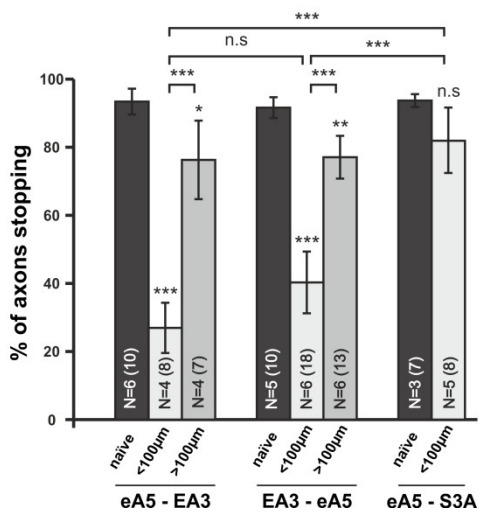
Figure 5: Co-adaptation of retinal growth cones in double-cue gap assays.

Subfigures in A each display a cartoon illustrating the experimental setup (left), the inverted signal of fluorescent phalloidin stained axonal actin (middle) and the underlying, antibody-labeled substrate (right) in a detailed view of a representative microscopic image (scale: 100μm).

A: Double-cue gap assays. Top row: naïve axons stop in front of a homogeneous field of EphA3-Fc (EA3, blue; nasal axons), ephrin-A5-Fc (eA5, red; temporal axons), or Sema3A-Fc (S3A, green; temporal axons). Bottom row: nasal, eA5 adapted growth cones ignore a field of EA3 after a small gap and, *vice versa*, temporal, EA3 adapted growth cones ignore eA5. In contrast, temporal, eA5 adapted growth cones are still strongly repelled by a field of S3A after a small gap. Substrates were labeled with anti Fc antibody; discrimination of proteins was achieved by transferring pencil marks on the stamp to the coverslip.

C: Quantification of double-cue gap assays. Combined data of assays with 65 and 90μm wide gaps in '<100μm' bars; 115 and 215μm in '>100μm' bars.

eA5-EA3: naïve: 93.4% stopping, <100μm: 26.9% stopping, >100μm: 76.3% stopping.

EA3-eA5: naïve: 91.6% stopping, <100μm: 40.3% stopping, >100μm: 77.1% stopping.

eA5-S3A: naïve: 93.7% stopping, <100μm: 81.9% stopping.

N: independent experimental days; n: analyzed culture dishes. Error bars represent standard errors. T-test with n.s.: $\alpha \geq 0.05$, *: $\alpha < 0.05$, **: $\alpha < 0.01$, ***: $\alpha < 0.001$.

(Figure 5A right and B; naïve: 93.7% stopping, eA5-S3A <100μm: 81.9% stopping) or Slit2 (data not shown).

Together, these findings perfectly support the prediction of the computational model and substantiate the existence of a so far undescribed cellular mechanism: co-adaptation.

II. THE CELLULAR MECHANISMS OF ADAPTATION

The modulation of the relative strength of *trans* FT and *cis* FF forward and reverse signaling during adaptation, as predicted by our model, could be achieved in various ways within the growth cone. Searching for the molecular implementation of adaptation, we first thought about a cellular re-localization of sensors during adaptation. In a parallel study, Markus Weschenfelder therefore tried to follow the dynamics of ephrin-As and EphAs on the growth cones' surface during adaptation (Weschenfelder, 2014). Since available antibodies for EphAs and ephrin-As lack specificity, he produced a SNAP-tagged ephrin-A5 expression construct (pSNAP-eA5-IRES-GFP). RGCs were transfected with this construct via electroporation of whole-mount E7 retinae (Weschenfelder, 2014). The SNAP tag is a self-labeling enzyme, which provides covalent coupling of fluorescent dyes to the SNAP tag that ensures stable labeling and, due to the small size of the labeled tag, the label does not impede protein function (Keppler et al., 2003; Gautier et al., 2008; Jing and Cornish, 2011).

A big advantage of the SNAP system comes with the use of cell permeant and non-permeant SNAP substrates, allowing to specifically target the total or the surface-bound population of SNAP-tagged proteins of a cell, respectively. Thus, the system allows to follow the dynamics of membrane proteins localization easily.

In experiments with SNAP-ephrin-A5 expressing RGCs, Weschenfelder could show that SNAP-ephrin-A5 surface levels are dramatically reduced on growth cones growing on EphA3-Fc substrates, i.e. when adapting towards reverse signals, compared to naïve growth cones growing on control Fc substrates. Notably, SNAP-ephrin-A5 surface levels were also reduced on growth cones growing on ephrin-A5-Fc

substrates, indicating a concurrent regulation of reverse and forward signaling (Weschenfelder, 2014).

In this work, I focused on identifying the mechanisms underlying ephrin-A and EphA sensor uptake into the cell and how they can be potentially brought back to the surface upon resensitization.

Inhibition of Endocytosis During Growth Cone Desensitization

To identify the mechanism by which ephrin-A (and potentially EphA) sensors are internalized into the cell during growth cone adaptation, I treated growth cones with a pharmacological inhibitor, Pitstop2, that specifically blocks clathrin-mediated endocytosis (CME; von Kleist et al., 2011). CME is ubiquitously used for the internalization of numerous ligand-activated receptors and has been previously shown to be involved in the endocytosis of EphAs (Yoo et al., 2010; Boissier et al., 2013). Previous attempts to impede growth cone adaptation by the pharmacological inhibition of dynamin dependent endocytosis with the inhibitor Dynasore, however, were unsuccessful (Fritz, 2012).

In first tests, temporal explants, either placed on a contact-printed field of 15µg/ml ephrin-A5-Fc or in front of it on 20µg/ml laminin, were exposed to 30µM Pitstop2 and the number of outgrowing, i.e. desensitized axons was counted. While naïve growth cones encountering the ephrin-A5 field do show an unaltered stop reaction in presence of Pitstop2 (Figure 6A, left), the number of axons growing out from an explant placed on the field tends to be reduced in Pitstop2, but not in control (DMSO) treated cultures (Figure 6A, middle). This might indicate an effect of Pitstop2 on the desensitization of growth cones. However, application of Pitstop2 to naïve axons (grown on laminin) also results in a reduction of outgrowth compared to the control group

(Figure 6A, right). Similar results were found using 30μM Dyngo4a, a blocker of all dynamin dependent endocytotic pathways with much higher potency than Dynasore (McCluskey et al., 2013; data not shown). Those findings clearly demonstrate a negative effect of the inhibitors Pitstop2 and Dyngo4a on the general growth and elongation of axons, potentially masking effects on growth cone desensitization. Therefore, these preliminary experiments were stopped. To evaluate the role of endocytosis on adaptation necessitated another read-out for adaptation, which is not based on the outgrowth behavior of axons.

To this end, I performed collapse assays, typically used as a standard approach to evaluate the repulsive action of a potential guidance cue (Cox et al., 1990; Raper and Kapfhammer, 1990). Repulsive activity can be easily measured in these experiments by evaluating the percentage of collapsed growth cones. In case of an ephrin-A5 collapse assay, typically 80-90% of growth cones show a collapsed morphology after 20 minutes of incubation with ephrin-A5-Fc (Drescher et al., 1995; Wahl et al., 2000). Adaptation can be seen in these assays by the fact that, after prolonged incubation with 0.25μg/ml ephrin-A5-Fc (a concentration that triggers collapse in temporal but not nasal axons and is therefore assumed to be in a physiological range), temporal growth cones recover their morphology again (Fritz, 2012).

In accordance with this, also in presence of 30μM Pitstop2 application of 0.25μg/ml ephrin-A5-Fc results in a strong collapse of temporal growth cones after 20 minutes (eA5+DMSO: 85.4% collapsed; eA5+P: 83.1% collapsed), while 0.25μg/ml of human Fc fragment together with Pitstop2 does not trigger a collapse (Fc+P: 7.5% collapsed; Figure 6B). Pitstop2, therefore, clearly has no effect on the primary response of growth cones towards ephrin-A5. As a result of adaptation, ephrin-A5-Fc treated growth cones recover their morphology after 120 minutes (eA5+DMSO: 15.8% collapsed). However, recovery is completely abolished when growth cones are incubated with ephrin-A5-Fc together
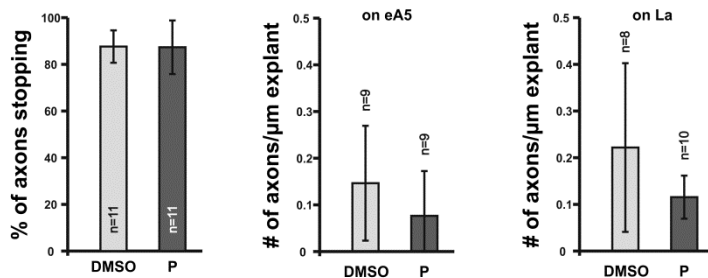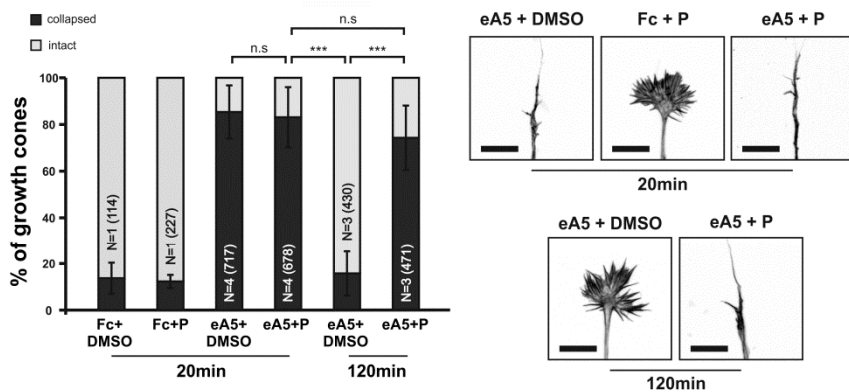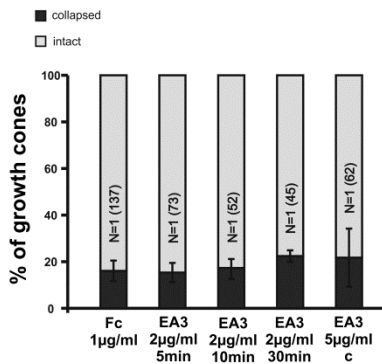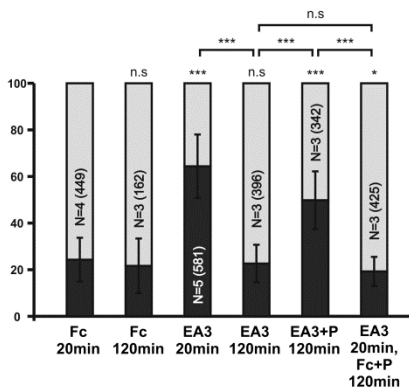
Figure 6: Inhibition of endocytosis during retinal growth cone desensitization.

A: Effects of Pitstop2 on adaptation towards substrate-bound ephrin-A5. Left: Naïve growth cones stop in front of a field of contact-printed ephrin-A5-Fc (eA5; 15μg/ml) in presence of 30μM Pitstop2 (P; 87.3% stopping) or control DMSO (87.6% stopping). Middle: The number of outgrowing axons from explants placed on eA5 is reduced in presence of 30μM P (0.08 axons/μm explant), compared to control situations (0.15 axons/μm explant). Right: However, P also impedes outgrowth of naïve axons growing on laminin (La; 0.12 axons/μm explant; control: 0.22 axons/μm explant). Combined data from nasal and temporal cultures. N=1 (independent experimental days); n: number of evaluated explants; error bars represent standard errors.

B: Effects of Pitstop2 on adaptation towards soluble ephrin-A5. Pitstop2 prevents temporal growth cones from desensitizing towards 0.25μg/ml ephrin-A5-Fc (eA5+DMSO 120min: 15.8% collapsed; eA5+P 120min: 74.3% collapsed). The initial response of growth cones towards eA5 is unaltered in presence of P (eA5+DMSO 20min: 85.4% collapsed; eA5+P: 83.1% collapsed). Neither P itself, nor does its carrier DMSO induce a collapse (Fc+DMSO 20min: 13.6% collapsed; Fc+P 20min: 7.5% collapsed). N: independent experimental days; number of analyzed growth cones in brackets. Error bars represent standard errors. T-test with n.s.: $\alpha \geq 0.05$, ***: $\alpha < 0.001$. Representative images of phalloidin stained growth cones on the right (scale bar: 10μm).

C: EphA3 collapse assays. Moderate concentrations of EphA3-Fc (EA3) do not trigger a collapse on nasal or temporal growth cones (1μg/ml Fc 20min: 16.1% collapsed; 2μg/ml EA3 5min: 15.3% collapsed; 10min: 17.3% collapsed; 30min: 22.4% collapsed; 5μg/ml antibody-clustered (c) EA3 20min: 21.7% collapsed). Combined data from nasal and temporal growth cones. N: independent experimental days; number of analyzed growth cones in brackets. Error bars represent standard errors.

D: Effects of Pitstop2 on adaptation towards soluble EphA3. Very high concentrations of soluble EphA3-Fc (EA3; 15μg/ml) trigger a collapse on nasal or temporal growth cones (EA3 20min: 64.4% collapsed; Fc (4.2μg/ml) 20min: 24.3% collapsed). Growth cones desensitize towards EA3 within 120 minutes (EA3 120min: 22.6% collapsed), but not in presence of 30μM Pitstop2 (EA3+P 120min: 49.8% collapsed). P does not impede growth cones from recovering their morphology in general (EA3 20min, then Fc+P 120min: 19.3% collapsed). Combined data from nasal and temporal growth cones. N: independent experimental days; number of analyzed growth cones in brackets. Error bars represent standard errors. T-test with n.s.: $\alpha \geq 0.05$, *: $\alpha < 0.05$, ***: $\alpha < 0.001$.

with Pitstop2 for 120 minutes (eA5+P: 74.3% collapsed; Figure 6B), indicating CME being required for growth cone desensitization.

To test, whether CME is also required for growth cone desensitization towards reverse signals, I first had to establish a reverse signaling collapse assay. Remarkably, application of even 2µg/ml soluble EphA3-Fc for 30 minutes does not trigger a collapse on nasal or temporal growth cones (22.4% collapsed; Figure 6C). As previous studies on EphB collapse assays reported a strong effect of EphB2 already after 5 minutes and most prominent at 10 minutes (Mann et al., 2003), I also checked for shorter incubation times in EphA3 collapse assays. However, growth cones show intact morphologies 5 or 10 minutes after application of 2µg/ml soluble EphA3-Fc (15.3% and 17.3% collapsed; Figure 6C).

In vivo, EphAs are thought to dimerize upon binding with ephrin-As and then form larger clusters that enhance signaling (Janes et al., 2012; Nikolov and Himanen, 2013). Potentially, ephrin-A reverse signaling also requires clustered EphAs in order to be most effective[4]. I, therefore, mixed 5µg/ml EphA3-Fc with anti human goat IgG in a molar ratio of 1:2 (1h at RT), in order to form artificial EphA clusters. Antibody-clustered EphA3, however, does also not trigger a collapse of nasal or temporal growth cones (21.7% collapsed; Figure 6C). In a last attempt, and inspired by the fact that substrate-bound EphA3 adsorbed from 15µg/ml EphA3-Fc solution does repel RGC growth cones (see Figure 2; Gebhardt et al., 2012), I applied 15µg/ml soluble EphA3-Fc to nasal and temporal growth cones. Surprisingly, this high concentration of EphA3 triggers a clear collapse response after incubation for 20 minutes (64.4% collapsed), whereas an equimolar concentration of Fc fragment does not (4.2µg/ml; 24.3% collapsed; Figure 6D). Thus, the collapse response is

---

[4]: evidence supporting this notion can be found in the *Supplement* section of this work: '*I. Ephrin-A/ EphA Binding Constants and Effects of EphA Clustering*'.

specific to EphA3 and, to the best of my knowledge, is the first evidence for repulsive ephrin-A reverse signaling, triggered by soluble EphA.

Moreover, RGC growth cones are able to desensitize towards soluble EphA3, when exposed to it for a longer period (22.6% collapsed growth cones after 120 minutes incubation; Figure 6D). Importantly, application of 15µg/ml EphA3-Fc together with 30µM Pitstop2 for 120 minutes results in a significant decrease in recovery rates of nasal and temporal growth cones (49.8% collapsed), reflecting the requirement of CME for reverse signal desensitization, as seen in ephrin-A5 collapse assays for forward signaling (cf. Figure 6B).

Noteworthy, Pitstop2 does not prevent collapsed growth cones from recovering their morphology *per se*, as seen with growth cones that were first treated with 15µg/ml EphA3-Fc for 20 minutes in the absence of Pitstop2 and then, after changing the medium, with 4.2µg/ml Fc plus 30µM Pitstop2 for another 120 minutes. While growth cones are expected to collapse upon EphA3 treatment, the abovementioned treatment does not prevent growth cones from recovering their morphology, when EphA3 is removed (19.3% collapsed; Figure 6C). Thus, Pitstop2 specifically inhibits desensitization towards the repulsive cue.

In sum, I hereby show that growth cone desensitization towards forward and reverse signals and the corresponding uptake of EphA/ ephrinA sensors strongly depend on clathrin-mediated endocytosis.

Dynamics of SNAP-Ephrin-A5 During Growth Cone Resensitization

But how do growth cones regain their sensitivity? Are sensors from internal storages brought back to the membrane during resensitization? To tackle this question, I transfected RGCs with SNAP-ephrin-A5 IRES GFP and specifically labeled the intracellular population of SNAP-ephrin-A5 in desensitized growth cones growing on a field of 15µg/ml ephrin-A5-Fc. Then, after a certain time period, I stained for the labeled molecules, which were now on the growth cones' surface. To ensure exclusive labeling of intracellular SNAP-ephrin-A5, cells were first treated with SNAP Surface block (a cell impermeant SNAP substrate) before staining with cell permeant SNAP Cell fluorescein. Axons were allowed to grow for another 20-22 hours afterwards, before an anti fluorescein antibody was applied to the medium. After washing and fixation, growth cones were stained for anti fluorescein. With this, all SNAP-ephrin-A5 molecules that had been transported from the growth cones' interior to the membrane during the second growth period are labeled (Figure 7A; see *Materials and Methods* for details).

After staining, growth cones growing on laminin show, contradicting a naïve expectation, a significant staining, indicating sensor turnover even in the absence of FT signaling (Figure 7C). In growth cones that never left the ephrin-A5-Fc field during the whole experiment, the anti fluorescein signal is weak compared to control growth cones growing on laminin (fold change in relative intensity compared to growth cones on laminin; on eA5: 0.85), which could either be explained by a reduced rate of SNAP-ephrin-A5 turnover, but might also mean a constant (or even elevated) turnover with a simultaneous increase in degradation of sensors (Figure 7B, C and D).

Interestingly, growth cones which have grown off the ephrin-A5-Fc field during the second growth phase, and therefore were able to

A

SNAP surface block — 22h

SNAP cell fluorescein — 22.5h

anti fluorescein 1st antibody — 44h

fixation and 2nd antibody — 45.5h

outside

inside

B

eA5

control

on

off

C

anti fluorescein

control

on ephrin-A5

off ephrin-A5

actin

GFP

substrate

D

fold change in rel. intensity

control

on eA5

off eA5

N=5 (22)

N=4 (15)

N=6 (21)

n.s

n.s

*
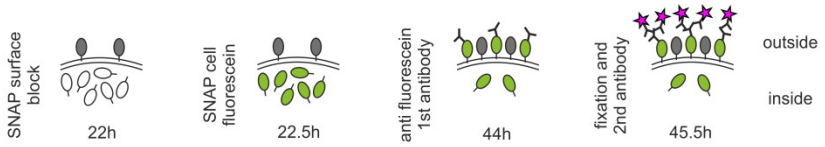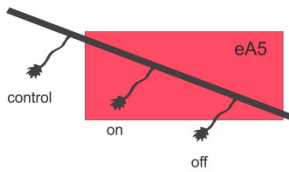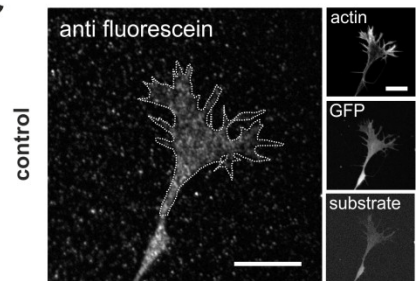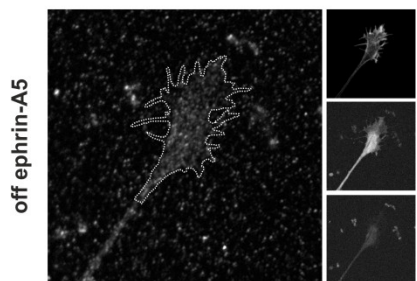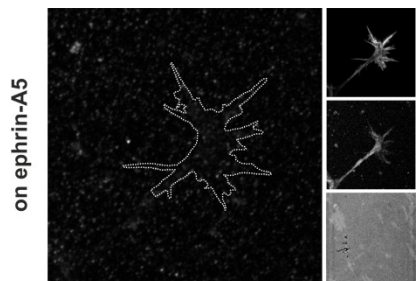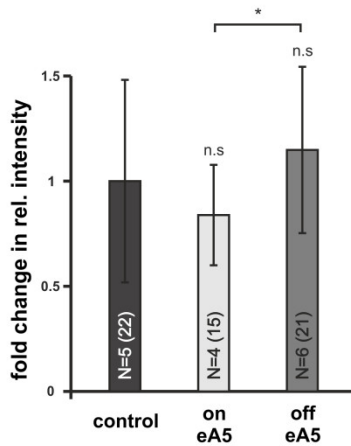
Figure 7: Dynamics of SNAP-ephrin-A5 during growth cone resensitization.

A: Staining for recycled SNAP-ephrin-A5. Extracellular SNAP-ephrin-A5 was blocked by SNAP Surface Block (gray), before the cell-permeant SNAP Cell fluorescein was applied for 40min (green). After washing, axons were allowed to grow for another 20-22 hours. Then, an anti fluorescein antibody was added to the medium for 15min, washed out and cells were fixed and stained for anti fluorescein (magenta stars).

B: Experimental setup. Retinal explants were placed on a contact-printed field of ephrin-A5-Fc (red) as indicated. SNAP Cell fluorescein was applied at a time point, when 'off eA5' category growth cones were still on the field.

C: SNAP-ephrin-A5 dynamics during forward signal resensitization. Representative images of growth cones, stained for anti fluorescein and actin. For quantification, the anti fluorescein signal was normalized to the GFP reporter signal of transfected growth cones, both measured in a mask drawn in the actin channel (white dotted line). The substrate was labeled with anti Fc antibody. Scale bar: 10µm.

D: Quantification of SNAP-ephrin-A5 dynamics. Ephrin-A5 desensitized growth cones show a reduced anti fluorescein signal compared to naïve control growth cones (fold change in relative intensity: control: 1; on eA5: 0.85). Upon resensitization, the anti fluorescein signal reappears and even slightly exceeds the signal of control growth cones (off eA5: 1.13). N: independent experimental days; number of analyzed growth cones in brackets. Error bars represent standard errors. T-test with n.s.: $\alpha \geq 0.05$, *: $\alpha < 0.05$.

recover their sensitivity towards forward signals, show a significantly higher surface staining, as compared to growth cones that still grow on the field (off eA5; 1.13; Figure 7B, C and D). Only this indicates that the lack of staining on growth cones growing on ephrin-A5-Fc was not due to degradation, but due to a reduced turnover of SNAP-ephrin-A5. To ensure that growth cones had enough time to regain sensitivity, only those growth cones that were located at least 200µm away from the ephrin-A5-Fc field were evaluated in the 'off eA5' category. The anti fluorescein signal on these growth cones even exceeds the signal measured on control growth cones slightly, suggesting that the exocytosis of SNAP-ephrin-A5 during resensitization exceeds endocytosis during normal turnover.

Receptor turnover typically involves the degradation of activated receptors and protein synthesis of new protein, as shown for Netrin-1, BDNF, or Sema3A (Ming et al., 2002; Piper et al., 2005). Alternatively, internalized receptors can also be recycled via recycling endosomes (Schindler et al., 2015). In RGC growth cones, von Philipsborn could previously show, that resensitization towards ephrin-A5-Fc is independent on protein synthesis. Growth cones treated with 40µM anisomycin were still able to detect the second ephrin-A5-Fc field after a 200µm wide gap in ephrin-A5-Fc gap assays (von Philipsborn, 2007). In my experiments, the detection of protein newly synthesized during resensitization is excluded by the staining procedure (no dye present during resensitization; Figure 7A). The abovementioned findings therefore indicate endosomal recycling of ephrin-A5 being utilized in forward signal resensitization.

It should be emphasized that these results were gained for ephrin-A5 on ephrin-A5 substrates. As ephrin-A5 is not a receptor for ephrin-A5-Fc, the regulation of ephrin-A5 has to be assumed to be a result of active or passive co-regulation with EphAs, corroborating the co-adaptation theory.

III. THE FUNCTION OF CO-ADAPTATION IN VIVO

Adaptation is typically used in biological systems to prevent the saturation of signaling and, thereby, to extend the dynamic range of sensor sensitivity, when for example a cell is moving in a concentration gradient of attractive or repulsive ligand. As shown by the model, however, there is no obvious need for adaptation in the mapping of retinal growth cones on the tectal gradient field, as they reliably find their correct target positions without any implementation of adaptation (cf. Figure 4B). What then might the *in vivo* function of adaptation be?

Modeling the Innervation of the Tectal Target by RGC Axons

In fact, adaptation might be needed for retinal axons to initially innervate the *tectum opticum* during development. As they reach the anterior tectum, RGC growth cones are confronted with high concentrations of EphAs, which they typically avoid (Figure 8; cf. Figure 2).
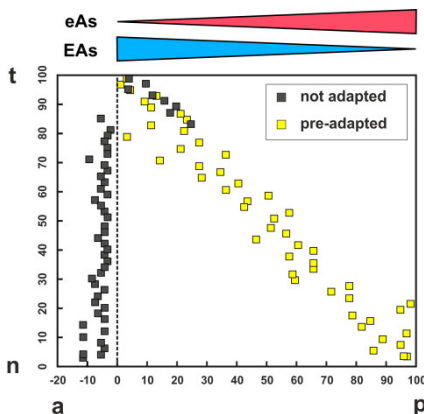
Figure 8: Modeling tectal innervation.

Co-adaptation enables fiber terminals to initially enter a tectal target field and allows correct mapping therein (yellow squares), whereas non-adapted terminals (dark gray squares) predominantly fail to enter. Graded distribution of EphAs (EAs, blue) and ephrin-As (eAs, red) indicated by colored wedges. n=50; C_0=1; q_x=0.3. R_F and L_F of adapted terminals initially deflected by a factor of 30.

Simulations with axonal terminals positioned in front of a tectal target field show that adapted terminals (sensors deflected manually by a factor of 30) are able to enter the target, whereas non-adapted terminals cannot (Figure 8). Moreover, adapted terminals reliably find their targets within the target field, demonstrating adaptation being theoretically reconcilable with topographic mapping. The hypothetical cue, desensitizing growth cones in front of the target, however, is yet to be identified.

In summary, the results presented in this work show clear evidence for a novel cellular mechanism of co-regulated adaptation towards EphA forward and ephrin-A reverse signals in RGC growth cones. The co-regulated uptake of sensors during desensitization is dependent on clathrin-mediated endocytosis, whereas resensitization in absence of forward or reverse signals seems to be mediated by endosomal recycling. It remains to be elucidated in detail, how EphAs and ephrin-As can be trafficked in strict proportion - an absolute requirement to reconcile adaptation and topographic mapping. Adaptation might be required for RGC axons to initially enter the tectal target field *in vivo*.

DISCUSSION

I. GROWTH CONE ADAPTATION AND RETINOTOPIC MAPPING

Growth Cone Adaptation Towards Substrate-Bound Ephrin-A and EphA

For my experiments, I have chosen recombinant ephrin-A5 and EphA3, as these proteins are expressed in conspicuous gradients along the a-p axis of the chicken tectum and have indeed been shown to be important for retinotectal guidance (Drescher et al., 1995; Cheng et al., 1995; Frisen et al., 1998). The used recombinant proteins each consist of the native proteins' extracellular domain, C-terminally fused to a human IgG fragment via a factor Xa recognition site linker, followed by a 6-His tag (R&D Systems). Although I used recombinant EphA3-Fc and ephrin-A5-Fc from mouse and human, respectively, the sequences share 81% and 89% similarity on the amino-acid level with their chicken equivalents (NCBI's BLAST). Experimentally, chick RGCs are repelled from soluble as well as substrate-bound ephrin-A5-Fc or EphA3-Fc. Thus, both recombinant proteins can be assumed to be recognized as functional ligands by chicken RGC growth cones.

Adaptation (including desensitization and resensitization) of retinal growth cones towards substrate-bound ephrin-A5-Fc was first fully[5] demonstrated by von Philipsborn (von Philipsborn, 2007) and could be confirmed in own experiments (Figure 2A). In ephrin-A5 gap assays, temporal RGC growth cones ignore a field of repulsive ephrin-A5-Fc after a small gap, when initially grown from an ephrin-A5 substrate,

---

[5]: The desensitization of growth cones towards ephrin-A-rich posterior tectal membranes was first shown by Rosentreter and co-workers (Rosentreter et al., 1998).

although they had the choice to stay in the ephrin-free gap. Increasing the width of the gap, and thereby the time axons grow in the absence of ephrin-A5, returns their sensitivity, as measured by an increasing rate of stopping in front of the second ephrin field. With this, the gap assay is a decisive *in vitro* experiment explicitly revealing the growth cones' ability to de- and re-sensitize towards repulsive EphA/ ephrin-A5 forward signals. Furthermore, although the individual growth cone only displays a binary decision (to cross or not to cross) when evaluating samples after fixation, the population behavior allows for quantification of the adaptation response. Using ephrin-A5 gap patterns with different gap sizes (50, 75, 100 and 200µm) reveals a gradual increase in the fraction of growth cones stopping with increasing gap sizes (15.3%, 43.0%, 59.2% and 81.0% stopping, respectively). Given that growth cones, having crossed a 200µm wide gap, still show a significantly weaker stop reaction compared to naïve growth cones (81.0% and 98.0%, respectively), resensitization seems to be not fully completed after this distance/ time of growth on laminin.

In EphA3-Fc gap assays, I could show for the first time that growth cones also adapt their reverse signaling (Figure 2B). Similar to the observations in ephrin-A5 gap assays, retinal growth cones desensitize towards reverse signals, when growing on substrate-bound EphA3-Fc, as they show a reduced stop reaction on the edge to the second field of EphA3 behind a small gap, compared to naïve growth cones (cf. Figure 2C; 25.0% and 92.6% stopping, respectively). They also regain sensitivity with increasing gap sizes (65µm: 25.0%, 90µm: 39.9%, 115µm: 60.1%, 215µm: 75.8% stopping) with a comparable course observed in ephrin-A5 gap assays. The fact, that both forward and reverse signal adaptation have surprisingly similar dynamics (cf. Figure 9; the combined data of ephrin-A5 and EphA3 gap assays can be fit with a
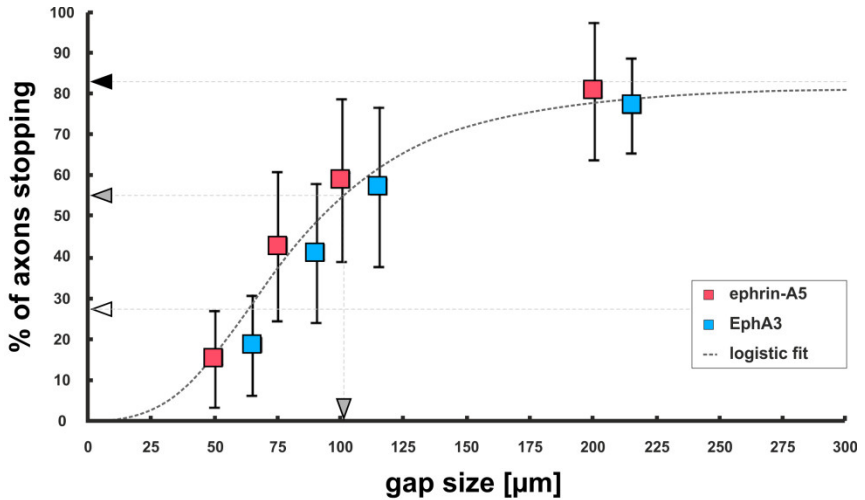
Figure 9: The dynamics of growth cone resensitization in ephrin-A5 and EphA3 gap assays.

The percentage of stopping fibers in ephrin-A5-Fc (red) and EphA3-Fc (blue) gap assays as a function of gap size, plotted on a continuous axis for distance. The combined data can be fitted with a correlation coefficient of r=0.98 by a logistic power function with $y = a/(1 + (x/b)^c)$, with a=82.6940; b=81.1634 and c=-3.0541. From the baseline stop rate of naïve growth cones (28.8%; white arrowhead) and the saturation value of the fit (~83%; black arrowhead), a dynamic range of growth cones can be estimated. Within this range, the half-maximum of resensitization (55.8% stopping) is reached after ~100µm (gray arrowheads). Error bars represent standard errors.

correlation coefficient of r=0.98 by a logistic power function with $y = a/(1 + (x/b)^c)$[6]), is a first indication of a common cellular adaptation mechanism.

---

[6]: a=82.6940; b=81.1634 and c=-3.0541; converging to saturation at ~82.7% stopping.

Notably, although not systematically explored, there is no obvious correlation between the distance growth cones grow on the first field of ephrin-A5 or EphA3 and their sensitivity when encountering the second field after a gap. Together with observations, showing that axons on substrate-bound ephrin-A5-Fc elongate with the same average velocity as axons on laminin substrates (von Philipsborn, 2007), growth cones seem to be fully desensitized from the moment they leave a retinal explant, placed on an EphA or ephrin-A substrate. As axons usually also need longer incubation until they emerge from explants placed on those substrates (own, not quantified observations), desensitization of growth cones is assumed to occur at the interface between explant and substrate before axons actually elongate.

The fact that the stop reactions of naïve growth cones at the edge to a field of Fc and those of adapted growth cones encountering ephrin-A5-Fc or EphA3-Fc after a small gap, are not significantly different (naive Fc: 28.8%; eA5 50µm: 15.3%; EA3 65µm: 25.0%), indicates that growth cones are still nearly completely desensitized after having crossed a 50µm or 65µm wide gap, respectively. Given the average growth rate of RGC axons of about 2.5µm/min (von Philipsborn, 2007), resensitization can be estimated to take >26 minutes of growth on laminin, until a change in the growth cones' stopping response, when re-encountering a field of ephrin-A5 or EphA3, can be measured. The half-maximum of resensitization, calculated from the logistic fit above as the mean between the maximum and the baseline stop rate of growth cones ((82.7%/2)+(28.8%/2)=55.8%), is reached at about 100µm or after ~40min of growth on laminin. Almost complete resensitization (98% saturation) is estimated to be reached after ~120 minutes, or 300µm.

Adaptation is expected to depend on the concentration of the stimulus. Ephrin-A5 and EphA3 gap assays were performed at nominally identical concentrations, however, it should be noted that the protein concentrations used for printing, are not obviously correlated to the concentrations present on the substrate after printing, as the transfer of protein will be incomplete and different for different proteins. Moreover, for the contact printing of EphA3-Fc it was necessary to pre-treat glass substrates with an epoxysilane, followed by coverage with poly-L-lysine (see *Material and Methods* for details), in order to transfer functionally active protein (Fiederling, 2012). This indicates that, upon printing, substantial amounts of protein can lose functionality, possibly because of denaturation or inaccessibility of ligand binding sites due to adsorption to the substrate in an unfavorable orientation. Therefore, the amount of active protein on the surface after printing cannot easily be predicted. It can also not be correlated to, for example, the signal of an antibody staining, as this will most likely detect all (also inactive) proteins. A comparison to the staining signal of protein adsorbed from solution with a similar concentration is also not possible, as adsorption from solution and printing potentially have different physical effects on the protein (15µg/ml EphA3-Fc adsorbed from solution does repel retinal growth cones, whereas the same concentration printed on untreated glass does not; Fiederling, 2012).

However, the amount of active protein present on the surface of ephrin-A5 or EphA3 gap assays, strongly repels nasal and temporal retinal growth cones, even if nasal growth cones (expressing low EphA levels) are least sensitive to forward signals and, respectively, temporal growth cones (expressing low ephrin-A levels) are expected to be rather insensitive towards reverse signals. This indicates that active proteins are present in quantities that potentially saturate repulsive signaling, repelling >90% of retinal growth cones.

Growth Cone Adaptation Towards Soluble Ephrin-A and EphA

As the applied effective concentration of ephrin-A5 cannot be controlled in gap assays (see above), but can be well titrated in a collapse assay, I used this assay to further investigate growth cone adaptation. In ephrin-A5 or EphA3 collapse assays, retinal growth cones growing on a laminin substrate collapse upon application of either cue, indicating the repulsive action of soluble ephrin-A5-Fc or EphA3-Fc. However, after a while, growth cones recover their morphology in the presence of either cue, as a result of adaptive desensitization. Thus, retinal growth cones not only adapt towards substrate-bound ephrin-A5-Fc or EphA3-Fc, as seen in gap assays, but also when either cue is presented in soluble form (cf. Figure 6).

In ephrin-A5 collapse assays, temporal growth cones incubated with 0.25μg/ml ephrin-A5-Fc for 20 minutes, show a collapse rate of 85.4%, whereas, after 120 minutes, the collapse rate drops down to 15.8% (cf. Figure 6B). Importantly, ephrin-A5-Fc has been shown to be still functionally active after prolonged incubation, illustrated by experiments in which the medium containing 0.25μg/ml ephrin-A5-Fc was kept on a first explant culture for 120 minutes and was then reused on a second culture of neurons for 20 minutes. While temporal growth cones are mostly intact in the first culture after 120 minutes, the 'recycled' ephrin-A5-Fc triggers full response on a fresh culture, ruling out the possibility that growth cones recover in the first culture because of ephrin-A5 being degraded or consumed in another way (Fritz, 2012). Note that the concentrations used in ephrin-A5 collapse assays are much lower than those used in ephrin-A5 gap assays (0.25μg/ml compared to 15μg/ml). We used the lowest possible ephrin-A5 concentration, that triggers a collapse in temporal, but not in nasal retinal growth cones (Fritz, 2012), to show that adaptation occurs at physiological concentrations of guidance cues.

To investigate a potential adaptation also towards soluble EphA3-Fc, I for the first time established an EphA3-Fc collapse assay in this work (cf. Figure 6D). It turned out that substantially higher concentrations of EphA3 are needed to induce a collapse response than previously tried. Notably, the initial collapse rates of growth cones exposed to 15μg/ml EphA3-Fc for 20 minutes are still overall lower than those of growth cones treated with ephrin-A5-Fc for 20 minutes (64.4% and 85.4% collapsed, respectively). Given, that the baseline collapse rates of growth cones in controls (treated with at least equimolar[7] concentration of Fc-fragment) are higher in EphA3 collapse assay controls compared to ephrin-A5 collapse assay controls (Fc 4.2μg/ml: 24.3% and Fc 0.25μg/ml: 13.6%, respectively), the applied EphA3 concentration cannot further be increased without intolerable unspecific collapse responses. Thus, at first glance, when ligands are applied in soluble form, forward signals seem to be stronger (or at least trigger a stronger collapse response) than reverse signals. However, as the clustering of EphAs seems to be important for the interaction with ephrin-As (Janes et al., 2012), there might (alternatively) be substantial differences in reverse signaling, depending on the oligomerization state of EphAs. The seemingly reduced collapse sensitivity might, therefore, be a consequence of partially inappropriate EphA3-Fc complexes, preventing optimal signaling. Hence, EphA3 clusters, which might form only at high concentrations and bind to ephrin-A5 with substantially higher affinity compared to dimeric EphA3-Fc (see *Supplement*: '*I. Ephrin-A/ EphA Binding Constants and Effects of EphA Clustering*'), seem to be essential for effective reverse signaling. Hence, the effective concentration of suitable EphA3 oligomers, needed to trigger a collapse might be much lower than 15μg/ml and is possibly in the range of the

[7]: Molecular masses of EphA3-Fc, ehrin-A5-Fc and Fc-fragment are roughly 90kDa, 50kDa and 25kDa, respectively. A 1:1 molar ratio of EphA3 to Fc or ephrin-A5 to Fc is achieved with 15μg/ml EA3 and 4.2μg/ml Fc, or 0.25μg/ml eA5 and 0.125μg/ml Fc.

active ephrin-A5 concentration. Indeed, when applied in substrate-bound form, there is no significant difference in the strength of forward and reverse signals, measured as stop rates in ephrin-A5 and EphA3 gap assays (98.0% and 92.6% stopping).

Even if the primary response of retinal growth cones towards high concentrations of soluble EphA3-Fc seems to be weaker than measured in ephrin-A5 collapse assays, a similar adaptive desensitization towards reverse signals can be observed after 120 minutes (from 64.4% and 22.6% collapse). Corroborating my findings in EphA3 gap assays, this is clear evidence for growth cone adaptation towards soluble EphA3-Fc.

In both, ephrin-A5 and EphA3 collapse assays, collapse rates of growth cones treated for 120 minutes with either cue are not significantly different from collapse rates of control (Fc treated) growth cones (eA5 120min: 15.8%, Fc 0.25µg/ml 20min: 13.6%; EA3 120min: 22.6%, Fc 4.2µg/ml 20min: 24.3%), indicating that desensitization is completed within 120 minutes.

Together, gap and collapse assays provide compelling evidence for the existence of adaptation in retinal growth cones, raising the question of how adaptation might be compatible with a topographic mapping mechanism that relies on quantitative signaling.

Growth Cone Adaptation Towards Fiber-Fiber Signaling

As growth cone fiber-fiber interactions are assumed to instruct retinotopic mapping even more than fiber-target interactions (Gebhardt et al., 2012; Weth et al., 2014), non-adapting FF interactions could possibly rescue topographic mapping in the face of adaptation. To see whether this is the case, I had to check, whether retinal growth cones

also adapt towards FF signaling. In collision experiments, the reactions of growth cones encountering other retinal fibers were evaluated using time lapse microscopy (Figure 3). As observed by others, temporal growth cones encountering nasal axons display a strong repulsive reaction (they collapse and retract, or collapse and stop; Raper and Grunewald, 1990; Lutz, 2011). Surprisingly, however, when FT forward signaling adapted temporal growth cones (explant placed on a field of substrate-bound ephrin-A5-Fc) meet nasal axons, they are no longer repelled (they predominantly overgrow or fasciculate with the nasal fiber; cf. Figure 3B). This clearly indicates that, upon forward FT desensitization, temporal growth cones concomitantly lose sensitivity towards forward FF signals. Growth cone adaptation, therefore, has to be considered to occur not only towards FT, but also towards FF signals. Because of nasal retinal growth cones being not responsive towards temporal fibers (cf. Figure 3B; an enigma that has been observed early on in *in vitro* experiments; Bonhoeffer and Huf, 1985; Raper and Grunewald, 1990), adaptation towards reverse FF interactions could not be addressed in those experiments. It is unclear yet, why nasal growth cones are generally less responsive *in vitro*. Potentially, the artificial *in vitro* situation lacks components of the growth cones' *in vivo* environment, necessary for effective FF reverse signaling, which is compensated for in FT adaptation experiments by the abundance of recombinant EphA protein.

Mathematical Modeling of Growth Cone Adaptation and Mapping

Through modeling, we searched for a possibility, how adaptation could be implemented into the retinotectal mapping system, without destroying its main feature - the formation of an accurate topographic map. In the model, mapping critically relies on the balancing of absolute

forward and reverse signals (Gebhardt et al., 2012). It is obvious, that affecting the relative proportion of both signals in a given growth cone through adaptation, will prevent this balancing at the growth cones' correct target position in the tectal gradient field. Instead, balancing might occur at a different position (if the target field provides for an EphA/ ephrin-A ratio matching the adapted growth cones' signals). Thereby, the minimum of the guidance potential is shifted within the tectal target field during adaptation, destroying correct topography. Thus, to retain topography, we conclude that adaptation might scale the guidance potential, but must not change its fundamental topology. This can be achieved only, when forward and reverse signaling are modified concordantly and, therefore, when the monotony of the potential function is not altered upon adaptation.

Implementing such a form of adaptation (co-adaptation), which regulates the activities of axonal sensors R_F and L_F without changing their relative strength, in fact preserves the topology of the guidance potential and allows accurate mapping of adapting fibers (cf. Figure 4C). Moreover, the co-adaptation model perfectly reproduces the results of *in vitro* adaptation assays like ephrin-A5 or EphA3 gap assays (cf. Figure 4D).

Except of implementing the adaptation mechanism, simulating the gap assays required several minor modifications of the model. Although, the model generally does not depend on the implementation of any forward bias of fibers in order to make them find their target positions in an tectal gradient field, the simulation of gap assays did necessitate the implementation of a preference to grow forward. Thus, the applied forward drive, q_x, is used to bias the growth cones' probabilistic choice of a surrounding position on the target field for subsequent potential evaluation towards the fields in front of the growth cone. The potential at the chosen position is than compared to the potential at the growth cones' current position, in order to decide the next step (see Gebhardt,

2009 for details). Note that q_x does not affect the actual step decision, which is only dependent on the guidance potentials calculated at the current and the tested target position.

While q_x was set $q_x=0$ for the simulations in tectal gradient fields, q_x had to be increased to $q_x=0.3$ in simulations of gap assays, because the laminin-covered areas on these substrates are defined as R_T, $L_T=0$ and, therefore, provide for a homogeneous area of guidance potential minimum with $D=0$, effectively causing a random walk of growth cones. Thus, in simulations with $q_x=0$, growth cones spent unpredictable periods of time with random, non-directional growth in the gap. Similarly, the homogeneous fields of EphA or ephrin-A on the substrates, defined as $R_T=4$ or $L_T=4$, respectively, provide higher, but also non-differential values of D, as long as a growth cone does not reach the edge of a field, causing growth cones to perform a random walk. Due to this randomness, it is impossible to correlate the time of growth to the distance a growth cone has covered, which is a prerequisite for the simulation of gap assays. As growth cones *in vitro* also do show a directed migration behavior, clearly different from a random walk, the assumption of an intrinsic forward drive seems reasonable. In fact, already with a moderate forward drive with $q_x=0.3$ (changing the probability, w, to consider a field in front of the growth cone for the next step from $w=1/3=0.33$ to $w=(1+q_x)/3=0.43$), the results from ephrin-A5 and EphA3 gap assays can be accurately reproduced by the model (cf. Figure 4D).

The forward bias observed in the migration of real growth cones might originate from the growth cones' internal polarity, which, most likely, does not allow for drastic changes in the direction of growth within very small increments of space. Microtubules, which extent from the axon through the central domain of the growth cone to individual filopodia, determine the direction of growth through stabilization of filopodia (Sabry et al., 1991; Tanaka and Kirschner, 1995). Due to the

stiffness of microtubules, it is unlikely that filopodia with an extreme angle to the axon shaft can be stabilized in this way. Thus, growth cones might predominantly grow rather straight.

In addition to q_x, the strength of fiber-fiber interactions was adjusted for simulations of *in vitro* assays. While the FF scaling factor, c, is set c=100 in simulations of full retinal projections, c was reduced to c=1 in simulations of gap assays. Simultaneously, the number of fibers was decreased from n=100 to n=15. Both parameters were changed in order to better match the real experimental conditions. As the number of axons emerging from one retinal explant strip in an *in vitro* experiment can be estimated to be in the range of 10^3, it is obvious that FF signals must be much weaker than *in vivo*, where roughly 10^6 RGCs (Naito and Chen, 2004) are expected to be involved in the mapping to the target. Moreover, the few growth cones from an retinal explant strip have a much bigger substrate to spread upon, compared to the multitude of retinal fibers, which are spatially restricted to the area of the optic tectum during *in vivo* mapping. Hence, the impact of FF interactions was reduced mainly through decreasing c for the simulation of *in vitro* assays, while the size of the substrate was only slightly increased by a factor of two, in order to safe simulation time.
Besides these adjustments, all simulations were run with a unique set of parameters.

In addition to mapping, the updated model, including adaptation, successfully reproduces other *in vitro* and *in vivo* experiments like single- and double-cue stripe assays, or map expansion experiments (Meyer et al., 1987; data not shown), as the previous model did (see Gebhardt et al., 2012). However, it has not been tested for all of the experimental conditions, described in Weth et al., 2014 so far. The full explanatory power of the new model, therefore, is still to be evaluated.

Growth Cone Co-Adaptation

The results of *in vitro* ephrin-A/ EphA double-cue gap assays are in perfect agreement with the prediction of the existence of co-adaptation from the model. This novel assay allows to investigate co-adaptation with a high level of control, and, therefore, generates highly reliable data, as the functionality of both proteins to either side of the gap can be tested on the same substrate in multiple ways: First, in a double-cue gap assay with growth cones adapting towards protein X, encountering protein Y after the gap, the repulsive activity of protein Y is controlled with a second explant strip from the same retina, that is placed onto laminin on the other side of the Y field, opposite to the test explant. Experiments were only evaluated, if the naïvely outgrowing growth cones from this control explant did show a significant stop reaction at the Y field. On the other hand, if growth cones from the test explant, placed on the X field, do not show a significant stop reaction (in contrast to the control growth cones), it is clear that this is due to the growth on X and, thereby, attests to the function of X and it can be concluded that X desensitizes growth cones towards Y through co-adaptation.

Hence, the results from double-cue gap assays shown in this work, provide robust evidence for the existence of co-adaptation towards forward and reverse EphA/ ephrin-A signaling, but not towards other repulsive cues like Sema3A, or Slit2 (data not shown).

More evidence, corroborating the existence of co-adaptation, comes from Weschenfelder's work with retinal growth cones overexpressing SNAP-tagged ephrin-A5. He could show, that growth cones downregulate the amount of surface SNAP-ephrin-A5 not only upon adaptation towards substrate-bound EphA3-Fc, but also towards ephrin-A5-Fc (Weschenfelder, 2014).

In own experiments, I could observe that the SNAP-ephrin-A5 that has been in the growth cones' interior during desensitization, is brought to the surface, when growth cones leave the underlying ephrin-A5 substrate and grow onto laminin (cf. Figure 7). However, although significant, the difference in the surface levels of recycled SNAP-ephrin-A5 on desensitized versus resensitized growth cones is much smaller (13%; Figure 7D), than the difference of surface SNAP-ephrin-A5 on control versus desensitized growth cones (~60%, Weschenfelder, 2014). This might be due to incomplete blocking of the surface SNAP-ephrin-A5 population before staining the intracellular population, incomplete labeling of the intracellular SNAP-ephrin-A5 population, or incomplete detection of the recycled SNAP-ephrin-A5 with the anti fluorescein antibody. Moreover, resensitization might have been incomplete at the time of staining, or there are other, non-labeled sources of recycled ephrin-A5 that contribute to resensitization. All these effects could explain, why the relative difference of the SNAP-ephrin-A5 surface signal is less pronounced upon resensitization (detected as described in Figure 7A), compared to the difference upon desensitization (detected by a SNAP Surface staining, Weschenfelder, 2014). It is to be evaluated, how internalized sensors can be brought back to the surface upon resensitization (see also *Discussion*: '*Growth Cone Resensitization: Protein Synthesis vs. Recycling*').

II. THE CELLULAR MECHANISMS OF ADAPTATION

Growth Cone Desensitization via Clathrin-Mediated Endocytosis

The results presented in Figure 6, clearly demonstrate that growth cone desensitization towards ephrin-A5-Fc and EphA3-Fc, respectively, is dependent on clathrin-mediated endocytosis. In ephrin-A5 collapse assays, application of 30µM Pitstop2 does not significantly alter the initial collapse response of temporal RGC axons towards 0.25µg/ml ephrin-A5-Fc, when exposed to it for 20 minutes. However, the adaptive desensitization of growth cones, observed after prolonged (120min) incubation with ephrin-A5-Fc is efficiently blocked, when Pitstop2 is present (Figure 6B). As collapse rates of Pitstop2 treated growth cones after 120 minutes are not significantly different from those of growth cones treated for 20 minutes (74.3% and 83.1%, respectively), CME is assumed to be necessary for adaptive desensitization towards forward signals.

Similarly, collapse rates of growth cones exposed to 15µg/ml EphA3-Fc for 120 minutes are significantly higher in the presence of Pitstop2 (49.8%, compared to 22.6% without Pitstop2), indicating that desensitization towards reverse signals also depends on CME, although there is a small difference (significant at $\alpha < 0.05$) between the collapse rates of Pitstop2 treated growth cones after 120min (49.8%) and Eph-only treated growth cones after 20min (64.4%; cf. Figure 6D) indicating some residual resensitization. This might hint at additional, clathrin independent mechanisms being involved in reverse signaling desensitization.

In contrast to adaptation, the primary forward signaling is not affected by Pitstop2 (eA5+DMSO 20min: 85.4%; eA5+P: 83.1% collapsed) and thus, seems to be independent of CME. For reasons of time, I could not

test yet, whether primary reverse signaling is also independent of CME in EphA3 collapse assays. Although the dynamics of adaptation towards forward and reverse signals are almost identical (cf. *Discussion*: '*Growth Cone Adaptation Towards Substrate-Bound Ephrin-A and EphA*'), making a common adaptation mechanism more likely, it cannot be ruled out that reverse signaling (fully or partially) depends on CME.

Notably, the inhibition of CME via Pitstop2, does not prevent growth cones from collapsing, indicating that the internalization of large fractions of plasma membrane during growth cone collapse involves clathrin independent endocytotic pathways, like, for example, macropinocytosis (Kabayama et al., 2009; Joset et al., 2010).

The pharmacological inhibitor Pitstop2, blocking the association of the clathrin terminal domain to the cargos to be endocytosed via the adaptor AP-2 (von Kleist et al., 2011), can be assumed to block clathrin-mediated endocytosis with high specifity, although the exact mechanism by which inhibition is achieved is controversially discussed (Lemmon and Traub, 2012; Willox et al., 2014).

The previously used Dynasore, designed to block all dynamin dependent endocytotic pathways (including CME), however, did surprisingly not prevent the desensitization of retinal growth cones towards ephrin-A5-Fc (Fritz, 2012). A possible explanation for this might be, that Dynasore targets the dynamin GTPases Dynamin-1 and Dynamin-2 (Macia et al., 2006), but has not been reported to inhibit Dynamin-3, which significantly contributes to the synaptic physiology of neurons (Raimondi et al., 2011; Lou et al., 2012). Moreover, Dynasore turned out to mediate strong off-target effects, as, for example, seen by the fact that even in Dynamin-1, -2 and -3 triple knockout cells, Dynasore induces an inhibition on fluid-phase endocytosis or membrane ruffling (Park et al., 2013). Another, more recent study showed that Dynasore disrupts the organization of lipid rafts by

modulating the homeostasis of cholesterol in the plasma membrane (Preta et al., 2015). The disruption of rafts in retinal growth cones might induce an adaptation pathway circumventing CME (cf. *Discussion*: '*Regulating Sensor Trafficking - Fyn the Raftsman*'). Thus, through unspecific effects, Dynasore might paradoxically prevent its own, specific action on the internalization of receptors involved in adaptation.

Another possible explanation might be that Dynasore binds to serum proteins and thereby loses its activity, as reported in Kirchhausen et al., 2008. Since Fritz applied Dynasore 30 minutes before the addition of ephrin-A5 to the F12MC culture medium (containing fetal calf serum and chicken serum) on a retinal culture (Fritz, 2012), the activity of the inhibitor might have been already strongly reduced or completely abolished, when the ephrin-A5 was added.

Together, a specific and effective inhibition of dynamin dependent endocytosis by Dynasore in those experiments must be doubted. Experiments with Pitstop2, on the other hand, provide more trustable evidence, as, upon application, a specific and significant effect can be measured.

Growth Cone Resensitization: Protein Synthesis vs. Recycling

As desensitization is dependent on the endocytosis of sensors, it is reasonable to assume that sensors are brought back to the cell surface during resensitization. Thus, adjusting the sensitivity of a growth cone towards forward and reverse signals by regulating the EphA/ ephrin-A surface levels could theoretically be realized by (at least) two generally different concepts: (i) internalization, degradation and local synthesis of new sensors, or (ii) internalization and endosomal recycling of sensors.

In the following, I will discuss the significance of both mechanisms for ephrin-A/ EphA co-adaptation.

Chick RGC growth cones move with an average velocity of about 2.5µm/min on laminin (von Philipsborn, 2007). To cross a 200µm wide gap in gap assay experiments, therefore takes them about 80 minutes. During this time period, ephrin-A5 or EphA3 adapted growth cones almost fully recover their sensitivity towards forward and reverse signals, as previously discussed.

Both, local protein synthesis and endosomal recycling occur at rates compatible to this period and could, thus, theoretically explain resensitization. Local protein synthesis involves the production of mRNA, its transport to the growth cone and the translation into protein, once arrived (Yoon et al., 2009; Holt & Bullock, 2009). For EphA3, as an example, the duration of this whole process can be estimated to occur within about 30 minutes in a cell with an axon of 1mm length (EphA3 transcript length: ~8kb; transcription and translation rates: ~20nt/s; average velocity of a kinesin motor: ~1800nm/s; Milo & Phillips, 2016). Evidence, suggesting that mRNAs can be locally stored in P-bodies (typically involved in mRNA degradation) until they are released for translation might actually render the transport of mRNA unnecessary for local protein synthesis and would provide for an even more rapid availability of new protein (Donnelly et al., 2010). Several studies show that local protein synthesis is critically involved in the motility of growth cones and their response to guidance cues like Sema3A, Netrin-1 or BDNF via the localized translation of cytoskeletal components and their effectors, e.g. ß-actin mRNA (Yao et al., 2006; Leung et al., 2007), RhoA mRNA (Wu et al., 2005), cofilin-1 mRNA (Piper et al., 2006) or ß-thymosin mRNA (van Kesteren et al., 2006). As mRNA localization, stability and translation are each subject to a tight regulatory machinery (Donnelly et al., 2010; Gumy et al., 2013), local protein synthesis could theoretically explain the fine-tuned adaptive

regulation of EphAs and ephrin-As, as documented in this work. However, neither the initial response to, nor adaptation towards ephrin-A5 were found to depend on local protein synthesis (von Philipsborn, 2007; Roche et al., 2009). EphA and ephrin-A signaling might therefore be peculiar in terms of the mechanisms utilized for guidance, compared to other guidance cues like Sema3A, Netrin-1 or BDNF, which do depend on protein synthesis (see above, although challenged by Roche et al., 2009).

The role of protein synthesis on the adaptation towards reverse signals has not been investigated, so far. As forward signal adaptation is independent of protein synthesis, and since forward and reverse signaling have to be tightly co-regulated during co-adaptation, it seems unlikely that both sensors are regulated by different mechanisms. However, it cannot be formally excluded, that reverse signal adaptation requires protein synthesis. Obviously, this issue needs further investigation.

As an alternative to local protein synthesis, the replenishment of EphAs and ephrin-As on the plasma membrane during resensitization could be achieved via endosomal recycling. Endosomal recycling can generally follow two separate routes, one fast and one slow recycling pathway, which are controlled by the small GTPases Rab4 and Rab11, respectively (van der Sluijs et al., 1992; Ullrich et al., 1996; Schindler et al., 2015). While fast recycling is thought of as a constitutive transport of cargo from early endosomes (EE) back to the membrane, slow recycling involves an additional sorting step in recycling endosomes (RE) or in multi-vesicular bodies (MVBs). In receptor tyrosine kinase trafficking, ubiquitination is used as a signal to sort internalized receptors via the ESCRT machinery into intraluminal vesicles (ILVs) of MVBs, targeting them for degradation as MVBs mature into late endosomes/ lysosomes (Huang et al., 2006; Eden et al., 2010; Goh and Sorkin, 2013). Non- or de-

ubiquitinated proteins can escape degradation by moving into tubular extensions of MVBs and recycle back to the cell surface (Goh and Sorkin, 2013). The rate of recycling thereby depends on the activity of deubiquitinating enzymes and ubiquitin ligases (Sabet et al., 2015) and, as the degradation pathway can be saturated, on the concentration of internalized receptors (shown for EGFR; Sorkin et al., 1991). Alternatively, RTKs can enter the slow recycling pathway via REs from EEs (Goh and Sorkin, 2013). How exactly proteins are tagged for recycling and by which mechanisms they are guided through a series of recycling endosomal structures is not well understood, but most likely involves special tethering complexes like the recently identified EARP (Schindler et al., 2015).

Recycling of EphA receptors has been observed only for EphA2 so far. While most activated EphA2 receptors are degraded in lysosomes, about 35% of internalized EphA2 is recycled back to the cell surface of human tumor cells in Rab4 and Rab11 positive endosomes (Boissier et al., 2013). As also GPI-anchored proteins, like ephrin-As, undergo recycling (Cai et al., 2011; Refaei et al., 2011), endosomal recycling fulfills the general requirements for EphA/ ephrin-A adaptive resensitization.

Special Requirements on Co-Adaptation - A Problem of Proportionality and Unligated Receptors

The concept of co-adaptation, however, implies some special, conceptually more challenging requirements on the trafficking of sensors. First, both EphAs and ephrin-As need to be regulated in strict proportion, as their relative signaling is essential for correct mapping (Figure 4B). Non-proportional uptake of sensors in a growth cone would inevitably shift its inherent sensitivity towards forward and

reverse signals, eventually preventing the balancing of impinging signals at a given position in the target gradient system (Gebhardt et al., 2012; Weth et al., 2014).

Second, such a co-regulated internalization of sensors must inevitably involve the uptake of non-occupied receptors. This is, at first glance, inconsistent with receptor-mediated endocytosis, i.e. CME, which is, according to text books, primarily accessible to ligand-activated receptors. Contradicting this prevailing view, however, work on EGFR trafficking revealed, that ligand-activation is not an absolute requirement for CME, as substantial amounts of unoccupied EGFR were found to be endocytosed upon inhibition of protein kinase A (PKA) in a clathrin dependent manner (Salazar and González, 2002). This could be similar for other RTKs and provide for a means to internalize non-activated EphAs via CME.

But what about GPI-anchored ephrin-As? Although the sensitivity towards reverse signals could theoretically be adjusted by just regulating the levels of the ephrin-A co-receptors (e.g. TrkB, p75NTR and Ret), which are amenable to CME upon activation (Deinhardt et al., 2007; Yap and Winckler, 2015), Weschenfelder's findings, showing that the amount of ephrin-A5 itself on the surface is reduced upon co-adaptation (Weschenfelder, 2014), argue against this theory. As the internalization of GPI-anchored proteins is generally mediated by clathrin independent endocytotic pathways (Skretting et al., 1999; Ricci et al., 2000; Fivaz et al., 2002; Sabharanjak et al., 2002), one might argue that ephrin-As are internalized together with their co-receptors. This scenario would require, that ephrin-As form complexes with their co-receptors even before they have bound their EphA ligands, and that these complexes can be endocytosed via CME. Indeed, p75NTR was found to form complexes with ephrin-A2 or ephrin-A5 in mouse RGCs, in absence of any external stimuli (Lim et al., 2008). Thus, ephrin-As

could be principally targeted for CME upon association with co-receptors.

Regulating Sensor Trafficking - Fyn the Raftsman

The amount of internalization as well as the trafficking of sensors back to the membrane has to be tightly controlled for proper adaptation. Although the mechanisms involved in controlling recycling are poorly understood, a study by Baba and co-workers suggests, that the Src family kinase Fyn, which is activated by ligand-bound ephrin-As via p75NTR (Lim et al., 2008), negatively regulates the amount of surface ephrin-A by influencing the metabolism of raft-associated lipids (Baba et al., 2009). They report an increased production of sphingomyelin upon ephrin-A2 reverse signaling, effectively reducing the amount of surface ephrin-A, potentially by impairing protein trafficking. Inhibition of sphingomyelin synthesis results in an increase of ephrin-A on the surface (Baba et al., 2009). This concept of regulating the surface levels of a receptor by modulating lipid metabolism is interesting. Ephrin-As, as many other GPI-anchored proteins, are assumed to localize to special microdomains of the plasma membrane, so called 'lipid rafts'. Changing the lipid composition of rafts, and thereby affecting their physical properties (e.g. curvature), has been shown to impact protein sorting, vesicle budding and membrane fusion (McMahon and Gallop, 2005; Kumar et al., 2015), and thus, the trafficking of raft-localized proteins. It is to be mentioned at this point, that the existence of lipid rafts, as passively forming lipid islands that incorporate specialized proteins, is under controversial debate for more than a decade, still (for reviews see Munro, 2003; Leslie, 2011). Skeptics argue that the formation of specialized membrane domains is a more active process and most likely initiated by proteins that the lipids follow, and not the other way

around (Leslie, 2011). The concept of lipid rafts should therefore be taken as a model rather than a fact. It is, however, without doubt that different cellular membranes differ in their lipid composition and that proteins are heterogeneously distributed in the plasma membrane (Munro, 2003). The Fyn dependent increase in sphingomyelin production upon ephrin-A2 reverse signaling might thus be a mechanism to actively regulate the trafficking of ephrin-As. Although there is no direct evidence for the activation of Fyn via EphAs, both proteins have been found to interact upon stimulation with ephrin-As (Knöll and Drescher, 2004), suggesting that forward and reverse signals could influence sphingomyelin metabolism. Co-adaptation could therefore be achieved by the regulation of specific lipids, involved in the trafficking of EphAs and ephrin-As.

The signal triggering this sorting would have to originate from somewhere downstream of the signaling potential and is yet to be identified. A possible effector of this signal might be the C-terminal Src kinase Csk, which is known to influence forward signaling (Knöll and Drescher, 2004) and, as the Csk homolog Chk associates with TrkA[8] (Yamashita et al., 1999), might also be involved in reverse signaling.

Csk has been shown to be part of a lateral inhibition mechanism, starting with the activation of a Src family kinase, which then phosphorylates the lipid raft-associated protein Cbp (Kawabuchi et al., 2000). Cbp, as an adaptor protein, recruits the cytosolic Csk to the membrane (Cary and Cooper, 2000), which in turn inhibits the activation of neighboring, inactive Src family kinases by phosphorylation of a conserved C-terminal tyrosine (Thomas and Brugge, 1997; Ingley, 2008). Thus, EphA forward activated Fyn might prevent the activation of Fyn through reverse signaling and *vice versa*.

[8]: TrkA is structurally very similar to TrKB, mainly differing in its preferred binding to NGF, compared to BDNF (TrkB) (Klein et al., 1989; Segal, 2003).

With this, the lateral inhibition of Fyn via Csk would perfectly explain how adaptation could be regulated in proportion to the signal potential, as this mechanism would provide for the means to effectively shut-down adaptation, when forward and reverse signals are balanced.

How Sensor Trafficking Controls Sensitivity - Predictions of the Model

Following the observations and interpretations given so far, one might naïvely think of adaptive desensitization being achieved by attenuating the incoming signals by reducing the amount of surface sensors. However, this is most likely not the explanation for adaptation. In fact, in the computational model, adaptive desensitization is realized by up-regulating signals. Although this seems counterintuitive, sensitivity and signaling strength must not be confused. In the model, the increase of sensor activities R_F and L_F intensifies the *trans* fiber-target interactions, but even more amplifies the *cis* fiber-fiber interactions, since the activities of both interacting partners R_F and L_F are elevated upon adaptation. As a result, *cis* interactions outbalance the other signaling contributors and predominate absolute forward and reverse signaling. Eventually, due to the signal balancing mechanism of the model, this results in a reduced absolute value of the guidance potential D, as constant signals (like *cis* signals) add constantly to nominator and denominator and contribute to the absolute value of D. Increasing absolute forward and reverse signals, therefore, brings D closer to zero, given $D=|\ln(\text{reverse}/\text{forward})|$ (cf. *Results*: '*Mathematical Modeling of Growth Cone Adaptation and Mapping*'). For a growth cone on a tectal target field, this results in a flattened potential minimum curve, i.e. desensitizes it towards positions anterior and posterior to the correct target position.

With analogy to everyday life, significant information from a conversation can easily be missed, when there are some guys chatting loudly next by. In case of EphA/ ephrin-A signaling, these 'guys' are *cis* interactions, which contribute a lot to the absolute signal in adapted growth cones and thereby mask the important information, namely signal differences resulting from small changes in the ligand concentration on the substrate.

Indeed, the *in vitro* observation of reduced sensors on the surface of desensitized growth cones could be reconciled with enhanced *cis* signaling, as I will elucidate shortly.

Before, however, it is to be noted that *cis* signaling must not be confused with *cis* attenuation, which has been proposed to prevent the involved sensors from signaling (Hornberger et al., 1999). *Cis* attenuation has been reported to occur between ephrin-As and EphAs located in the same membrane upon binding of the ephrins' receptor binding domain, not with the ligand binding domain of EphA, but with its second fibronectin type III domain (Carvalho et al., 2006). Such an interaction (termed 'parallel *cis*' here) is assumed to prevent the involved sensors from interacting with ligands in *trans* and has been postulated to not result in the phosphorylation of EphAs[9]. Others assume that the *cis* binding of Eph and ephrin involves their ligand/ receptor binding domains (Yin et al., 2004; Marquardt et al., 2005; termed 'anti-parallel *cis*' here). Although it is unclear, whether such an interaction is conformationally possible, it should result in the phosphorylation of EphA and, therefore, be indistinguishable from *trans* interactions.

With this, and the consideration of anti-parallel *cis* interactions between sensors located on filopodia that are in contact with parts of the same

---

[9]: Carvalho and co-workers detected a decreased level of global tyrosine phosphorylation, when over-expressing ephrin-A5 in EphA3 expressing HEK293 cells (Carvalho et al., 2006).

growth cone, *cis* interactions have also to be considered as signal transducing.

To prevent *cis* interactions to mutually exclude sensors from *trans* signaling, it has been suggested that EphAs and ephrin-As laterally segregate into distinct membrane domains (Gauthier and Robins, 2003; Marquardt et al., 2005; Kao and Kania, 2011).

Now, as sensors involved in adaptation are sorted for CME upon desensitization, their re-localization might bring them into a configuration that promotes anti-parallel *cis* interactions.

Together with the insights from the observations mentioned in the previous chapter (*Discussion*: '*Regulating Sensor Trafficking - Fyn the Raftsman*'), a hypothetical mechanism explaining the sensor trafficking during adaptation towards forward and reverse signals can be formulated: Upon EphA or ephrin-A activation, the Src family kinase Fyn is activated, which induces the production of sphingomyelin, effectively liberating ephrin-A5 from its *cis* signaling incompetent state in rafts, sorting it to membrane domains in which it can bind EphAs in a parallel, non-signaling *cis* configuration. Those complexes assumedly undergo CME. As a result, the amount of surface EphAs and ephrin-As is reduced. Upon internalization, the interaction of ephrin-As and EphAs might switch from a parallel to a signaling competent anti-parallel *cis* interaction, favored by the high curvature of the membrane in endosomal vesicles, potentially explaining the relative increase of *cis* over *trans* signaling during growth cone desensitization. Thus, *cis* signaling might predominantly originate from signaling endosomes, which have been previously shown to be involved in the signaling of EphAs and other RTKs (McPherson et al., 2001; Yoo et al., 2010; Boissier et al., 2013). As parallel *cis* complexes most likely lack an ubiquitin signal, they might be primarily sorted for endosomal recycling, which,

however, is outbalanced by the massive internalization of newly forming *cis* complexes.

When the impinging *trans* signals are weaker or completely absent, Fyn switches to a predominantly inactive state and allows ephrin-As to be sorted back into rafts, segregating them from EphAs and thereby preventing *cis* interaction. Thus, during resensitization, internalization of *cis* complexes abates, whilst ongoing recycling restores the original EphA and ephrin-A surface concentrations.

Notably, as I show, that adaptation is dependent on CME, whereas forward repulsive signaling is not (cf. Figure 6), the sensors that operate both tasks most likely belong to two, independently regulated populations. Hence, together with the arguments mentioned earlier, the internalization of EphA/ ephrin-A *cis* complexes is assumed to be clathrin-mediated and required for adaptation, whereas *trans* activated EphAs most likely signal from the cell surface upon blocking their internalization.

An Intracellular Storage of Ephs and Ephrins

In contrast to protein synthesis independent adaptation towards forward signals, it has not been investigated so far, whether reverse signaling, and adaptation towards it, initially depend on local protein synthesis. Over longer time periods, both forward and reverse signaling (and also adaptation) must involve either transport or local translation of EphAs and ephrin-As, respectively, as active sensors are continuously degraded and have to be replaced. This is difficult to test experimentally, however, because inhibitors act globally on protein synthesis and, eventually, kill the cells after some hours (von Philipsborn, 2007). Possibly, intracellular sensors are stored in vesicular

structures, as for example the RE and ER- or Golgi-like outposts in the peripheral growth cone (Merianda et al., 2009), from which they can be transported to the membrane on demand. Such a storage could be filled by local translation and from retrograde transport of (recycling) endosomes, as reported to occur towards the trans-Golgi network (Johannes & Popoff, 2008; Cullen & Korswagen, 2012). Sensor storages might explain why adaptation is independent on protein synthesis for a certain time period and could provide for a trafficking platform, from which the relative amount of surface EphAs and ephrin-As could be controlled. A graphical model about the trafficking of sensors (shown for EphAs) during signaling and adaptation is given in Figure 10A.

With this, enhanced *cis* signaling, followed or caused by a clathrin dependent reduction of the surface sensor levels, might outbalance the relative contribution of *trans* signals to total signaling and could, thereby, desensitize retinal growth cones (Figure 10B). When the outside signal is gone, the sensors are recycled back to the surface and *trans* signals regain dominance over *cis* signals.

Notably, even if the concepts of *cis* attenuation and *cis* signaling are completely contradictory, the result of ephrin-A/ EphA *cis* interactions is always reported to decrease the relative strength of *trans* signaling and, thereby, to desensitize growth cones towards *trans* signals (Hornberger et al., 1999; Yin et al., 2004; Marquardt et al., 2005; Carvalho et al., 2006; Kao and Kania, 2011). Thus, regardless on the mechanism their effect is based on, *cis* interactions are a good candidate to instrument the adaptive responses of retinal growth cones as predicted by our model.
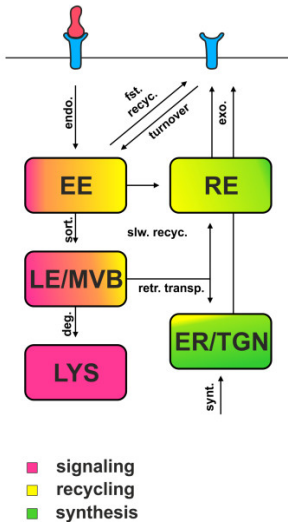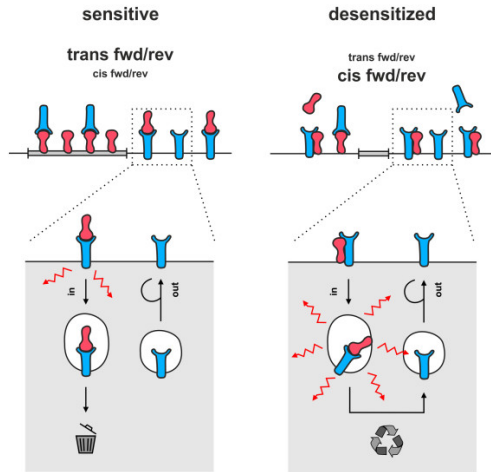
Figure 10: Concepts of Sensor Trafficking, Signaling and Adaptation.

A: Sensor trafficking during signaling and adaptation. Multiple endosomal comparments (colored boxes) are involved in the trafficking of EphAs (blue) during signaling and adaptation. Arrows indicate direction of transport. EE: Early endosome; LE/ MVB: Late Endosome and multivesicular bodies; RE: Recycling endosome; ER/ TGN: Endoplasmatic reticulum and trans-Golgi network; LYS: Lysosome. Endo.: endocytosis; sort.: sorting; deg.: degradation; fst. recycling: fast recycling; slw. recyc.: slow recycling; retr. transp.: retrograde transport; synt.: synthesis; exo.; exocytosis. A similar diagram can be drawn for ephrin-A trafficking (not shown).

B: A hypothetical model for adaptive desensitization. Ephrin-As (red) localize to lipid raft microdomains (gray box) and are, thereby, laterally segregated from EphAs (blue) on naïve growth cones. In this sensitive state, forward and reverse *trans* interactions dominate signaling. Activated sensors are internalized with a rate 'in' and primarily undergo degradation. Fresh sensors are brought to the cell surface with a rate 'out'. Upon adaptation, ephrin-As are liberated from rafts by the action of Fyn and bind EphAs in a parallel *cis* conformation. *Cis* complexes are internalized via CME and mainly targeted for endosomal recycling. Inside endosomes, a signal producing anti-parallel *cis* interaction is favored over parallel *cis* interactions. As a result, increasing *cis* signals desensitize growth cones towards *trans* signals. As in>out, the surface level of sensors are decreased. However, as ephrin-As are sorted back into rafts upon resensitisation, recycling restores the original EphA and ephrin-A surface concentrations. In the figure, only forward signal adaptation is illustrated.

III. THE FUNCTION OF CO-ADAPTATION

The results of this work provide first compelling evidence for the co-regulated adaptation of retinal growth cones towards repulsive ephrin-A and EphA signals. However, as the system even without adaptation is highly adaptive, demonstrated by the flexibility in mapping for example after experimental ablation of parts of the retina or the tectum (Gaze and Sharma, 1970; Yoon, 1971; Sharma, 1972; Schmidt et al., 1978), it remains to be elucidated, what the *in vivo* function of co-adaptation might be.

During map formation, retinal growth cones are assumed to be guided by gradients of EphAs and ephrin-As on the tectum. However, as guidance cue gradients are rather shallow (Reber et al., 2004), the individual growth cones have to detect extremely small differences in the concentrations of these cues, in order to read out the directional information encoded in the gradients. A growth cone with an average diameter of 15μm navigating in a gradient with an estimated slope of ~1% (in an optimal case centered on a concentration of about the dissociation constant of EphA/ ephrin-A binding; K_D=10nM), therefore, is assumed to detect the difference of some few single molecules across its width. Thus, as reviewed recently, growth cone guidance is on the edge to the physical limits of chemotaxis (Goodhill, 2016).

Although adaptation can most likely not overcome physical constrains like thermal noise and receptor binding noise (Goodhill, 2016) and growth cones move too slow for an effective time averaging of individual measurements (as for example utilized in bacterial chemotaxis; reviewed in Micali and Endres, 2016), it might help to prevent the saturation of downstream signaling pathways. Thus, reducing the amount of receptors available for *trans* interactions by

promoting *cis* interactions at high ligand concentrations, might keep *trans* signaling in the dynamic range of the signaling system, though, at the cost of sensitivity. However, this would require different signaling pathways for *trans* and *cis* signaling, or a *cis* interaction that does not result in signaling (see above).

Moreover, adaptation might be needed for retinal growth cones to innervate the tectum from its anterior pole during development. The anterior tectum expresses high levels of EphAs and should, therefore, repel the growth cones in the optic tract, arriving at E6 (Mueller et al., 2000). Through modeling, I could show that adaptation could theoretically enable growth cones to overcome this EphA barrier and would still allow the formation of a topographic map, once entered (cf. Figure 8). This hypothesis, however, would require the presence of a cue, which desensitizes growth cones in front of the tectum. Studies in *Xenopus* propose a role for FGF2 on tectal innervation, as retinal axons, expressing a dominant negative FGF receptor (FGFR), avoid the tectum and do not enter (McFarlane et al., 1996). Therefore, FGFR signaling might potentially be involved in adaptation towards EphA and ephrin-A signals. In *Xenopus*, FGF2 is expressed at high levels in front of the tectum, but not within the tectum at developmental stage 39. Masking this discrete expression pattern by global application of soluble FGF2 causes retinal growth cones to completely overgrow the tectum (McFarlane et al., 1995), further supporting the desensitizing role of FGFR signaling towards EphA and ephrin-A signals. In the early chick tectum (E3), FGF gradients have been reported to induce the graded expression of EphAs and ephrin-As (Chen et al., 2009). Although it has to be elucidated, whether there is FGF expression in front of the chicken tectum at E6, the link between FGF and EphAs/ ephrin-As makes FGF an excellent candidate for the predicted, pre-tectal desensitization source. Thus, adaptation might play a role in bringing RGC growth cones into the tectum.

IV. OUTLOOK AND OPEN QUESTIONS

To better understand the mechanisms and the function of adaptation, several questions should be addressed in the future:

First of all, it is to be confirmed that internalized sensors are indeed recycled back to the growth cones' surface upon resensitization. A co-staining of SNAP-ephrin-A5 and markers for recycling endosomes, like Rab11, could provide for an answer to this question.

Moreover, one should further investigate the dynamics of desensitization, for example by evaluating the collapse rates of growth cones at different time points in ephrin-A5 and EphA3 collapse assays and try to understand the role of *cis* interactions for adaptation. To investigate *cis* interactions, a tagged EphA expression construct would be extremely helpful. Tagged ephrin-A and EphA could then be used (e.g. in a FRET study) to localize and quantify their interaction within the same growth cone. Additionally, one should find an approach to check, whether *cis* interactions are able to activate the involved sensors, or not. In parallel, it would be interesting to search for a possible implementation of non-signaling *cis* interactions within the computational model. As a complete masking of EphAs through ephrin-As will prevent nasal growth cones (high expression of ephrin-As; low EphAs) from correct mapping, limiting the fraction of sensors that can be engaged for *cis* interactions might reconcile them with mapping. Modeling could also be used to address the question, whether *cis* interactions would have to attenuate both, EphA forward and ephrin-A reverse signals, for the latter of which there is no experimental evidence.

Finally, although the basic performance of the updated model including adaptation seems unaltered, its full power in reproducing the existing *in vitro* and *in vivo* evidence from regeneration and genetic experiments is still to be evaluated.

SUPPLEMENT

I. Ephrin-A/ EphA Binding Constants and Effects of EphA Clustering

Interactions of ephrins and Ephs (at least within the same subclass) are commonly assumed to be highly promiscuous, meaning that all EphAs bind all ephrin-As with about the same affinity (Pasquale, 2004; Dai et al., 2014). Although binding constants of different Eph-ephrin pairs have been repeatedly measured (Gale et al., 1996; Himanen et al., 2004; Noberini et al., 2012), those measurements were performed under widely diverging conditions with different measuring systems, making it difficult to compare the existing results. Thus, in contrast to the general assumption of promiscuity, it might be possible that interactions between all of the six ephrin-As and nine EphAs are not completely redundant in their signaling outcome. In fact, it has been proposed that spatial clustering of EphAs enhances forward signaling (Janes et al., 2012), bringing into play a new feature of signaling quality that might depend on specific EphA - ephrin-A interactions. Moreover, some recent findings raise serious doubts on the promiscuity of ephrin-Eph binding (Rohani et al., 2014; Reber, 2015, unpublished data), endorsing a substantial degree of specificity to individual ephrin-A - EphA pairs.

To shed new light on this controversy, I used the BLItz biolayer interferometer (Pall ForteBio, Menlo Park, USA) to measure the binding constants of selected ephrin-A and EphA candidates at different EphA concentrations. The BLItz system utilizes light interference to measure the immobilization of protein to an optical biosensor. Biosensors are functionalized glas fibers to which a protein-sensor of choice can be coupled (e.g. via the streptavidin-biotin system). Using the interference pattern from a loaded biosensor as reference, any change in the number of protein on the sensor (e.g. through interaction with a ligand) can be

detected as a shift in the interference pattern (http://www.fortebio.com/bli-technology.html, access date: 2016/05/11). For my experiments, streptavidin coated biosensors were loaded with 5µg/ml biotinylated ephrin-A2-Fc (mouse; #BT603), -A3-Fc (human, #BT359) or -A5-Fc (human, #BT374; all from R&D Systems) and the binding kinetics was measured using concentration series of 0, 3, 15, 33 and 100µg/ml EphA3-Fc or EphA4-Fc (mouse, #641-A4; R&D Systems), (loading: 120sec, baseline: 30sec, association: 120sec, dissociation: 120sec; all in BLItz kinetics buffer). KDs were calculated from on and off rates derived by software from local curve fits corrected for start of association and dissociation.

Notably, some ephrin-As bound EphA3 or EphA4 with substantially lower affinity at low concentrations of Eph, compared to higher concentrations, hinting at a potential difference in detecting Eph clusters, which are assumed to be only present at high concentrations. In those cases, namely for ephrin-A5 - EphA3 and ephrin-A2 - EphA4, K_{DS} shifted from >25nM to <10nM with increasing Eph concentration (Figure S1A, C). For ephrin-A5 - EphA4, a less pronounced shift was observed, whereas ephrin-A2 - EphA3 and ephrin-A3 - EphA3 showed a constant K_D of <10nM at all concentrations (Figure S1C, D). These results imply a differential specificity of ephrin-As in their ability to discriminate between individual, clustered and non-clustered EphAs. The mean K_{DS} (averaged over all concentrations) of my measurements are very similar to the binding constants reported by others (in the low nanomolar range; Gale et al., 1996; Himanen et al., 2004; Noberini et al., 2012).
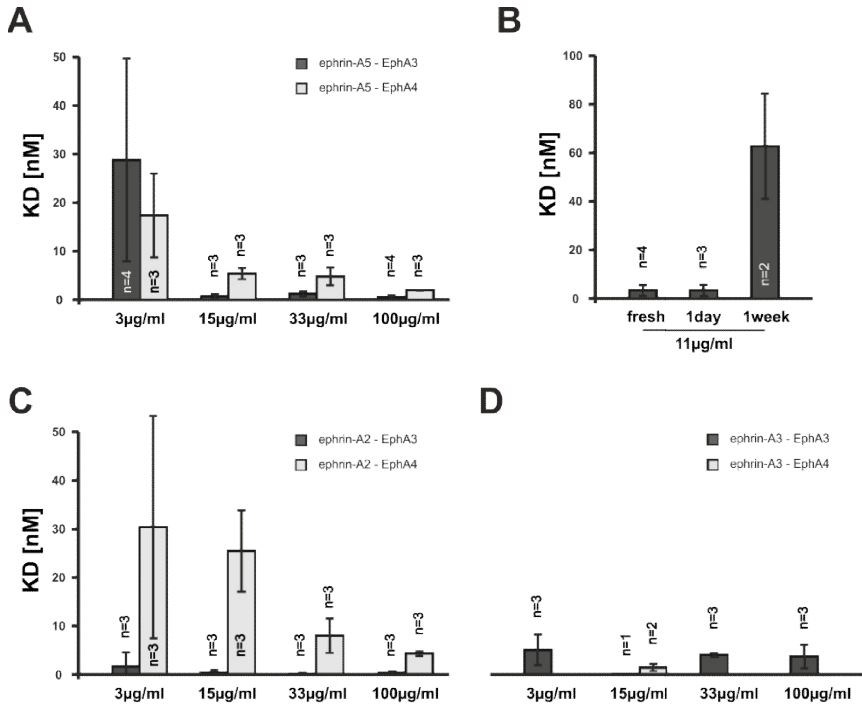
Figure S1: Binding constants of selected ephrin-A - EphA interactions derived from BLItz measurements.

A: Ephrin-A5 binding to EphA3 or EphA4. Binding constants (K_D in nM) of ephrin-A5 and EphA3 or EphA4, respectively. Ephrin-A5 binds both EphAs with substantially decreased affinity at low concentrations (<15µg/ml).

B: Stability of Eph clusters. Potential EphA3 clusters are stable for at least one day at a concentration of 11µg/ml and disassemble and/ or degrade after one week in solution as indicated by a strong increase in K_D.

C: Ephrin-A2 binding to EphA3 or EphA4. K_Ds of ephrin-A2 - EphA4 binding show the same trend as seen for ephrin-A5, whereas ephrin-A2 binds EphA3 with overall low K_D at all concentrations.

D: Ephrin-A3 binding to EphA3 or EphA4. Ephrin-A3 - EphA3 as seen for ephrin-A2 - EphA3. Ephrin-A3 binds EphA4 with high affinity at 15µg/ml.

However, while it has been reported of dimeric ephrin-A5-Fc binding with much higher affinity to EphA3 compared to ephrin-A5 monomers (Pabbisetty et al., 2006), an effect of concentration-dependent EphA multimerization on the binding to specific ephrin-As is undescribed so far and might have interesting implications for ephrin-A reverse signaling *in vitro* and *in vivo*.

Further studies are needed to confirm these findings and it should be checked, at which concentrations EphAs begin to cluster in solution. For *in vitro* assays, it would be moreover important to know how long these clusters are stable in solution. First tests indicate, that EphA3 forms clusters at concentrations ≥11µg/ml, which are stable at least for one day when kept at 4°C and are completely dissolved and/ or degraded after one week in solution (Figure S1B).

II. Model Code

```
%-------------------Version 1.11-----------------------------------------000
clear all

%% GENERAL PARAMETERS-----------------------------------------------------

NoGrowthCone    = 200;
SizeGrowthCone  = 3;
offset          = (SizeGrowthCone-1)/2;
GCcutoff        = 0.01;
steps           = 30000;
Qx              = 0;                                                       010
Qy              = 0;
sigma           = 0.12;
mu              = 0.006;
lambda          = 0.0045;
knockIn         = 0;
cis_factor      = 1;
pre_adap        = 1;


no_adap         = 10;
x_shift         = 0;                                                      020
C_dynamic       = 1;
C               = 100;


Pedestal_Receptor_Retina=0;
Pedestal_Ligand_Retina=0;
Pedestal_Receptor_Target=0;
Pedestal_Ligand_Target=0;



FieldSizeX      = 50;                                                     030
FieldSizeXtd    = FieldSizeX + 2*offset;
o               = 100/FieldSizeX;
FieldSizeY      = 8;
FieldSizeYtd    = FieldSizeY + 2*offset;
kappa_retina    = o*0.025;
omega_retina    = 0.4;


ftw = 0;

adap            = 1;                                                      040
adapHistory     = 10;



%% DEFINING VECTORS AND MATRICES-----------------------------------------


YDrang = [(1-Qy)/3 1/3+(1-Qy)/3 1];

GrowthConeLigand   = zeros(FieldSizeXtd,FieldSizeYtd);
Lxy   = zeros(FieldSizeXtd,FieldSizeYtd);
                                                                         050
GrowthConeReceptor = zeros(FieldSizeXtd,FieldSizeYtd);
Rxy = zeros(FieldSizeXtd,FieldSizeYtd);

AxonReceptor = zeros(1,NoGrowthCone);
AxonLigand   = zeros(1,NoGrowthCone);
```

```
        AxonReceptor_REF = zeros(1,NoGrowthCone);
        AxonLigand_REF   = zeros(1,NoGrowthCone);


        xtHistory  = zeros(steps,NoGrowthCone);
060     ytHistory  = zeros(steps,NoGrowthCone);


        DxHistory        = zeros(steps,NoGrowthCone);
        AbsDxHistory     = zeros(steps,NoGrowthCone);
        QxHistory        = zeros(steps,NoGrowthCone);
        FactorHistory    = zeros(steps,1);


        adapmeandenom    = sum(1:adapHistory);


        ValAdapRec          = zeros(1,NoGrowthCone);
070     ValAdapLig          = zeros(1,NoGrowthCone);
        ValAdapRecHistory   = zeros(steps,NoGrowthCone);
        ValAdapLigHistory   = zeros(steps,NoGrowthCone);
        AbsAdapRec          = zeros(1,NoGrowthCone);
        AbsAdapLig          = zeros(1,NoGrowthCone);
        AbsAdapRecHistory   = zeros(1,NoGrowthCone);
        AbsAdapLigHistory   = zeros(1,NoGrowthCone);


        ValResRec           = zeros(steps,NoGrowthCone);
        ValResLig           = zeros(steps,NoGrowthCone);
080     ValResRecHistory    = zeros(steps,NoGrowthCone);
        ValResLigHistory    = zeros(steps,NoGrowthCone);


        AdapCoeff        = zeros(steps,NoGrowthCone);
        AdapmeanCoeff    = ones (steps,NoGrowthCone);
        ResRecCoeff      = ones (steps,NoGrowthCone);
        ResLigCoeff      = ones (steps,NoGrowthCone);


        ReceptorHistory = zeros(steps,NoGrowthCone);
        LigandHistory   = zeros(steps,NoGrowthCone);
090
        GC_GCfactor_History = zeros(1,steps);


        %% SUBSTRATES-------------------------------------------------

        SubstrateExpon;
        %SubstrateLigandGap;
        %SubstrateReceptorGap;
        %SubstrateTectalInnervation;

100     %% ALLOCATION OF STARTPOSITIONS-------------------------------------

        if NoGrowthCone == 1
         YStartPos = ceil(FieldSizeX/2);
        else
         YStartPos =  round(linspace(offset,FieldSizeX,NoGrowthCone));
        end

        a=0.5;c=0.5;
        [W, V] = meshgrid(1:FieldSizeY, 1:FieldSizeX);
110     gaussian = @(x0,y0) exp(-(a*(V-x0).^2 + c*(W-y0).^2));
        weightxtd = zeros(FieldSizeXtd, FieldSizeYtd);

        tic
        datestr(now);
```

```
%% INITIALISATION---------------------------------------------------------

for n=1:NoGrowthCone
    xt  = 1+x_shift+offset;
                                                                        120
    if NoGrowthCone == 1
        yt  = ceil(FieldSizeY/2);
    else
        yt  = round(((FieldSizeY-1)/(NoGrowthCone-1))*...
            n+((NoGrowthCone-FieldSizeY)/(NoGrowthCone-1))) + offset;
    end


    AxonReceptor(n) = ((2*(omega_retina*exp(kappa_retina*(YStartPos(n)-...
                    FieldSizeX/2))))+Pedestal_Receptor_Retina)*...     130
                    pre_adap;
    AxonLigand(n)   = ((2*(omega_retina*exp(-kappa_retina*(YStartPos(n)-...
                    1-FieldSizeX/2))))+Pedestal_Ligand_Retina)*pre_adap;

    AxonReceptor_REF(n) = ((2*(omega_retina*exp(kappa_retina*...
                        (YStartPos(n)-FieldSizeX/2))))+...
                        Pedestal_Receptor_Retina)*pre_adap;
    AxonLigand_REF(n)   = ((2*(omega_retina*exp(-kappa_retina*...
                        (YStartPos(n)-1-FieldSizeX/2))))+...
                        Pedestal_Ligand_Retina)*pre_adap;             140

    ReceptorHistory(1,n)= AxonReceptor(n);
    LigandHistory(1,n)= AxonLigand(n);


if knockIn > 0
    for f=1:floor(NoGrowthCone/2)
        if n==2*f
            AxonReceptor(n) = AxonReceptor(n)+knockIn;
            AxonLigand(n)   = AxonLigand(n);                          150
            break
        else
            AxonReceptor(n) = AxonReceptor(n);
            AxonLigand(n)   = AxonLigand(n);
        end
    end

end

    xrandom = rand;                                                   160
    if(xrandom < (1-Qx)/SizeGrowthCone)
        xtDirection = -1;
    elseif(xrandom < 1/SizeGrowthCone+(1-Qx)/SizeGrowthCone)
        xtDirection = 0;
    else
        xtDirection = 1;
    end

    yrandom = rand;
    if(yrandom < YDrang(1))                                           170
        ytDirection = -1;
    elseif(yrandom < YDrang(2))
        ytDirection = 0;
    else
        ytDirection = 1;
    end
```

```
          if xt+xtDirection<1+offset
                  xtDirection=0;
          elseif xt+xtDirection>FieldSizeX+offset
180               xtDirection=0;
          end

          if yt+ytDirection<1+offset
                  ytDirection=0;
          elseif yt+ytDirection>FieldSizeY+offset
                  ytDirection=0;
          end


190       Lxy = SubstrateLigand;
          Rxy = SubstrateReceptor;

          Dx1 = abs(log(((AxonReceptor(n)*(Lxy(xt,yt)+AxonLigand(n)))/...
              (AxonLigand(n)*(Rxy(xt,yt)+AxonReceptor(n))))));
          Dx2 = abs(log(((AxonReceptor(n)*...
              (Lxy(xt+xtDirection,yt+ytDirection)+ AxonLigand(n)))/...
              (AxonLigand(n)*(Rxy(xt+xtDirection,yt+ytDirection)+...
              AxonReceptor(n))))));

200       DxHistory(1,n) = Dx1;

          WDx1 = wkeitpd(Dx1,sigma);
          WDx2 = wkeitpd(Dx2,sigma);

          if ftw == 1;
                  xt=xt+1;
                  yt=yt;

          elseif ftw == 0;
210           if rand>wkeit01(WDx1,WDx2);
                  xt = xt+xtDirection;
                  yt = yt+ytDirection;
              end
          end

          xtHistory(1,n) = xt;
          ytHistory(1,n) = yt;

          AdapCoeff(1,n) = 1;
220   end




      %% ITERATION--------------------------------------------------------

      for ii=2:steps

          if C_dynamic == 1
230           GC_GCfactor=C*(-exp(-log(2.^((ii./(steps./2)).^5)))+1);
          elseif C_dynamic == 0
              GC_GCfactor=C;
          end

          FactorHistory(ii)=GC_GCfactor;
          GC_SUBfactor=1;
```

100

```
allGrowthConeLigand   = zeros(FieldSizeXtd,FieldSizeYtd);
allGrowthConeReceptor = zeros(FieldSizeXtd,FieldSizeYtd);
                                                                        240
for nn=1:NoGrowthCone

    xn=xtHistory(ii-1,nn)-1;
    yn=ytHistory(ii-1,nn)-1;
    weight=gaussian(xn,yn);
    weight(weight<GCcutoff)=0;
    weightxtd(2:FieldSizeXtd-1,2:FieldSizeYtd-1)= ...
              weight(1:FieldSizeX,1:FieldSizeY);

    allGrowthConeLigand   = allGrowthConeLigand + ...             250
                            AxonLigand(nn).*weightxtd;
    allGrowthConeReceptor = allGrowthConeReceptor + ...
                            AxonReceptor(nn).*weightxtd;

end

for n=1:NoGrowthCone

    if ii<=no_adap                                                260
    ReceptorHistory(ii,n)=ReceptorHistory(1,n);
    LigandHistory(ii,n)=LigandHistory(1,n);
end

    xt = xtHistory(ii-1,n);
    yt = ytHistory(ii-1,n);

    weight=gaussian(xt-1,yt-1);
    weight(weight<GCcutoff)=0;
    weightxtd(2:FieldSizeXtd-1,2:FieldSizeYtd-1) = ...            270
              weight(1:FieldSizeX,1:FieldSizeY);

    currentGrowthConeLigand   = AxonLigand(n)  .*weightxtd;
    currentGrowthConeReceptor = AxonReceptor(n).*weightxtd;

    meancurrentGCLigand   = sum(sum(currentGrowthConeLigand))/...
                            nnz(currentGrowthConeLigand);
    meancurrentGCReceptor = sum(sum(currentGrowthConeReceptor))/...
                            nnz(currentGrowthConeReceptor);
                                                                        280

    currentGCLigandRef   = AxonLigand_REF(n)  .*weightxtd;
    currentGCReceptorRef = AxonReceptor_REF(n).*weightxtd;

    meancurrentGCLigandRef   = sum(sum(currentGCLigandRef))/...
                               nnz(currentGCLigandRef);
    meancurrentGCReceptorRef = sum(sum(currentGCReceptorRef))/...
                               nnz(currentGCReceptorRef);

                                                                        290
    GrowthConeLigand   = allGrowthConeLigand   - ...
                         currentGrowthConeLigand;
    GrowthConeReceptor = allGrowthConeReceptor - ...
                         currentGrowthConeReceptor;
            xrandom = rand;
            if(xrandom < (1-Qx)/SizeGrowthCone)
                xtDirection = -1;
```

```
300              elseif(xrandom < 1/SizeGrowthCone+(1-Qx)/SizeGrowthCone)
                     xtDirection = 0;
                 else
                     xtDirection = 1;
                 end

                 yrandom = rand;
                 if(yrandom < YDrang(1))
                     ytDirection = -1;
                 elseif(yrandom < YDrang(2))
310                  ytDirection = 0;
                 else
                     ytDirection = 1;
                 end

                 if xt+xtDirection<1+offset
                     xtDirection=0;
                 elseif xt+xtDirection>FieldSizeX+offset
                     xtDirection=0;
                 end
320              if yt+ytDirection<1+offset
                     ytDirection=0;
                 elseif yt+ytDirection>FieldSizeY+offset
                     ytDirection=0;
                 end


                 rev = GC_SUBfactor.*currentGrowthConeLigand.*...
                 SubstrateReceptor+GC_GCfactor.*currentGrowthConeLigand.*...
330              GrowthConeReceptor+cis_factor.*currentGrowthConeLigand.*...
                 currentGrowthConeReceptor;

                 fwd = GC_SUBfactor.*currentGrowthConeReceptor.*...
                 SubstrateLigand+GC_GCfactor.*currentGrowthConeReceptor.*...
                 GrowthConeLigand+cis_factor.*currentGrowthConeReceptor.*...
                 currentGrowthConeLigand;


                 fwdmean=sum(sum(fwd))/nnz(fwd);
340              revmean=sum(sum(rev))/nnz(rev);


                 Dx=abs(log(revmean/fwdmean));
                 DxHistory(ii,n) = Dx;


                 weight=gaussian(xt-1+xtDirection,yt-1+ytDirection);
                 weight(weight<GCcutoff)=0;
                 weightxtd(2:FieldSizeXtd-1,2:FieldSizeYtd-1) = ...
350                  weight(1:FieldSizeX,1:FieldSizeY);

                 currentGrowthConeLigand_target   = AxonLigand(n).*...
                 weightxtd;
                 currentGrowthConeReceptor_target = AxonReceptor(n).*...
                 weightxtd;

         rev_target = GC_SUBfactor.*currentGrowthConeLigand_target.*...
                     SubstrateReceptor+GC_GCfactor.*...
                     currentGrowthConeLigand_target.*GrowthConeReceptor+...
```

```
                cis_factor.*currentGrowthConeLigand_target.*...      360
                currentGrowthConeReceptor_target;


    fwd_target = GC_SUBfactor.*currentGrowthConeReceptor_target.*...
                SubstrateLigand+GC_GCfactor.*...
                currentGrowthConeReceptor_target.*GrowthConeLigand+...
                cis_factor.*currentGrowthConeReceptor_target.*...
                currentGrowthConeLigand_target;



    fwdmean_target=sum(sum(fwd_target))/nnz(fwd_target);            370
    revmean_target=sum(sum(rev_target))/nnz(rev_target);


    Dx_target=abs(log(revmean_target/fwdmean_target));
    AbsDxHistory(ii,n) = log(revmean_target/fwdmean_target);




%% ------------------------Adaptation------------------------------------
                                                                   380
    if adap==1

        adaprev = currentGrowthConeLigand.*...
                 (currentGrowthConeReceptor+SubstrateReceptor);
        adapfwd = currentGrowthConeReceptor.*...
                 (currentGrowthConeLigand+SubstrateLigand);
        adaprevmean = sum(sum(adaprev))/nnz(adaprev);
        adapfwdmean = sum(sum(adapfwd))/nnz(adapfwd);

        AdapCoeff(ii,n)=1/(1+(mu*(abs(log(adaprevmean/...          390
         adapfwdmean)))));

        ResRecCoeff(ii,n) = lambda*(meancurrentGCReceptorRef-...
                           meancurrentGCReceptor);
        ResLigCoeff(ii,n) = lambda*(meancurrentGCLigandRef-...
                           meancurrentGCLigand);

        ResRecCoeff(2,n) = 1;
        ResLigCoeff(2,n) = 1;
                                                                   400

        if ii>adapHistory && ii>no_adap
           AdapmeanCoeff(ii,n) = 0;

            for k=0:adapHistory
                AdapmeanCoeff(ii,n) = AdapmeanCoeff(ii,n) + ...
                                     k*AdapCoeff(ii-adapHistory+k,n);
            end

          AdapmeanCoeff(ii,n) = AdapmeanCoeff(ii,n)/adapmeandenom;  410

          AxonReceptor(n) = AxonReceptor(n)/...
                           AdapmeanCoeff(ii,n)+ResRecCoeff(ii,n);
          AxonLigand(n)   = AxonLigand(n)/...
                           AdapmeanCoeff(ii,n)+ResLigCoeff(ii,n);

                    ReceptorHistory(ii,n) = AxonReceptor(n);
                    LigandHistory(ii,n)   = AxonLigand(n);
```

```
                    end
420
                else
                    ReceptorHistory(ii,n) = AxonReceptor(n);
                    LigandHistory(ii,n)   = AxonLigand(n);
                end


        %%----------------------------------------------------------------
430
                wDx = wkeitpd(Dx,sigma);
                wDx_target = wkeitpd(Dx_target,sigma);

                if ftw == 1;
                    xt=xt+1;
                    yt=yt;

                elseif ftw == 0;

440                 if rand>=wkeit01(wDx,wDx_target);
                        xt = xt+xtDirection;
                        yt = yt+ytDirection;
                    end
                end

                xtHistory(ii,n) = xt;
                ytHistory(ii,n) = yt;

            end
450
            clc;
            steps-ii
        end
```

Alternative Implementation of Adaptation:

```
% ------------------------Adaptation--------------------------------000

    %independent adaptation of fwd and rev:

        if adap==1

        AdapCoeff_rec(ii,n)=(log(1/ReceptorHistory(1,n)*...
                            SubstrateLigand(xt,yt)));
        AdapCoeff_lig(ii,n)=(log(1/LigandHistory(1,n)*...
                            SubstrateReceptor(xt,yt)));              010


        AxonReceptor(n)=((AxonReceptor(n)-SubstrateReceptor(xt,yt))*...
                        exp(-(abs(tau*AdapCoeff_rec(ii,n)^2))))+...
                        SubstrateReceptor(xt,yt);
        AxonLigand(n)=(AxonLigand(n)-SubstrateLigand(xt,yt))*...
                        exp(-(abs(tau*AdapCoeff_lig(ii,n)^2)))+...
                        SubstrateLigand(xt,yt);

        ReceptorHistory(ii,n) = AxonReceptor(n);                    020

        LigandHistory(ii,n) = AxonLigand(n);


        else
            ReceptorHistory(ii,n) = AxonReceptor(n);
            LigandHistory(ii,n)   = AxonLigand(n);

        end
                                                                    030

%%----------------------------------------------------------------------
```

Substrates:

Tectal gradient field (SubstrateExpon.m):

```
000     SubstrateLigand=zeros(FieldSizeXtd,FieldSizeYtd);
        SubstrateReceptor=zeros(FieldSizeXtd,FieldSizeYtd);

        omega_target=1;
        kappa_target=0.05;


        for zi=1:1:FieldSizeX
            for zn=1:1:FieldSizeY
                SubstrateLigand(zi+offset,zn+offset) = omega_target*...
010             exp(kappa_target*(zi-FieldSizeX/2))+Pedestal_Ligand_Target;

                 SubstrateReceptor(zi+offset,zn+offset) = omega_target*...
                exp(-kappa_target*(zi-1-FieldSizeX/2))+...
                 Pedestal_Receptor_Target;
            end
        end
```

ephrin-A gap assay substrate (SubstrateLigandGap.m):

```
000     SubstrateLigand=zeros(FieldSizeXtd,FieldSizeYtd);
        SubstrateReceptor=zeros(FieldSizeXtd,FieldSizeYtd);


        l=4;
        lueckenbreite=ceil(0.1*FieldSizeX);
        unterkante=ceil(0.25*FieldSizeX);
        oberkante=unterkante+lueckenbreite;


010     for zi=1:1:FieldSizeY
            for zn=1:1:unterkante
                SubstrateLigand(zn+offset,zi+offset) = l;
                SubstrateReceptor(zn+offset,zi+offset) = 0;
            end

            for zn=unterkante+1:1:oberkante
                SubstrateLigand(zn+offset,zi+offset) = 0;
                SubstrateReceptor(zn+offset,zi+offset) = 0;
            end
020
            for zn=oberkante+1:1:FieldSizeX
                SubstrateLigand(zn+offset,zi+offset) = l;
                SubstrateReceptor(zn+offset,zi+offset) = 0;
            end
        end
```

EphA gap assays (SubstrateReceptorGap.m):

```
SubstrateLigand=zeros(FieldSizeXtd,FieldSizeYtd);                        000
SubstrateReceptor=zeros(FieldSizeXtd,FieldSizeYtd);


r=4;
lueckenbreite=ceil(0.1*FieldSizeX);
unterkante=ceil(0.25*FieldSizeX);
oberkante=unterkante+lueckenbreite;


for zi=1:1:FieldSizeY                                                    010
    for zn=1:1:unterkante
        SubstrateLigand(zn+offset,zi+offset) = 0;
        SubstrateReceptor(zn+offset,zi+offset) = r;
    end

    for zn=unterkante+1:1:oberkante
        SubstrateLigand(zn+offset,zi+offset) = 0;
        SubstrateReceptor(zn+offset,zi+offset) = 0;
    end
                                                                         020
    for zn=oberkante+1:1:FieldSizeX
        SubstrateLigand(zn+offset,zi+offset) = 0;
        SubstrateReceptor(zn+offset,zi+offset) = r;
    end
end
```

III. GUI and Code of the Fiber-Counting Tool

GUI:
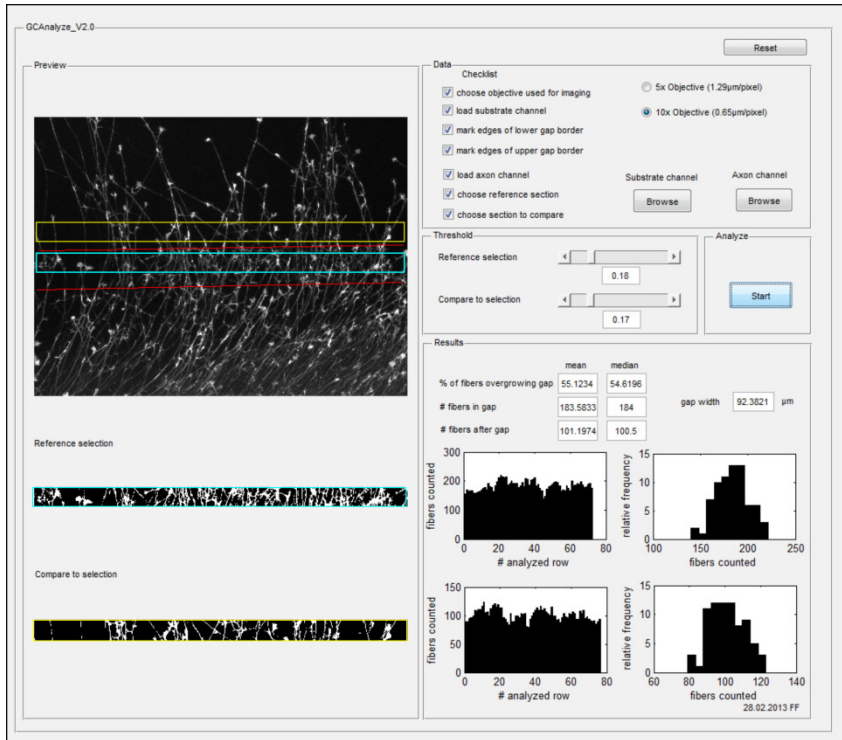
Figure S2: Graphical user interface of the fiber-counting tool

To evaluate the percentage of stopping fibers (e.g. in an EphA3 gap assay), two rectangular regions of interest (ROIs) were drawn on the images' axon channel, parallel to the edges of the gap (ROI 1, blue, in the gap, ROI 2, yellow, immediately behind the gap). The position of the gap was previously determined in the substrate channel and marked in the GUI (red lines). After manual thresholding, ROIs were line-scanned and a histogram of each pixel row was evaluated counting signal peaks. Peaks broader than average axon widths were either divided into several counts, or excluded from evaluation when reaching the average size of a growth cone. Counts from all pixel rows in one ROI were averaged and the percentage of stopping fibers was calculated from mean counts in ROI 1 and ROI 2 (% $F_{stopping}$ = 100-[(F_{ROI2}*100)/F_{ROI1}]).

Code:

```
function varargout = gcanalyze_v2_0(varargin)
gui_Singleton = 1;
gui_State = struct('gui_Name',       mfilename, ...
                   'gui_Singleton',  gui_Singleton, ...
                   'gui_OpeningFcn', @gcanalyze_v2_0_OpeningFcn, ...
                   'gui_OutputFcn',  @gcanalyze_v2_0_OutputFcn, ...
                   'gui_LayoutFcn',  [] , ...
                   'gui_Callback',   []);
if nargin && ischar(varargin{1})
    gui_State.gui_Callback = str2func(varargin{1});
end

if nargout
    [varargout{1:nargout}] = gui_mainfcn(gui_State, varargin{:});
else
    gui_mainfcn(gui_State, varargin{:});
end

% --- Executes just before gcanalyze_v2_0 is made visible.
function gcanalyze_v2_0_OpeningFcn(hObject, ~, handles, varargin)
handles.output = hObject;

guidata(hObject, handles);

% --- Outputs from this function are returned to the command line.
function varargout = gcanalyze_v2_0_OutputFcn(~, ~, handles)
varargout{1} = handles.output;


%_____BROWSE 1_____

% --- Executes on button press in browse_1.
function browse_1_Callback(hObject, ~, handles)
handles.output=hObject;
[filename,path]=uigetfile('*.tif');
filegap=fullfile(path,filename);
savepath ('padthdef.m')

imshow(filegap,'Parent',handles.preview_whole);
set(handles.checkbox1,'Value', 1);

global unterkante_positionen;
unterkante_positionen=ginput(2);
unterkante=polyfit(unterkante_positionen(:,1),unterkante_positionen(:,2),1);

x=0:0.1:100;
y=polyval(unterkante,x);
hold on
plot(x,y,'k')
plot(unterkante_positionen(:,1),unterkante_positionen(:,2),'r')
set(handles.checkbox2,'Value', 1);

global oberkante_positionen
oberkante_positionen=ginput(2);
oberkante=polyfit(oberkante_positionen(:,1),oberkante_positionen(:,2),1);

w=0:0.1:100;
z=polyval(oberkante,w);
hold on
plot(w,z,'k')
```

110

```
plot(oberkante_positionen(:,1),oberkante_positionen(:,2),'r')
set(handles.checkbox3,'Value', 1);

global dist
global dist_txt
global pixscale

if get(handles.button_5Ob,'Value')==1
    pixscale=1.29;
elseif get(handles.button_10Ob,'Value')==1
    pixscale=0.65;
else
    pixscale=0;
end

dist1=abs((unterkante_positionen(3))-(oberkante_positionen(3)));
dist1_txt=num2str(dist);
dist2=abs((unterkante_positionen(4))-(oberkante_positionen(4)));
dist2_txt=num2str(dist);
dist=((dist1+dist2)/2)*pixscale;
dist_txt=num2str(dist);

set(handles.gap_width,'String',dist_txt);


function gap_width_Callback(hObject, eventdata, handles)
global dist_txt
set(hObject,'String',dist_txt);


% --- Executes during object creation, after setting all properties.
function gap_width_CreateFcn(hObject, eventdata, handles)
if ispc && isequal(get(hObject,'BackgroundColor'),
get(0,'defaultUicontrolBackgroundColor'))
    set(hObject,'BackgroundColor','white');
end

% --- Executes on button press in button_5Ob.
function button_5Ob_Callback(hObject, eventdata, handles)
global pixscale

get(hObject,'Value')
if get(handles.button_5Ob,'Value')==1
    set(handles.button_10Ob,'Value',0);
    pixscale=1.29;
    set(handles.checkobjective,'Value',1);
end

% --- Executes on button press in button_10Ob.
function button_10Ob_Callback(hObject, eventdata, handles)
global pixscale

get(hObject,'Value')
if get(handles.button_10Ob,'Value')==1
    set(handles.button_5Ob,'Value',0);
    pixscale=0.65;
    set(handles.checkobjective,'Value',1);
end


%_____BROWSE 2_____

% --- Executes during object creation, after setting all properties.
```

```
function browse_2_Callback(~, ~, handles)
 [filename,path]=uigetfile('*.tif');

file=fullfile(path,filename);
imshow(file,'Parent',handles.preview_whole);

global unterkante_positionen;
global oberkante_positionen;

hold on
plot(unterkante_positionen(:,1),unterkante_positionen(:,2),'r')
plot(oberkante_positionen(:,1),oberkante_positionen(:,2),'r')
set(handles.checkbox4,'Value', 1);

global ingap;
ingap=imcrop(gcf);
set(handles.checkbox5,'Value', 1);

global aftergap;
aftergap=imcrop(gcf);
set(handles.checkbox6,'Value', 1);
ingapbw=im2bw(ingap,0.2);
aftergapbw=im2bw(aftergap,0.2);

imshow(ingapbw,'Parent',handles.preview_select1);
imshow(aftergapbw,'Parent',handles.preview_select2);

threshvalue=0.2;
set(handles.thresh1,'Value',0.2);
set(handles.thresh1_text,'String',num2str(threshvalue));
set(handles.thresh2,'Value',0.2);
set(handles.thresh2_text,'String',num2str(threshvalue));


%_____THRESH 1_____
% --- Executes on slider movement.
function thresh1_Callback(~, ~, handles)
global ingap;
global ingapbw;
threshvalue = get(handles.thresh1,'Value');
set(handles.thresh1_text,'String',num2str(threshvalue));

ingapbw=im2bw(ingap,threshvalue);
imshow(ingapbw,'Parent',handles.preview_select1);

% --- Executes during object creation, after setting all properties.
function thresh1_CreateFcn(hObject, ~, ~)
if ispc && isequal(get(hObject,'BackgroundColor'),
get(0,'defaultUicontrolBackgroundColor'))
    set(hObject,'BackgroundColor','white');
end


function thresh1_text_Callback(~, ~, ~)


% --- Executes during object creation, after setting all properties.
function thresh1_text_CreateFcn(hObject, ~, ~)
if ispc && isequal(get(hObject,'BackgroundColor'),
get(0,'defaultUicontrolBackgroundColor'))
    set(hObject,'BackgroundColor','white');
end
```

112

```
%_____THRESH 2_____
% --- Executes on slider movement.
function thresh2_Callback(~, ~, handles)
global aftergap;
global aftergapbw;
threshvalue = get(handles.thresh2,'Value');
set(handles.thresh2_text,'String',num2str(threshvalue));
aftergapbw=im2bw(aftergap,threshvalue);
imshow(aftergapbw,'Parent',handles.preview_select2);

% --- Executes during object creation, after setting all properties.
function thresh2_CreateFcn(hObject, ~, ~)
if ispc && isequal(get(hObject,'BackgroundColor'),
get(0,'defaultUicontrolBackgroundColor'))
    set(hObject,'BackgroundColor','white');
end

function thresh2_text_Callback(~, ~, ~)


% --- Executes during object creation, after setting all properties.
function thresh2_text_CreateFcn(hObject, ~, ~)
if ispc && isequal(get(hObject,'BackgroundColor'),
get(0,'defaultUicontrolBackgroundColor'))
    set(hObject,'BackgroundColor','white');
end

% --- Executes during object creation, after setting all properties.
function preview_whole_CreateFcn(hObject, ~, ~)
if ispc && isequal(get(hObject), get(0,'defaultUicontrolBackgroundColor'))
    set(hObject,'BackgroundColor','white');
end

function figure1_CreateFcn(hObject, ~, ~)
if ispc && isequal(get(hObject), get(0,'defaultUicontrolBackgroundColor'))
    set(hObject,'BackgroundColor','white');
end

function uipanel1_CreateFcn(hObject, ~, ~)
if ispc && isequal(get(hObject), get(0,'defaultUicontrolBackgroundColor'))
    set(hObject,'BackgroundColor','white');
end


%_____START_____
% --- Executes on button press in start.
function start_Callback(~, ~, handles)
global ingapbw;
global aftergapbw;

if get(handles.button_10Ob,'Value')==1
    gcsize=20;
elseif get(handles.button_5Ob,'Value')==1
    gcsize=12;
end

axsize=2;

sizeingapbw=size(ingapbw);
colingapbw=sizeingapbw(:,1);
lineingapbw=length(ingapbw);

sizeaftergapbw=size(aftergapbw);
```

```
colaftergapbw=sizeaftergapbw(:,1);
lineaftergapbw=length(aftergapbw);

ingapfiber=zeros(colingapbw,1);
aftergapfiber=zeros(colaftergapbw,1);


for ii=1:colingapbw
    signlin(ii)=0;

    for jj=2:lineingapbw
        if ingapbw(ii,jj)==1 && ingapbw(ii,jj-1)==0
            if signlin(ii)==0;
                sigcountin=1;
                signlin(ii)=1;

            else
                sigcountin=sigcountin+1;
                signlin(ii)=signlin(ii)+1;

            end
            stimein(signlin)=jj;

            intiin=1;

        elseif ingapbw(ii,jj)==0 && ingapbw(ii,jj-1)==1
            entiin=1;
            if exist('intiin','var')==0
                intiin=0;
            end
            if intiin==1 && entiin==1

                signallengthin(ii,sigcountin)=jj-stimein(sigcountin);


                entiin=0;
                intiin=0;

                if signallengthin(ii,sigcountin) >= axsize
                    if signallengthin(ii,sigcountin) <= gcsize

ingapfiber(ii)=ingapfiber(ii)+(ceil((signallengthin(ii,sigcountin))/...
axsize));
                    else
                        ingapfiber(ii)=ingapfiber(ii)+1;
                    end
                else
                    ingapfiber(ii)=ingapfiber(ii)+1;

                end
            end
        end

    end
end


for ii=1:colaftergapbw
    signlaf(ii)=0;

    for jj=2:lineaftergapbw
        if aftergapbw(ii,jj)==1 && aftergapbw(ii,jj-1)==0
            if signlaf(ii)==0;
                sigcountaf=1;
```

```
                    signlaf(ii)=1;

                else
                    sigcountaf=sigcountaf+1;
                    signlaf(ii)=signlaf(ii)+1;

                end
                stimeaf(signlaf)=jj;

                intiaf=1;

            elseif aftergapbw(ii,jj)==0 && aftergapbw(ii,jj-1)==1
                entiaf=1;
                if intiaf==1 && entiaf==1

                    signallengthaf(ii,sigcountaf)=jj-stimeaf(sigcountaf);

                    entiaf=0;
                    intiaf=0;

                    if signallengthaf(ii,sigcountaf) >= axsize
                        if signallengthaf(ii,sigcountaf) <= gcsize
                            aftergapfiber(ii)=aftergapfiber(ii)+...
                            (ceil((signallengthaf(ii,sigcountaf))/axsize));
                        else
                            aftergapfiber(ii)=aftergapfiber(ii)+1;
                        end
                    else
                        aftergapfiber(ii)=aftergapfiber(ii)+1;

                    end
                end
            end
        end
end


fibers_in_gap=mean(ingapfiber);
fibers_after_gap=mean(aftergapfiber);
fibers_in_gap_med=median(ingapfiber);
fibers_after_gap_med=median(aftergapfiber);

fibers_crossing_gap_percent=fibers_after_gap/(fibers_in_gap/100);
fibers_crossing_gap_percent_med=fibers_after_gap_med/...
(fibers_in_gap_med/100);


res1=num2str(fibers_crossing_gap_percent);
set(handles.result,'String',num2str(res1));

res2=num2str(fibers_in_gap);
set(handles.ingap,'String',num2str(res2));

res3=num2str(fibers_after_gap);
set(handles.aftergap,'String',num2str(res3));

res4=num2str(fibers_crossing_gap_percent_med);
set(handles.median1,'String',num2str(res4));

res5=num2str(fibers_in_gap_med);
set(handles.median2,'String',num2str(res5));
```

```
res6=num2str(fibers_after_gap_med);
set(handles.median3,'String',num2str(res6));

bar(ingapfiber,'Parent',handles.result1);
xlabel(handles.result1,'# analyzed row');
ylabel(handles.result1,'fibers counted');

hist(ingapfiber,'Parent',handles.result2);
xlabel(handles.result2,'fibers counted');
ylabel(handles.result2,'relative frequency');

bar(aftergapfiber,'Parent',handles.result3);
xlabel(handles.result3,'# analyzed row');
ylabel(handles.result3,'fibers counted');

hist(aftergapfiber,'Parent',handles.result4);
xlabel(handles.result4,'fibers counted');
ylabel(handles.result4,'relative frequency');


%_____% OF AXONS OVERGROWING_____

function result_Callback(~, ~, ~)

% --- Executes during object creation, after setting all properties.
function result_CreateFcn(hObject, ~, ~)
if ispc && isequal(get(hObject,'BackgroundColor'),
get(0,'defaultUicontrolBackgroundColor'))
    set(hObject,'BackgroundColor','white');
end

%_____CHECKBOXES_____

% --- Executes on button press in checkbox1.
function checkbox1_Callback(~, ~, ~)

% --- Executes on button press in checkbox2.
function checkbox2_Callback(~, ~, ~)

% --- Executes on button press in checkbox3.
function checkbox3_Callback(~, ~, ~)

% --- Executes on button press in checkbox4.
function checkbox4_Callback(~, ~, ~)

% --- Executes on button press in checkbox5.
function checkbox5_Callback(~, ~, ~)

% --- Executes on button press in checkbox6.
function checkbox6_Callback(~, ~, ~)

% --- Executes on button press in checkobjective.
function checkobjective_Callback(hObject, eventdata, handles)


%_____AXONS IN GAP_____
function ingap_Callback(~, ~, ~)

% --- Executes during object creation, after setting all properties.
function ingap_CreateFcn(hObject, ~, ~)
if ispc && isequal(get(hObject,'BackgroundColor'),
get(0,'defaultUicontrolBackgroundColor'))
    set(hObject,'BackgroundColor','white');
end
```

```
%_____AXON AFTER GAP_____
function aftergap_Callback(~, ~, ~)

% --- Executes during object creation, after setting all properties.
function aftergap_CreateFcn(hObject, ~, ~)
if ispc && isequal(get(hObject,'BackgroundColor'),
get(0,'defaultUicontrolBackgroundColor'))
    set(hObject,'BackgroundColor','white');
end


%_____RESULTS 1 MEDIAN_____
function median1_Callback(~, ~, ~)

% --- Executes during object creation, after setting all properties.
function median1_CreateFcn(hObject, ~, ~)
if ispc && isequal(get(hObject,'BackgroundColor'),
get(0,'defaultUicontrolBackgroundColor'))
    set(hObject,'BackgroundColor','white');
end


%_____RESULTS 2 MEDIAN_____
function median2_Callback(~, ~, ~)

% --- Executes during object creation, after setting all properties.
function median2_CreateFcn(hObject, ~, ~)
if ispc && isequal(get(hObject,'BackgroundColor'),
get(0,'defaultUicontrolBackgroundColor'))
    set(hObject,'BackgroundColor','white');
end


%_____RESULTS 3 MEDIAN_____
function median3_Callback(~, ~, ~)

% --- Executes during object creation, after setting all properties.
function median3_CreateFcn(hObject, ~, ~)
if ispc && isequal(get(hObject,'BackgroundColor'),
get(0,'defaultUicontrolBackgroundColor'))
    set(hObject,'BackgroundColor','white');
end


%_____RESET_____
% --- Executes on button press in reset.
function reset_Callback(~, ~, ~)

evalin('base','clear all');
close(gcbf)
gcanalyze_v2_0
```

REFERENCES

Akiyama, H., Fukuda, T., Tojima, T., Nikolaev, V.O., Kamiguchi, H., 2016. Cyclic Nucleotide Control of Microtubule Dynamics for Axon Guidance. J. Neurosci. 36, 5636–5649.

Atapattu, L., Saha, N., Llerena, C., Vail, M.E., Scott, A.M., Nikolov, D.B., Lackmann, M., Janes, P.W., 2012. Antibodies binding the ADAM10 substrate recognition domain inhibit Eph function. J. Cell Sci. 125, 6084–6093.

Baba, A., Akagi, K., Takayanagi, M., Flanagan, J.G., Kobayashi, T., Hattori, M., 2009. Fyn tyrosine kinase regulates the surface expression of glycosylphosphatidylinositol-linked ephrin via the modulation of sphingomyelin metabolism. J. Biol. Chem. 284, 9206–9214.

Bearce, E.A., Erdogan, B., Lowery, L.A., 2015. TIPsy tour guides: how microtubule plus-end tracking proteins (+TIPs) facilitate axon guidance. Front. Cell. Neurosci. 9, 241.

Boissier, P., Chen, J., Huynh-Do, U., 2013. Epha2 signaling following endocytosis: Role of tiam1. Traffic 14, 1255–1271.

Bonhoeffer, F., Huf, J., 1985. Position-dependent properties of retinal axons and their growth cones. Nature 315, 409–410.

Brown, A., Yates, P.A., Burrola, P., Ortuño, D., Vaidya, A., Jessell, T.M., Pfaff, S.L., O'Leary, D.D., Lemke, G., 2000. Topographic mapping from the retina to the midbrain is controlled by relative but not absolute levels of EphA receptor signaling. Cell 102, 77–88.

Cai, B., Katafiasz, D., Horejsi, V., Naslavsky, N., 2011. Pre-sorting endosomal transport of the GPI-anchored protein, CD59, is regulated by EHD1. Traffic 12, 102–120.

Cang, J., Feldheim, D.A., 2013. Developmental Mechanisms of Topographic Map Formation and Alignment. Annu. Rev. Neurosci 36, 51–77.

Carvalho, R.F., Beutler, M., Marler, K.J.M., Knöll, B., Becker-Barroso, E., Heintzmann, R., Ng, T., Drescher, U., 2006. Silencing of EphA3 through a cis interaction with ephrinA5. Nat. Neurosci. 9, 322–330.

Cary, L.A., Cooper, J.A., 2000. Molecular switches in lipid rafts. Nature 406, 466–467.

Chen, Y., Mohammadi, M., Flanagan, J.G., 2009. Graded levels of FGF protein span the midbrain and can instruct graded induction and repression of neural mapping labels. Neuron 62, 773–780.

Cheng, H.J., Nakamoto, M., Bergemann, A.D., Flanagan, J.G., 1995. Complementary gradients in expression and binding of ELF-1 and Mek4 in development of the topographic retinotectal projection map. Cell 82, 371–81.

Chklovskii, D.B., Koulakov, A.A., 2004. MAPS IN THE BRAIN: What Can We Learn from Them? Annu. Rev. Neurosci. 27, 369–392.

Connor, R.J., Menzel, P., Pasquale, E.B., 1998. Expression and tyrosine phosphorylation of Eph receptors suggest multiple mechanisms in patterning of the visual system. Dev. Biol. 193, 21–35.

Cox, E.C., Müller, B., Bonhoeffer, F., 1990. Axonal guidance in the chick visual system: posterior tectal membranes induce collapse of growth cones from the temporal retina. Neuron 4, 31–7.

Cullen, P.J., Korswagen, H.C., 2012. Sorting nexins provide diversity for retromer-dependent trafficking events. Nat. Cell Biol. 14, 29–37.

Dai, D., Huang, Q., Nussinov, R., Ma, B., 2014. Promiscuous and specific recognition among ephrins and Eph receptors. Biochim. Biophys. Acta - Proteins Proteomics 1844, 1729–1740.

Day, B., To, C., Himanen, J.P., Smith, F.M., Nikolov, D.B., Boyd, A.W., Lackmann, M., 2005. Three distinct molecular surfaces in Ephrin-A5 are essential for a functional interaction with EphA3. J. Biol. Chem. 280, 26526–26532.

Deinhardt, K., Reversi, A., Berninghausen, O., Hopkins, C.R., Schiavo, G., 2007. Neurotrophins redirect p75NTR from a clathrin-independent to a clathrin-dependent endocytic pathway coupled to axonal transport. Traffic 8, 1736–1749.

Donnelly, C.J., Fainzilber, M., Twiss, J.L., 2010. Subcellular communication through RNA transport and localized protein synthesis. Traffic 11, 1498–1505.

Drescher, U., Kremoser, C., Handwerker, C., Löschinger, J., Noda, M., Bonhoeffer, F., 1995. In vitro guidance of retinal ganglion cell axons by RAGS, a 25 kDa tectal protein related to ligands for Eph receptor tyrosine kinases. Cell 82, 359–70.

Eden, E.R., White, I.J., Tsapara, A., Futter, C.E., 2010. Membrane contacts between endosomes and ER provide sites for PTP1B-epidermal growth factor receptor interaction. Nat. Cell Biol. 12, 267–72.

Eph Nomenclature Comitee, 1997, 1997. Unified Nomenclature for Eph Family Receptors and Their Ligands, the Ephrins. Cell 90, 403–404.

Feldheim, D.A., O'Leary, D.D.M., 2010. Visual Map Development: Bidirectional Signaling, Bifunctional Guidance Molecules, and Competition. Cold Spring Harb. Perspect. Biol. 1–20. doi: 10.1101/cshperspect.a001768

Fiederling, F., 2012. Modellierung und experimentelle Untersuchung der Adaptation des Reverse Signaling in retinalen Wachstumskegeln. Master's Thesis, Zool. Institute, Karlsruhe Institute of Technology (KIT).

Fivaz, M., Vilbois, F., Thurnheer, S., Pasquali, C., Abrami, L., Bickel, P.E., Parton, R.G., Van der Goot, F.G., 2002. Differential sorting and fate of endocytosed GPI-anchored proteins. EMBO J. 21, 3989–4000.

Frisén, J., Yates, P.A., McLaughlin, T., Friedman, G.C., O'Leary, D.D.M., Barbacid, M., 1998. Ephrin-A5 (AL-1/RAGS) is essential for proper retinal axon guidance and topographic mapping in the mammalian visual system. Neuron 20, 235–243.

Fritz, M., 2012. Mechanismen der Adaptation retinaler Wachstumskegel an das axonale Lenkungssignal Ephrin-A5. PhD Thesis, Zool. Institute, Karlsruhe Institute of Technology (KIT).

Gale, N.W., Holland, S.J., Valenzuela, D.M., Flenniken, A., Pan, L., Ryan, T.E., Henkemeyer, M., Strebhardt, K., Hirai, H., Wilkinson, D.G., Pawson, T., Davis, S., Yancopoulos, G.D., 1996. Eph receptors and ligands comprise two major specificity subclasses and are reciprocally compartmentalized during embryogenesis. Neuron 17, 9–19.

Gauthier, L.R., Robbins, S.M., 2003. Ephrin signaling: One raft to rule them all? One raft to sort them? One raft to spread their call and in signaling bind them? Life Sci. 74, 207–216.

Gautier, A., Juillerat, A., Heinis, C., Corrêa, I.R., Kindermann, M., Beaufils, F., Johnsson, K., 2008. An Engineered Protein Tag for Multiprotein Labeling in Living Cells. Chem. Biol. 15, 128–136.

Gaze, R.M., Jacobson, M., Székely, G., 1963. The retino-tectal projection in Xenopus with compound eyes. J. Physiol. 165, 484–499.

Gaze, R.M., Sharma, S.C., 1970. Axial differences in the reinnervation of the goldfish optic tectum by regenerating optic nerve fibres. Exp. Brain Res. 10, 171–181.

Gebhardt, C., 2009. Development & Experimental Validation of a Novel Computational Model of Retinotopic Mapping. PhD Thesis, Zool. Institute, University of Karlsruhe (TH).

Gebhardt, C., Bastmeyer, M., Weth, F., 2012. Balancing of ephrin/Eph forward and reverse signaling as the driving force of adaptive topographic mapping. Development 139, 335–45.

Goh, L.K., Sorkin, A., 2013. Endocytosis of receptor tyrosine kinases. Cold Spring Harb. Perspect. Biol. doi: 10.1101/cshperspect.a017459.

Gomez, T.M., Letourneau, P.C., 2014. Actin dynamics in growth cone motility and navigation. J. Neurochem. 129, 221–234.

Goodhill, G.J., 2016. Can Molecular Gradients Wire the Brain? Trends Neurosci. 39, 202–11.

Gumy, L.F., Katrukha, E.A., Kapitein, L.C., Hoogenraad, C.C., 2014. New insights into mRNA trafficking in axons. Dev. Neurobiol. 74, 233–244.

Hattori, M., Osterfield, M., Flanagan, J.G., 2000. Regulated cleavage of a contact-mediated axon repellent. Science 289, 1360–1365.

Himanen, J.P., 2012. Ectodomain structures of Eph receptors. Semin. Cell Dev. Biol. 23, 35–42.

Himanen, J.P., Yermekbayeva, L., Janes, P.W., Walker, J.R., Xu, K., Atapattu, L., Rajashankar, K.R., Mensinga, A., Lackmann, M., Nikolov, D.B., Dhe-Paganon, S., 2010. Architecture of Eph receptor clusters. Proc. Natl. Acad. Sci. U. S. A. 107, 10860–5.

Himanen, J.-P., Chumley, M.J., Lackmann, M., Li, C., Barton, W.A., Jeffrey, P.D., Vearing, C., Geleick, D., Feldheim, D.A., Boyd, A.W., Henkemeyer, M., Nikolov, D.B., 2004. Repelling class discrimination: ephrin-A5 binds to and activates EphB2 receptor signaling. Nat. Neurosci. 7, 501–509.

Holt, C.E., Harris, W.A., 1983. Order in the initial retinotectal map in Xenopus: a new technique for labelling growing nerve fibres. Nature 301, 150–152.

Holt, C.E., Bullock, S.L., 2009. Subcellular mRNA Localization in Animal Cells and Why It Matters. Science 1212, 1212–6.

Hornberger, M.R., Dütting, D., Ciossek, T., Yamada, T., Handwerker, C., Lang, S., Weth, F., Huf, J., Weßel, R., Logan, C., Tanaka, H., Drescher, U., 1999. Modulation of EphA receptor function by coexpressed EphrinA ligands on retinal ganglion cell axons. Neuron 22, 731–742.

Huang, F., Kirkpatrick, D., Jiang, X., Gygi, S., Sorkin, A., 2006. Differential regulation of EGF receptor internalization and degradation by multiubiquitination within the kinase domain. Mol. Cell 21, 737–748.

Ingley, E., 2008. Src family kinases: Regulation of their activities, levels and identification of new pathways. Biochim. Biophys. Acta - Proteins Proteomics 1784, 56–65.

Janes, P.W., Saha, N., Barton, W.A., Kolev, M. V., Wimmer-Kleikamp, S.H., Nievergall, E., Blobel, C.P., Himanen, J.P., Lackmann, M., Nikolov, D.B., 2005. Adam meets Eph: An ADAM substrate recognition module acts as a molecular switch for ephrin cleavage in trans. Cell 123, 291–304.

Janes, P.W., Nievergall, E., Lackmann, M., 2012. Concepts and consequences of Eph receptor clustering. Semin. Cell Dev. Biol. 23, 43–50.

Jing, C., Cornish, V.W., 2011. Chemical Tags for Labeling Proteins Inside Living cells. Acc. Chem. Res. 2, 943.

Johannes, L., Popoff, V., 2008. Tracing the Retrograde Route in Protein Trafficking. Cell 135, 1175–1187.

Joset, A., Dodd, D.A., Halegoua, S., Schwab, M.E., 2010. Pincher-generated Nogo-A endosomes mediate growth cone collapse and retrograde signaling. J. Cell Biol. 188, 271–285.

Kabayama, H., Nakamura, T., Takeuchi, M., Iwasaki, H., Taniguchi, M., Tokushige, N., Mikoshiba, K., 2009. Ca2+ induces macropinocytosis via F-actin depolymerization during growth cone collapse. Mol. Cell. Neurosci. 40, 27–38.

Kania, A., Klein, R., 2016. Mechanisms of ephrin–Eph signalling in development, physiology and disease. Nat. Rev. Mol. Cell Biol. 17, 240-56.

Kao, T.J., Kania, A., 2011. Ephrin-Mediated cis-Attenuation of Eph Receptor Signaling Is Essential for Spinal Motor Axon Guidance. Neuron 71, 76–91.

Kawabuchi, M., Satomi, Y., Takao, T., Shimonishi, Y., Nada, S., Nagai, K., Tarakhovsky, A., Okada, M., 2000. Transmembrane phosphoprotein Cbp regulates the activities of Src-family tyrosine kinases. Nature 404, 999–1003.

Keppler, A., Gendreizig, S., Gronemeyer, T., Pick, H., Vogel, H., Johnsson, K., 2003. A general method for the covalent labeling of fusion proteins with small molecules in vivo. Nat. Biotechnol. 21, 86–9.

Kirchhausen, T., Macia, E., Pelish, H.E., 2008. Use of Dynasore, the Small Molecule Inhibitor of Dynamin, in the Regulation of Endocytosis. Methods Enzymol. 438, 77–93.

Klein, R., Parada, L.F., Coulier, F., Barbacid, M., 1989. TrkB, a novel tyrosine protein kinase receptor expressed during mouse neural development. EMBO J. 8, 3701–9.

Knöll, B., Drescher, U., 2004. Src Family Kinases Are Involved in EphA Receptor-Mediated Retinal Axon Guidance. J. Neurosci. 24, 6248–6257.

Kullander, K., Klein, R., 2002. Mechanisms and functions of Eph and ephrin signalling. Nat. Rev. Mol. Cell Biol. 3, 475–486.

Kumar, A., Baycin-Hizal, D., Zhang, Y., Bowen, M.A., Betenbaugh, M.J., 2015. Cellular traffic cops: The interplay between lipids and proteins regulates vesicular formation, trafficking, and signaling in mammalian cells. Curr. Opin. Biotechnol. 36, 215–221.

Lackmann, M., Mann, R.J., Kravets, L., Smith, F.M., Bucci, T.A., Maxwell, K.F., Howlett, G.J., Olsson, J.E., Vanden Bos, T., Cerretti, D.P., Boyd, A.W., 1997. Ligand for EPH-related kinase (LERK) 7 is the preferred high affinity ligand for the HEK receptor. J. Biol. Chem. 272, 16521–16530.

Lauterbach, J., Klein, R., 2006. Release of full-length EphB2 receptors from hippocampal neurons to cocultured glial cells. J. Neurosci. 26, 11575–11581.

Lemke, G., Reber, M., 2005. Retinotectal mapping: new insights from molecular genetics. Annu. Rev. Cell Dev. Biol. 21, 551–80.

Lemmon, S.K., Traub, L.M., 2012. Getting in Touch with the Clathrin Terminal Domain. Traffic 13, 511–519.

Leslie, M., 2011. Do Lipid Rafts Exist? Science 334, 1047–1048.

Leung, K., Horck, F.P.G. Van, Lin, A.C., Allison, R., Holt, C.E., 2007. Asymmetrical β -actin mRNA translation in growth cones mediates attractive turning to netrin-1. Nat. Neurosci. 9, 1247–1256.

Lim, Y.S., McLaughlin, T., Sung, T.C., Santiago, A., Lee, K.F., O'Leary, D.D.M., 2008. p75NTR Mediates Ephrin-A Reverse Signaling Required for Axon Repulsion and Mapping. Neuron 59, 746–758.

Liu, G., Dwyer, T., 2014. Microtubule dynamics in axon guidance. Neurosci. Bull. 30, 569–583.

Lisabeth, E.M., Falivelli, G., Pasquale, E.B., 2014. Eph Receptor Signaling and Ephrins. Cold Spring Harb. Perspect. Biol. doi:10.1016/j.surg.2006.10.010.

Lou, X., Fan, F., Messa, M., Raimondi, A., Wu, Y., Looger, L.L., Ferguson, S.M., De Camilli, P., 2012. Reduced release probability prevents vesicle depletion and transmission failure at dynamin mutant synapses. Proc. Natl. Acad. Sci. U. S. A. 109, E515–23.

Luo, L., Flanagan, J.G., 2007. Development of continuous and discrete neural maps. Neuron 56, 284–300.

Lutz, N., 2011. The role of axonal ephrin-As in fiber / fiber interactions of retinal ganglion cells. Bachelor's Thesis, Zool. Institute, Karlsruhe Institute of Technology (KIT).

Macia, E., Ehrlich, M., Massol, R., Boucrot, E., Brunner, C., Kirchhausen, T., 2006. Dynasore, a cell-permeable inhibitor of dynamin. Dev. Cell 10, 839–50.

Mann, F., Miranda, E., Weinl, C., Harmer, E., Holt, C.E., 2003. B-Type Eph Receptors and Ephrins Induce Growth Cone Collapse through Distinct Intracellular Pathways. J. Neurobiol. 57, 323–336.

Marín, O., Blanco, M.J., Nieto, M. a, 2001. Differential expression of Eph receptors and ephrins correlates with the formation of topographic projections in primary and secondary visual circuits of the embryonic chick forebrain. Dev. Biol. 234, 289–303.

Marler, K.J.M., Becker-Barroso, E., Martínez, A., Llovera, M., Wentzel, C., Poopalasundaram, S., Hindges, R., Soriano, E., Comella, J., Drescher, U., 2008. A TrkB/EphrinA interaction controls retinal axon branching and synaptogenesis. J. Neurosci. 28, 12700–12.

Marquardt, T., Shirasaki, R., Ghosh, S., Andrews, S.E., Carter, N., Hunter, T., Pfaff, S.L., 2005. Coexpressed EphA receptors and ephrin-A ligands mediate opposing actions on growth cone navigation from distinct membrane domains. Cell 121, 127–139.

Marston, D.J., Dickinson, S., Nobes, C.D., 2003. Rac-dependent trans-endocytosis of ephrinBs regulates Eph-ephrin contact repulsion. Nat. Cell Biol. 5, 879–888.

Mccluskey, A., Daniel, J.A., Hadzic, G., Chau, N., Clayton, E.L., Mariana, A., Whiting, A., Gorgani, N.N., Lloyd, J., Quan, A., Moshkanbaryans, L., Krishnan, S., Perera, S., Chircop, M., von Kleist, L., Mcgeachie, A.B., Howes, M.T., Parton, R.G., Campbell, M., Sakoff, J.A., Wang, X., Sun, J.Y., Robertson, M.J., Deane, F.M., Nguyen, T.H., Meunier, F.A., Cousin, M.A., Robinson, P.J., 2013. Building a better dynasore: The dyngo compounds potently inhibit dynamin and endocytosis. Traffic 14, 1272–1289.

McFarlane, S., Cornel, E.M., Amaya, E., Holt, C.E., 1996. Inhibition of FGF receptor activity in retinal ganglion cell axons causes errors in target recognition. Neuron 17, 245–254.

McFarlane, S., McNeill, L., Holt, C.E., 1995. FGF signaling and target recognition in the developing Xenopus visual system. Neuron 15, 1017–28.

McMahon, H.T., Gallop, J.L., 2005. Membrane curvature and mechanisms of dynamic cell membrane remodelling. Nature 438, 590–596.

McPherson, P.S., Kay, B.K., Hussain, N.K., 2001. Signaling on the endocytic pathway. Traffic 2, 375–384.

Menzel, P., Valencia, F., Godement, P., Dodelet, V.C., Pasquale, E.B., 2001. Ephrin-A6, a new ligand for EphA receptors in the developing visual system. Dev. Biol. 230, 74–88.

Merianda, T.T., Lin, A.C., Lam, J.S.Y., Vuppalanchi, D., Willis, D.E., Karin, N., Holt, C.E., Twiss, J.L., 2009. A functional equivalent of endoplasmic reticulum and Golgi in axons for secretion of locally synthesized proteins. Mol. Cell. Neurosci. 40, 128–142.

Meyer, R.L., 1979. Retinotectal projection in goldfish to an inappropriate region with a reversal in polarity. Science 205, 819–820.

Meyer, R.L., Wolcott, L.L., 1987. Compression and expansion without impulse activity in the retinotectal projection of goldfish. J. Neurobiol. 18, 549–567.

Micali, G., Endres, R.G., 2016. Bacterial chemotaxis: Information processing, thermodynamics, and behavior. Curr. Opin. Microbiol. 30, 8–15.

Milo, R., Phillips, R., 2016. Cell Biology by the Numbers, 1st ed. Garland Science, Taylor & Francis Group, LLC.

Ming, G., Wong, S.T., Henley, J., Yuan, X., Song, H., Spitzer, N.C., Poo, M., 2002. Adaptation in the chemotactic guidance of nerve growth cones. Nature 417, 411–418.

Mueller, B.K., Ledig, M.M., Wahl, S., 2000. The Receptor Tyrosine Phosphatase CRYPalpha Affects Growth Cone Morphology. J. Neurobiol. 4695, 219–229.

Munro, S., 2003. Lipid Rafts: Elusive or Illusive? Cell 115, 377–388.

Naito, J., Chen, Y., 2004. Morphological features of chick retinal ganglion cells. Anat. Sci. Int. 79, 213–225.

Nakamura, H., O'Leary, D.D.M., 1989. Inaccuracies in initial growth and arborization of chick retinotectal axons followed by course corrections and axon remodeling to develop topographic order. J. Neurosci. 9, 3776–3795.

NicholIV, R.H., Hagen, K.M., Lumbard, D.C., Dent, E.W., Gómez, T.M., 2016. Guidance of Axons by Local Coupling of Retrograde Flow to Point Contact Adhesions. J. Neurosci. 36 , 2267–2282.

Nievergall, E., Janes, P.W., Stegmayer, C., Vail, M.E., Haj, F.G., Teng, S.W., Neel, B.G., Bastiaens, P.I., Lackmann, M., 2010. PTP1B regulates Eph receptor function and trafficking. J. Cell Biol. 191, 1189–1203.

Nikolov, D.B., Xu, K., Himanen, J.P., 2013. Eph/ephrin recognition and the role of Eph/ephrin clusters in signaling initiation. Biochim. Biophys. Acta - Proteins Proteomics 1834, 2160–2165.

Noberini, R., Rubio De La Torre, E., Pasquale, E.B., 2012. Profiling Eph receptor expression in cells and tissues: A targeted mass spectrometry approach. Cell Adhes. Migr. 6, 102–112.

Pabbisetty, K.B., Yue, X.I.N., Li, C., Himanen, J., Zhou, R., Nikolov, D.B., Hu, L., 2007. Kinetic analysis of the binding of monomeric and dimeric ephrins to Eph receptors : Correlation to function in a growth cone collapse assay. Protein Sci. 16, 355–361.

Park, R.J., Shen, H., Liu, L., Liu, X., Ferguson, S.M., De Camilli, P., 2013. Dynamin triple knockout cells reveal off target effects of commonly used dynamin inhibitors. J. Cell Sci. 126, 5305–12.

Pasquale, E.B., 2005. Eph receptor signalling casts a wide net on cell behaviour. Nat. Rev. Mol. Cell Biol. 6, 462–75.

Pasquale, E.B., 2004. Eph-ephrin promiscuity is now crystal clear. Nat. Neurosci. 7, 417–8.

Piper, M., Anderson, R., Dwivedy, A., Weinl, C., van Horck, F., Leung, K.M., Cogill, E., Holt, C., 2006. Signaling mechanisms underlying Slit2-induced collapse of Xenopus retinal growth cones. Neuron 49, 215–28.

Piper, M., Salih, S., Weinl, C., Holt, C.E., Harris, W.A., 2005. Endocytosis-dependent desensitization and protein synthesis-dependent resensitization in retinal growth cone adaptation. Nat. Neurosci. 8, 179–86.

Preta, G., Cronin, J.G., Sheldon, I.M., 2015. Dynasore - not just a dynamin inhibitor. Cell Commun. Signal. 13, 24.

Raimondi, A., Ferguson, S.M., Lou, X., Armbruster, M., Paradise, S., Giovedi, S., Messa, M., Kono, N., Takasaki, J., Cappello, V., O'Toole, E., Ryan, T.A., De Camilli, P., 2011. Overlapping Role of Dynamin Isoforms in Synaptic Vesicle Endocytosis. Neuron 70, 1100–1114.

Raper, J.A., Kapfhammer, J.P., 1990. The enrichment of a neuronal growth cone collapsing activity from embryonic chick brain. Neuron 4, 21–29.

Raper, J.A., Grunewald, E.B., 1990. Temporal retinal growth cones collapse on contact with nasal retinal axons. Exp. Neurol. 109, 70–74.

Reber, M., Burrola, P., Lemke, G., 2004. A relative signalling model for the formation of a topographic neural map. Nature 431, 847–853.

Refaei, M., Leventis, R., Silvius, J.R., 2011. Assessment of the roles of ordered lipid microdomains in post-endocytic trafficking of glycosyl-phosphatidylinositol-anchored proteins in mammalian fibroblasts. Traffic 12, 1012–1024.

Ricci, V., Galmiche, A, Doye, A, Necchi, V., Solcia, E., Boquet, P., 2000. High cell sensitivity to Helicobacter pylori VacA toxin depends on a GPI-anchored protein and is not blocked by inhibition of the clathrin-mediated pathway of endocytosis. Mol. Biol. Cell 11, 3897–909.

Roche, F.K., Marsick, B.M., Letourneau, P.C., 2009. Protein Synthesis in Distal Axons Is Not Required for Growth Cone Responses to Guidance Cues. J. Neurosci. 29, 638–652.

Rohani, N., Parmeggiani, A., Winklbauer, R., Fagotto, F., 2014. Variable Combinations of Specific Ephrin Ligand/Eph Receptor Pairs Control Embryonic Tissue Separation. PLoS Biol. 12, 1-20.

Rosentreter, S., Davenport, R.W., Löschinger, J., Huf, J., Jung, J., Bonhoeffer, F., 1998. Response of retinal ganglion cell axons to striped linear gradients of repellent guidance molecules. J. Neurobiol. 37, 541–62.

Sabet, O., Stockert, R., Xouri, G., Brüggemann, Y., Stanoev, A., Bastiaens, P.I.H., 2015. Ubiquitination switches EphA2 vesicular traffic from a continuous safeguard to a finite signalling mode. Nat. Commun. 6, 8047.

Sabharanjak, S., Sharma, P., Parton, R.G., Mayor, S., 2002. GPI-anchored proteins are delivered to recycling endosomes via a distinct cdc42-regulated clathrin-independent pinocytic pathway. Dev. Cell 2, 411–423.

Sabry, J.H., O'Connor, T.P., Evans, L., Toroian-Raymond, A., Kirschner, M., Bentley, D., 1991. Microtubule behavior during guidance of pioneer neuron growth cones in situ. J. Cell Biol. 115, 381–395.

Salazar, G., González, A., 2002. The bending rigidity of mitotic chromosomes. Mol. Biol. Cell 13, 2170–2179.

Schaupp, A., Sabet, O., Dudanova, I., Ponserre, M., Bastiaens, P., Klein, R., 2014. The composition of EphB2 clusters determines the strength in the cellular repulsion response. J. Cell Biol. 204, 409–422.

Schindler, C., Chen, Y., Pu, J., Guo, X., Bonifacino, J.S., Program, M., 2015. EARP, a multisubunit tethering complex involved in endocytic recycling. Nat. Cell Biol. 17, 639–650.

Schlessinger, J., 2000. Cell Signaling by Receptor Tyrosine Kinases A large group of genes in all eukaryotes encode for. October 103, 211–225.

Schmidt, J.T., Cicerone, C.M., Easter, S.S., 1978. Expansion of the half retinal projection to the tectum in goldfish: an electrophysiological and anatomical study. J. Comp. Neurol. 177, 257–277.

Segal, R.A., 2003. Selectivity in Neutrophin Signaling: Theme and Variations. Annu. Rev. Neurosci. 26, 299–330.

Seiradake, E., Harlos, K., Sutton, G., Aricescu, A.R., Jones, E.Y., 2010. An extracellular steric seeding mechanism for Eph-ephrin signaling platform assembly. Nat Struct Mol Biol 17, 398–402.

Seiradake, E., Schaupp, A., del Toro Ruiz, D., Kaufmann, R., Mitakidis, N., Harlos, K., Aricescu, A.R., Klein, R., Jones, E.Y., 2013. Structurally encoded intraclass differences in EphA clusters drive distinct cell responses. Nat. Struct. Mol. Biol. 20, 958–64.

Sharma, S.C., 1972. Reformation of retinotectal projections after various tectal ablations in adult goldfish. Exp. Neurol. 34, 171–182.

Simon, D.K., O'Leary, D.D.M., 1992. Responses of retinal axons in vivo and in vitro to position-encoding molecules in the embryonic superior colliculus. Neuron 9, 977–989.

Singh, D.R., Cao, Q., King, C., Salotto, M., Ahmed, F., Zhou, X.Y., Pasquale, E.B., Hristova, K., 2015. Unliganded EphA3 dimerization promoted by the SAM domain. Biochem. J. 471, 101–9.

Skretting, G., Torgersen, M.L., van Deurs, B., Sandvig, K., 1999. Endocytic mechanisms responsible for uptake of GPI-linked diphtheria toxin receptor. J. Cell Sci. 112 (Pt 2), 3899–909.

Smith, F.M., Vearing, C., Lackmann, M., Treutlein, H., Himanen, J., Chen, K., Saul, A., Nikolov, D., Boyd, A.W., 2004. Dissecting the EphA3/Ephrin-A5 interactions using a novel functional mutagenesis screen. J Biol Chem 279, 9522–9531.

Sorkin, A., Westermark, B., Heldin, C.-H., Claesson-Welsh, L., 1991. Effect of Receptor Kinase Inactivation on the Rate of Internalization and Degradation of PDGF and the PDGF ß-Receptor. J. Cell Biol. 112, 469–478.

Sperry, R.W., 1963. Chemoaffinity in the Orderly Growth of Nerve Fiber Patterns and Connections. Proc. Natl. Acad. Sci. U. S. A. 50, 703–710.

Tamariz, E., Varela-Echavarría, A., 2015. The discovery of the growth cone and its influence on the study of axon guidance. Front. Neuroanat. 9, 51.

Tanaka, E., Kirschner, M.W., 1995. The role of microtubules in growth cone turning at substrate boundaries. J. Cell Biol. 128, 127–137.

Thanos, S., Mey, J., 2001. Development of the visual system of the chick II. Mechanisms of axonal guidance. Brain Res. Rev. 35, 205–245.

Thomas, S., Brugge, J., 1997. Cellular functions regulated by Src family kinases. Annu Rev Cell Dev Biol 13, 513–609.

Tojima, T., Itofusa, R., Kamiguchi, H., 2014. Steering neuronal growth cones by shifting the imbalance between exocytosis and endocytosis. J. Neurosci. 34, 7165–78.

Trinidad, E.M., Zapata, A.G., Alonso-Colmenar, L.M., 2010. Eph-ephrin bidirectional signaling comes into the context of lymphocyte transendothelial migration. Cell Adhes. Migr. 4, 363–367.

Ullrich, O., Molecular, E., 1996. Rab11 Regulates Recycling through the Pericentriolar Recycling Endosome. J. Cell Biol. 135, 913–924.

Van der Sluijs, P., Hull, M., Webster, P., Male, P., Goud, B., Mellman, I., 1992. the Small Gtp-Binding Protein Rab4 Controls an Early Sorting Event on the Endocytic Pathway. Cell 70, 729–740.

Van Kesteren, R.E., Carter, C., Dissel, H.M.G., Minnen, J. Van, Gouwenberg, Y., Syed, N.I., Spencer, G.E., Smit, A.B., 2006. Local Synthesis of Actin-Binding Protein ß -Thymosin Regulates Neurite Outgrowth. J. Neurosci. 26, 152–157. Van Meer, G., Sprong, H., 2004. Membrane lipids and vesicular traffic. Curr. Opin. Cell Biol. 16, 373–378.

Von Kleist, L., Stahlschmidt, W., Bulut, H., Gromova, K., Puchkov, D., Robertson, M.J., MacGregor, K.A., Tomlin, N., Pechstein, A., Chau, N., Chircop, M., Sakoff, J., Von Kries, J.P., Saenger, W., Kräusslich, H.G., Shupliakov, O., Robinson, P.J., McCluskey, A., Haucke, V., 2011. Role of the clathrin terminal domain in regulating coated pit dynamics revealed by small molecule inhibition. Cell 146, 471–484.

Von Philipsborn, A.C., Lang, S., Bernard, A., Loeschinger, J., David, C., Lehnert, D., Bastmeyer, M., Bonhoeffer, F., 2006a. Microcontact printing of axon guidance molecules for generation of graded patterns. Nat. Protoc. 1, 1322–8.

Von Philipsborn, A.C., Lang, S., Loeschinger, J., Bernard, A., David, C., Lehnert, D., Bonhoeffer, F., Bastmeyer, M., 2006b. Growth cone navigation in substrate-bound ephrin gradients. Development 133, 2487–2495.

Von Philipsborn, A.C., 2007. Axon guidance in substrate-bound protein gradients. PhD Thesis, Zool. Institute, University of Karlsruhe (TH).

Wahl, S., Barth, H., Ciossek, T., 2000. Ephrin-A5 induces collapse of growth cones by activating Rho and Rho kinase. J. Cell Biol. 149, 263–270.

Wedeen, V.J., Rosene, D.L., Wang, R., Dai, G., Mortazavi, F., Hagmann, P., Kaas, J.H., Tseng, W.-Y.I., 2012. The Geometric Structure of the Brain Fiber Pathways. Science 335, 1628–1634.

Weschenfelder, M., 2014. Expression rekombinanter Sensoren zur Visualisierung der Oberflächendynamik des Eph / ephrin-Systems in retinalen Wachstumskegeln des Huhns. PhD Thesis, Zool. Institute, Karlsruhe Institute of Technology (KIT).

Weth, F., Fiederling, F., Gebhardt, C., Bastmeyer, M., 2014. Chemoaffinity in topographic mapping revisited - Is it more about fiber-fiber than fiber-target interactions? Semin. Cell Dev. Biol. 35, 126–135.

Willox, A.K., Sahraoui, Y.M.E., Royle, S.J., 2014. Non-specificity of Pitstop2 in clathrin-mediated endocytosis. Biol. Open 3, 326–31.

Wimmer-Kleikamp, S.H., Janes, P.W., Squire, A., Bastiaens, P.I.H., Lakmann, M., 2004. Recruitment of Eph receptors into signaling clusters does not require ephrin contact. J. Cell Biol. 164, 661–666.

Wimmer-Kleikamp, S.H., Nievergall, E., Gegenbauer, K., Adikari, S., Yeadon, T., Boyd, A.W., Patani, N.R., Lackmann, M., Mansour, M., 2009. Eph / ephrin-facilitated adhesion of pre-B leukemia cells Elevated protein tyrosine phosphatase activity provokes Eph / ephrin-facilitated adhesion of pre-B leukemia cells. Cell 112, 721–732.

Wu, K.Y., Hengst, U., Cox, L.J., Macosko, E.Z., Jeromin, A., Urquhart, E.R., Jaffrey, S.R., 2005. Local translation of RhoA regulates growth cone collapse. Nature 436, 1020–4.

Xu, K., Tzvetkova-Robev, D., Xu, Y., Goldgur, Y., Chan, Y.-P., Himanen, J.P., Nikolov, D.B., 2013. Insights into Eph receptor tyrosine kinase activation from crystal structures of the EphA4 ectodomain and its complex with ephrin-A5. Proc. Natl. Acad. Sci. U. S. A. 110, 14634–9.

Yamashita, H., Avraham, S., Jiang, S., Dikic, I., Avraham, H., 1999. The Csk homologous kinase associates with TrkA receptors and is involved in neurite outgrowth of PC12 cells. J. Biol. Chem. 274, 15059–15065.

Yao, J., Sasaki, Y., Wen, Z., Bassell, G.J., Zheng, J.Q., 2006. An essential role for beta-actin mRNA localization and translation in Ca2+-dependent growth cone guidance. Nat. Neurosci. 9, 1265–1273.

Yap, C.C., Winckler, B., 2015. Adapting for endocytosis: roles for endocytic sorting adaptors in directing neural development. Front. Cell. Neurosci. 9, 1–17.

Yates, P.A., Roskies, A.L., McLaughlin, T., O'Leary, D.D.M., 2001. Topographic-specific axon branching controlled by ephrin-As is the critical event in retinotectal map development. J. Neurosci. 21, 8548–8563.

Yin, Y., Yamashita, Y., Noda, H., Okafuji, T., Go, M.J., Tanaka, H., 2004. EphA receptor tyrosine kinases interact with co-expressed ephrin-A ligands in cis. Neurosci. Res. 48, 285–296.

Yoo, S., Shin, J., Park, S., 2010. EphA8-ephrinA5 signaling and clathrin-mediated endocytosis is regulated by Tiam-1, a Rac-specific guanine nucleotide exchange factor. Mol. Cells 29, 603–609.

Yoon, B.C., Zivraj, K.H., Holt, C.E., 2009. Local Translation and mRNA Trafficking in Axon Pathfinding. Results Probl. Cell Differ. 48, 339–351.

Yoon, M.G., 1971. Reorganization of Retinotectal Projection Following Surgical Operations on the Optic Tectum in Goldfish. Exp. Neurol. 33, 395–411.

Yoon, M.G., 1972. Transposition of the visual projection from the nasal hemiretina onto the foreign rostral zone of the optic tectum in goldfish. Exp. Neurol. 37, 451–462.

Zimmer, M., Palmer, A., Köhler, J., Klein, R., 2003. EphB-ephrinB bi-directional endocytosis terminates adhesion allowing contact mediated repulsion. Nat. Cell Biol. 5, 869–878.

LIST OF ABBREVIATIONS

ABBREVIATIONS

a/ p	anterior/ posterior
Abl	Abelson murine leukemia viral oncogene homolog
ADAM	A disintegrin and metalloproteinase domain-containing protein
BDNF	Brain-derived neurotrophic factor
CAG	CMV early enhancer/ chicken β-actin promotor/enhancer
Cbp	Csk-binding protein
ChK	Csk homologous kinase
CME	Clathrin-mediated endocytosis
CMV	Cytomegalovirus
CRD	Cysteine-rich domain
Crk	CT10 regulator of kinase
Csk	C-terminal Src kinase
d/ v	dorsal/ ventral
DiO	3,3'-Dioctadecyloxacarbo-cyanine perchlorate
DiI	1,1'-Dioctadecyl-3,3,3',3'-tetramethylindocarbocyanine perchlorate
DMF	Dimethylformamide
DMSO	Dimethylsulfoxide
EARP	Endosome-associated recycling protein
EE	Early endosome
Eph	Erythropoetin producing hepatocyte
ER	Endoplasmatic reticulum
ESCRT	Endosomal sorting complexes required for transport
FF	Fiber-Fiber
FGF	Fibroblast growth factor
FGFR	FGF receptor
FNIII	Fibronectin type III domain
FT	Fiber-Target

GAP	GTPase activating protein
GEF	Guanosine nucleotide exchange factor
GC	Growth cone
GFP	Green fluorescent protein
GPI	Glycosylphosphatidylinositol
HBSS	Hanks' balanced salt solution
ILV	Intraluminal vesicle
IRES	Internal ribosomal entry site
K_D	Dissociation constant
l/ m	lateral/ medial
LBD	Ligand binding domain
LE	Late endosome
L_F	Ligand (ephrin-A) on a simulated fiber
L_T	Ligand (ephrin-A) on a simulated target cell
MC	Methylcellulose
MVB	Multi vesicular bodies
n/ t	nasal/ temporal
Nck	non-catalytic region of tyrosine kinase
p75NTR	p75 neutrophin receptor
PDMS	Polydimethylsiloxane
PDZ	PSD-95/ disc large/ zonula occludens-1 binding motif
PI3K	Phosphatidylinositol-4,5-bisphosphate 3-kinase
PKA	Protein kinase A
PLL	Poly-L-lysine
PTP1B	Protein-tyrosine phosphatase 1B
Rab	Ras-related in brain
Rac	Ras-related C3 botulinum toxin substrate
Ras	Rat sarcoma
RE	Recycling endosome
Ret	Rearranged during transfection
R_F	Receptor (EphA) on a simulated fiber

RGC	Retinal ganglion cell
RhoA	Ras homolog gene family member A
R_T	Receptor (EphA) on a simulated target cell
RT	Room temperature
RTK	Receptor tyrosine kinase
SAM	Sterile alpha motif
SC	*Superior colliculus*
Sema3A	Semaphorin 3A
Src	Sarcoma
TGN	Trans-golgi network
Trk	Tropomyosin receptor kinase
v/v	volume per volume
w/v	weight per volume

DANKSAGUNG

Mein herzlicher Dank gilt allen, die zur Fertigstellung dieser Arbeit beigetragen haben.

Inbesonders möchte ich danken:

Prof. Dr. Martin Bastmeyer für das Ermöglichen einer Promotion an seinem Lehrstuhl und seine Unterstützung bei organisatorischen und fachlichen Fragen.

Prof. Dr. Peter Nick für die Begutachtung meiner Arbeit als Korefferent.

Dr. Franco Weth für die hervorragende Betreuung meiner Arbeit und sein Engagement in der Förderung meiner wissenschaftlichen Kompetenz.

Prof. Dr. Martin Wegener, der es ermöglichte technische Bauteile in seiner Werkstatt anfertigen zu lassen.

Dr. Benjamin Richter für die Anfertigung einiger Stempel Master und für hilfreiche Disskussionen und Anregungen bei der Entwicklung von CPAD.

Dr. Bastian Rapp, Dr. Ansgar Waldbauer und Frederik Kotz für die Bereitstellung einiger Stempel Master.

Dr. Christoph Gebhardt, Dr. Martin Fritz und Dr. Markus Weschenfelder für ihre Hilfe im Labor und ihr kritisches Interesse an meiner Arbeit.

Meiner Familie und Anna für ihre Unterstützung.